2022-08-01

Water Sourcing Strategies Of Desert Vegetation In Varying Soil Textures With Vegetation Competition: A Stable Isotope Analysis

Martha Elizabeth Gardea
University of Texas at El Paso

WATER SOURCING STRATEGIES OF DESERT VEGETATION IN VARYING SOIL TEXTURES WITH VEGETATION COMPETITION: A STABLE ISOTOPE ANALYSIS

MARTHA ELIZABETH GARDEA

Master's Program in Environmental Science

APPROVED:

Hugo Gutierrez-Jurado, Ph.D., Chair

Anthony Darrouzet-Nardi, Ph.D.

Lin Ma, Ph.D.

Stephen Crites, Ph.D.
Dean of the Graduate School

WATER SOURCING STRATEGIES OF DESERT VEGETATION IN VARYING SOIL TEXTURES WITH VEGETATION COMPETITION: A STABLE ISOTOPE ANALYSIS

by

MARTHA ELIZABETH GARDEA, B.S.

THESIS

Presented to the Faculty of the Graduate School of
The University of Texas at El Paso
in Partial Fulfillment
of the Requirements
for the Degree of

MASTER OF SCIENCE

Department of Earth, Environmental and Resource Sciences
THE UNIVERSITY OF TEXAS AT EL PASO
August 2022

ACKNOWLEDGEMENTS

First of all, I would like to acknowledge and express my deepest appreciation to my committee members who make this work possible. To Dr. Hugo Gutierrez, the Chair of this thesis, who provided me the guidance and advice that carried me through all of the stages of this thesis. I'm extremely grateful to my committee members, Hugo Gutierrez, Lin Ma, and Dr. Nardi for your insightful comments and suggestions that lead to the success of this thesis.

I would also like to extend my gratitude to Dr. Craig Tweedie and Marguerite Mauritz-Tozer with the Systems Ecology Laboratory at the University of Texas at El Paso. Without their collaborative effort with moisture data from Jornada, this project would have not been possible. Nohemi Valenzuela and Mark Engle, thank you for allowing me to use your laboratory to process soil samples that were instrumental for this thesis. Nohemi, thank you for your assistance and patience whilst guiding me through the process.

Thank you to my colleagues, Orlando Ramirez-Valle and Alfredo Dagda-Torres for graciously helping me with sample collection and always answering my questions. Orlando y Alfredo, les agradesco mucho por su apoyo. No les puedo agradecer lo suficiente por su conocimiento, consejos, y mas de todo, su paciencia.

Nobody has been more important to be in the pursuit of this thesis than my family and friends. As a first generational student, I'd like to thank my parents for making sacrifices in order for me to succeed, they are my ultimate role models. Colin, thank you for always brightening my day and providing me with unending inspiration.

ABSTRACT

Recent studies have suggested an ecohydrological separation of water exists in the northern Chihuahuan Desert, where vegetation types, rainfall regimes, and location in the terrain seem to determine the type of water (e.g. isotopically depleted or enriched in ^{18}O and ^{2}H) plants are able to source and use throughout their growing cycle. That work found evidence of creosote (*Larrea tridentata*) and mesquite (*Prosopis glandulosa*) using tightly bound soil water at both a site on an ephemeral channel and a site in higher elevated flat area because the isotopic signature of plant water at the beginning of the study did not match that of precipitation but matched the soil samples. This behavior suggested tightly bound soil water was utilized and was sufficient to meet dry period vegetation demand. Additionally, soils from the channelized site were shown to become both enriched and depleted faster in $\delta^{18}O$ and ^{2}H than the flatter site, showing clear differences in hydrologic dynamics of the shallow soils possibly due to the influence of runoff on the channel soils. However, questions remain about the influence of soil properties and vegetation competition on the water sourcing dynamics of desert vegetation. This study will be adding two vegetation dense, finer soil sites to the existing low-lying channel sites and higher, flatter piedmont sites.

This study uses stable water isotope data to determine the relationship between subsurface water storage and desert vegetation in a dry piedmont in the Northern Chihuahuan Desert. Soil texture analyses were conducted on an instrument that measures suspension pressure, called PARIO. Vegetation xylem water was extracted using the cryogenic method to avoid isotopic fractionation. Soil samples were processed using the induction module (IM) attachment in the Picarro L2130-i CRDS. Quantitative observations of $\delta^{18}O$ and Deuterium from precipitation, soil water, and stem water samples from Creosote Bush (*Larrea tridentata*), Honey Mesquite (*Prosopis glandulosa*), Tarbush (*Flourensia cernua*), and Poaceae sp. were obtained using laser-based cavity

ringdown spectroscopy during two growing cycle periods for a total of 37 months in a piedmont location within the western side of the Jornada Experimental Range (JER).

The results of this study at the JER show that there are factors influencing the available water for the four desert vegetation species studied throughout their growing season. When assessing the soil texture influence on water availability, it is apparent that VD/FS (Vegetation Dense/Finer Soil) areas experience little evaporation due to their finer soil texture and possibly increasing their soil water residence time. When assessing the vegetation competition influence on water sourcing, we observed that the plants have different water sources strategies depending on the site and species. The isotopic signature of the stem water in the vegetation at the VD/FS areas tend to follow that of precipitation more closely than those of the vegetation on the other sites. This may be due to the inability of vegetation in the VD/FS areas to obtain water past the shallow soils due to the presence of a highly indurated caliche interfering with deeper infiltration. At the FA (Flat Area), honey mesquite tends to show a more relatively isotopically depleted water suggesting a deeper source in the soil profile, whereas, creosote shows a more enriched water resembling that found on shallower soil. The CA (Channel Area) shows that the vegetation may have a similar source in the soil profile. We also observed that landscape may have an influence on water availability. The channel area has a wide range of isotopic values that may indicate additional runoff from upstream that is combining with water previously in the soil profile. The interpretation of these results illuminates the plant water use dynamics and strategies of highly resilient desert vegetation communities as affected by the structure of the shallow critical zone.

TABLE OF CONTENTS

CHAPTER 1: INTRODUCTION 1
1.1 MOTIVATION 1
1.2 STABLE WATER ISOTOPES AS A VEGETATION WATER SOURCE TRACER 5
1.3 SOIL TEXTURE INFLUENCE ON WATER SOURCING 6
1.4 VEGETATION COMPETITION INFLUENCE ON WATER SOURCING 7
1.5 LANDSCAPE INFLUENCE ON WATER SOURCING 8
1.6 IMPORTANCE 8
1.7 OBJECTIVES 9
CHAPTER 2: METHODS 10
2.1 SITE DESCRIPTION 10
2.2 SAMPLE COLLECTION FOR ISOTOPIC ANALYSIS OF VEGETATION, SOIL AND RAINFALL WATER 13
2.3 MICROMETEORLOGICAL DATA 14
2.4 WATER EXTRACTION FROM VEGETATION AND SOIL SAMPLES 15
2.5 STABLE WATER ISOTOPE ANALYSIS 17
2.6 SOIL TEXTURE ANALYSES AT EACH SAMPLING LOCATION 19
2.7 VEGETATION COVER ANALYSES AT EACH SAMPLING LOCATION 19
CHAPTER 3: RESULTS 21
3.1 HYDROLOGICAL CONDITIONS 21
3.1.1 Precipitation 21
3.1.2 Vapor Pressure Deficit 23
3.1.3 Cumulative Precipitation 25
3.2 SOIL TEXTURE ANALYSIS 26
3.3 CANFIELD'S LINE INTERCEPT SURVEY 27
3.4 STABLE WATER ISOTOPES 29
3.4.1 Precipitation 29
3.4.2 Soil Water 31
3.4.3 Vegetation Stem Water 38
3.5 RELATIONSHIPS BETWEEN PRECIPITATION, SOIL WATER, AND VEGETATION STEM WATER 39

CHAPTER 4: DISCUSSION 48
4.1 SOIL TEXTURE INFLUENCE ON VEGETATION WATER SOURCING 48
4.2 VEGETATION SPECIES INFLUENCE ON VEGETATION WATER SOURCING 50
4.3 LANDSCAPE INFLUENCE ON VEGETATION WATER SOURCING 52
CHAPTER 5: CONCLUSIONS 54
5.1 FUTURE WORK 56
REFERENCES 57
APPENDIX A: 62
APPENDIX B: 66
APPENDIX C: 80
VITA 82

LIST OF FIGURES

Figure 1: Model of the soil-vegetation-atmosphere continuum 4
Figure 2: Illustration of hypothetical plant activity and soil moisture residence dynamics 6
Figure 3: Map of the study area 10
Figure 4: Satellite image of the sampling locations within the JER. 12
Figure 5: Satellite image of the eddy covariance towers relative to the study sites 15
Figure 6: Cryogenic vacuum extraction line for vacuum distillation of plant samples 17
Figure 7: Satellite image of the Canfield line intercept survey 20
Figure 8: Half hourly precipitation (mm) and air temperature (C) 22
Figure 9: Half-hourly precipitation (mm) and VPD (hPA) 24
Figure 10: Half hourly precipitation expressed as cumulative precipitation (mm). 25
Figure 11: Soil textural triangle containing samples from each site and depth 26
Figure 12: Bar graph containing data from a Canfield's line intercept survey 28
Figure 13: $\delta^{18}O$ (‰) of precipitation samples collected from the years 2018 to 2021 29
Figure 14: The Global Meteoric Water Line (GMWL) and Local Meteoric Water Line (LMWL) 30
Figure 15: Scatter plots for δ2H and δ18O (‰) for precipitation and soils for the study period 32
Figure 16: Linear regression plot of $\delta^{18}O$ and $\delta^{2}H$ (‰) soils with precipitation 32
Figure 17: $\delta^{18}O$ and $\delta^{2}H$ (‰) plot of 10 cm vs 20 cm of $\delta^{18}O$ for the soils 33
Figure 18: Plots comparing the soil behavior of samples 34
Figure 19: Plots comparing the soil behavior of samples each of the study sites 36
Figure 20: Continuation of plots comparing soil behavior 37
Figure 21: $\delta^{18}O$ and $\delta^{2}H$ (‰) concentration plot of the vegetation 38
Figure 22: Violin plots for data within each study site in units of $\delta^{18}O$ (‰) 40
Figure 23: Violin plots for data of vegetation within each study site in units of $\delta^{18}O$ (‰) 41
Figure 24: Polar plots of CA $\delta^{18}O$ (‰) concentration of precipitation, soil water at 10 cm and 20 cm, and vegetation 42
Figure 25: Polar plots of FA $\delta^{18}O$ concentration of precipitation, soil water at 10 cm and 20 cm, and vegetation 44
Figure 26: Polar plots of VD/FS Area 1 $\delta^{18}O$ concentration of precipitation, soil water at 10 cm and 20 cm, and vegetation 45
Figure 27: Polar plots of VD/FS Area 2 $\delta^{18}O$ concentration of precipitation, soil water at 10 cm and 20 cm, and vegetation 47

CHAPTER 1: INTRODUCTION

1.1 MOTIVATION

In the Northern Chihuahuan Desert, vegetation species such as creosote (*Larrea tridentata*) and honey mesquite (*Prosopis glandulosa*) thrive in arid and semiarid conditions. These desert plants are able to remain active nearly continually during their growing cycle despite low shallow moisture and high evaporative conditions. Recent studies have suggested that an ecohydrological separation of water exists, in which vegetation types, rainfall regimes and location in the terrain seem to determine the type of water (e.g. isotopically depleted or enriched) plants are able to acquire and use throughout their growing cycle (Renée Brooks et al., 2010; Szutu and Papuga, 2019; Qian et al., 2017). However, questions remain about the influence of soil properties and vegetation competition on the water sourcing dynamics of desert vegetation during their growing season.

Previous work in the area (Thompson et al. 2020) found evidence of creosote and honey mesquite using tightly bound soil water at an ephemeral channel and at a site in a higher elevated flat area. The isotopic signature of both plant stems' waters at the beginning of the study did not match that of precipitation but matched the soil water signatures (Thompson et al. 2020). This behavior suggested tightly bound soil water was utilized and was sufficient to meet dry period vegetation demand and coincides with the two water worlds hypothesis, which states that one water source is used by trees (tightly bound soil water not mixing with precipitation water) and another source is associated to infiltration, groundwater recharge, runoff, and streamflow (McDonnell, 2014; Renée Brooks et al., 2010; Dubbert et al., 2019). To expand on these findings, we will be observing the influence of soil properties and vegetation competition on water sourcing of desert vegetation. The interpretation of the results will help us decipher plant water use dynamics and

strategies of highly resilient desert vegetation communities as affected by the structure of the shallow critical zone.

The vegetation species we focus on are Creosote (*Larrea tridentata*), Honey Mesquite (*Prosopis glandulosa*), Grass (Poaceae sp.), and Tarbush (*Flourensia cernua*) in the Northern Chihuahuan Desert within the Jornada Experimental Range (JER). The Chihuahuan Desert (350,000 km^2) is the largest desert in North America and covers part of the U.S. Southwest (Morafka, 1989). The Chihuahuan Desert is characterized by low plant biomass, low primary productivity, and high plant species diversity (Kemp, 1983; Huenneke et al., 2001). Parts of the desert are classified as grassland and contains 3,300+ species of vegetation (MacMahon, 1979; Henrickson and Johnston, 2007) ranging from grass to shrubs and trees to pure stands of shrubs. On the northern portion of the Chihuahuan desert, the Jornada Basin, a long term ecological research station spanning more than a hundred years of vegetation records, is located on a plain 100 m above the Rio Grande east of the river and is characterized as a shrubland/grassland ecosystem (Gibbens et al. 2005). This ecosystem has been subjected to woody plant encroachment (Van Auken, 2009; Gibbens et al. 2005) and has since been documented in the 1858 (Gibbens et al., 2005). This woody plant encroachment has been attributed to various phenomena; among them, a changing climate, reduced fire frequency, and over grazing (Drewa and Havstad, 2001; Gibbens et al. 2005; Caracciolo et al., 2016).

Studies have determined that coexistence of plant communities in desert environments are partly due to differences in their utilization and partitioning of resources (Kemp, 1983; Fargione and Tilman, 2005). For instance, rooting patterns reaching differing depths in the soil profile can be utilized by different species, and in some cases allowing them to access moisture and nutrients from different pools (Grieu et al., 2001). This study focuses on deciphering the water sourcing

strategies for some of the dominant species in the Northern Chihuahuan Desert: creosote (*Larrea tridentata*) and honey mesquite (*Prosopis glandulosa*). Tarbush (*Flourensia cernua),* and grass (*Bouteloa spp.*) were also of interest due to their distinct root systems that perhaps enables them to tap into different water sources. Creosote is known to have shallow, wide reaching tap roots that extract water from a large volume of soil, in some cases within 2-5 m in depth and superficial roots within the top meter (Jorquera et al, 2012). Honey mesquite can behave as a phreatophytic species producing both a taproot and extensive lateral roots allowing the plant to absorb moisture from near the surface and up to 15 m laterally, while going 5-12 m deep into the soil when needed (Meyer, 1971). Tarbush roots can reach depths of 5 m or more with a radial reach of 1.5-5 m (10 cm within the soil surface) (Hyder et al., 2002). *Bouteloa spp*. has relatively shallower root systems and obtain shallow soil moisture when it becomes available, typically after significant (>5mm/d) rainfall events in the late Spring, Summer or early Fall. Furthermore, and similar to other semiarid and desert environments, caliche layers ($CaCO_3$) tend to develop in soils in the Jornada region (Hennessy, 1983). Caliche formation may affect soil-plant-water relations and plant distribution, which in turn will influence ecosystem primary production (Grieu et al., 2001). Because caliche is often produced within the rooting zone of plants in these environments (Hennessy, 1983), these layers can be a barrier to root growth, while at the same time have the ability to absorb and store water that may be available to plants under certain conditions (Schlesinger et al., 1989). The caliche found within the study sites may or may not store sufficient water for plants for plants to use.

The study included eight creosotes, eight honey mesquites, two tarbushes, and two grass plant samples from four distinct sites. The sites include an ephemeral channel (CA), a flat area (FA) in higher elevated terrain, and two vegetation-dense/finer-soil areas (VD/FS) within a piedmont at

the Jornada Experimental Range. Our goal is to determine how differences in landscape, soil texture, and vegetation species influences water sourcing of plants. We hypothesize that the isotopic signature of soil water varies with soil depth and time of the year as the isotopic signature of the rainfall changes with the seasons. Further, we hypothesize that plant water sourcing will vary with species (responding to different rooting depth and phenology), landscape, soil texture, and time of the year.

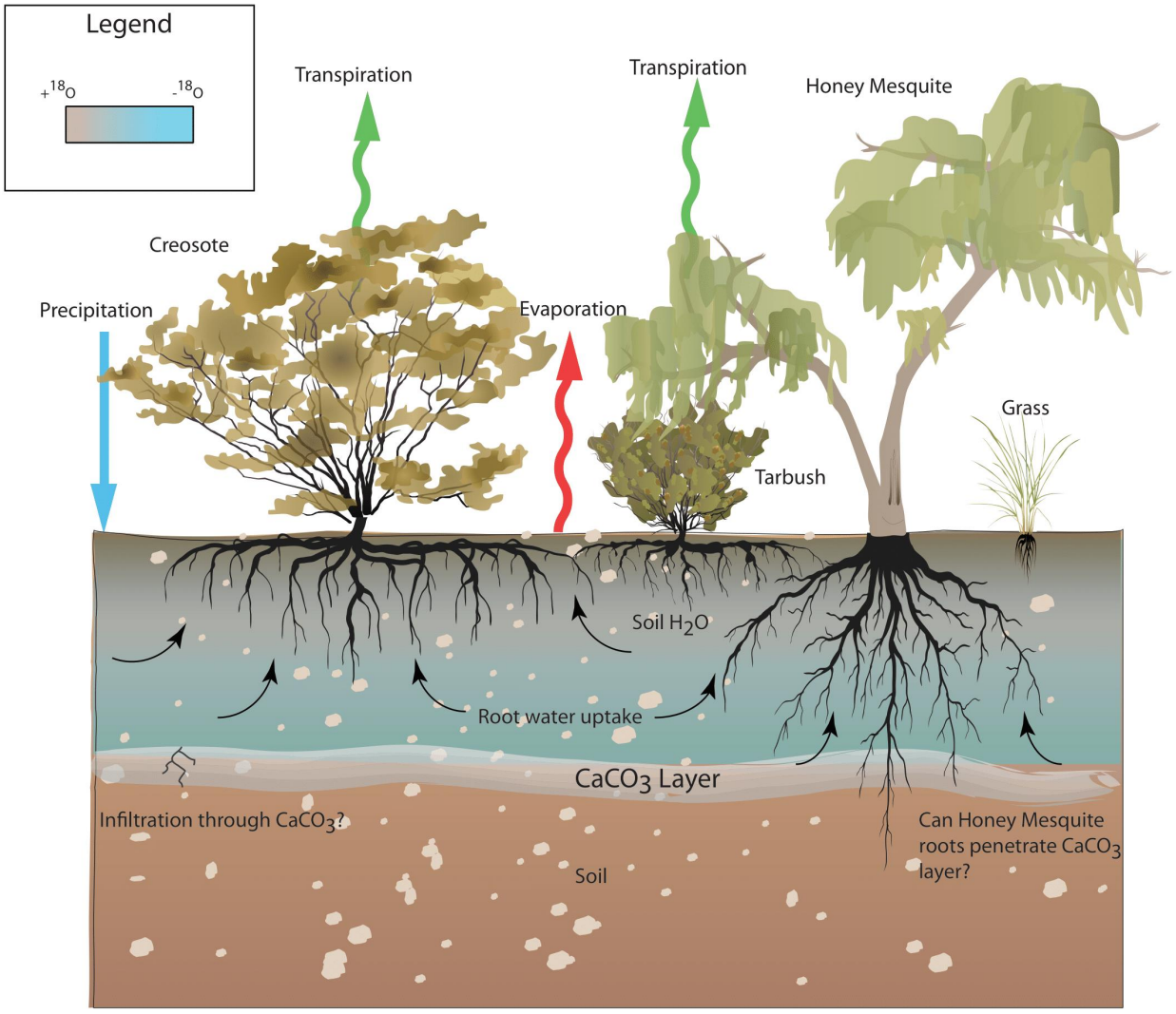

Figure 1: Model of the soil-vegetation-atmosphere continuum affecting stable water isotope composition and plant water uptake within the Jornada Experimental Range in the Northern Chihuahuan Desert.

1.2 STABLE WATER ISOTOPES AS A VEGETATION WATER SOURCE TRACER

Stable isotopes of hydrogen (δ^2H) and oxygen ($\delta^{18}O$) have been used as a diagnostic tool in ecohydrological studies aimed to decipher the temporal, spatial, and partitioning patterns of plant water sourcing (Walker and Richardson, 1991; Wu et al, 2019; McCole and Stern 2007; Szutu and Papuga, 2019; Sohel et al 2021). Soil water is under most situations the only source of water for plants in arid and semi-arid ecosystems where groundwater too deep or too difficult to access. Soil water undergoes variations in δ^2H and $\delta^{18}O$ isotopic composition due to mixing, evaporation, and precipitation (Figure 1) of isotopically different water throughout the year. During the winter season, precipitation events deliver isotopically depleted (δ^2H and $\delta^{18}O$) moisture into the soil and during summer, monsoonal precipitation is isotopically enriched. This moisture is pushed down into the soil profile and mixed with existing soil water or evaporates within the topsoil. The arrows represent biotic and abiotic flow paths of water. The rooting depths of vegetation demonstrate their ability to reach for resources within differing soil profiles. On the other hand, plant xylem water is typically an isotopic mixture of different water source pools from recent precipitation, groundwater (where available to plants), and soil water retained tightly on soil pores from previous rain events. Because δ^2H and $\delta^{18}O$ values found in soil water can be linearly correlated they can reveal the amount of isotopic enrichment attributed to evaporation. However, hydrogen and oxygen do not undergo fractionation during the plant water uptake process, so it can be assumed it resembles the isotopic signature of its source (Ehleringer and Dawson, 1992; Brunel et al. 1995, Dawson et al., 2002). In this research we will look into landscape position, soil texture and vegetation competition to better understand plant water sourcing for the dominant species in the Chihuahuan Desert.

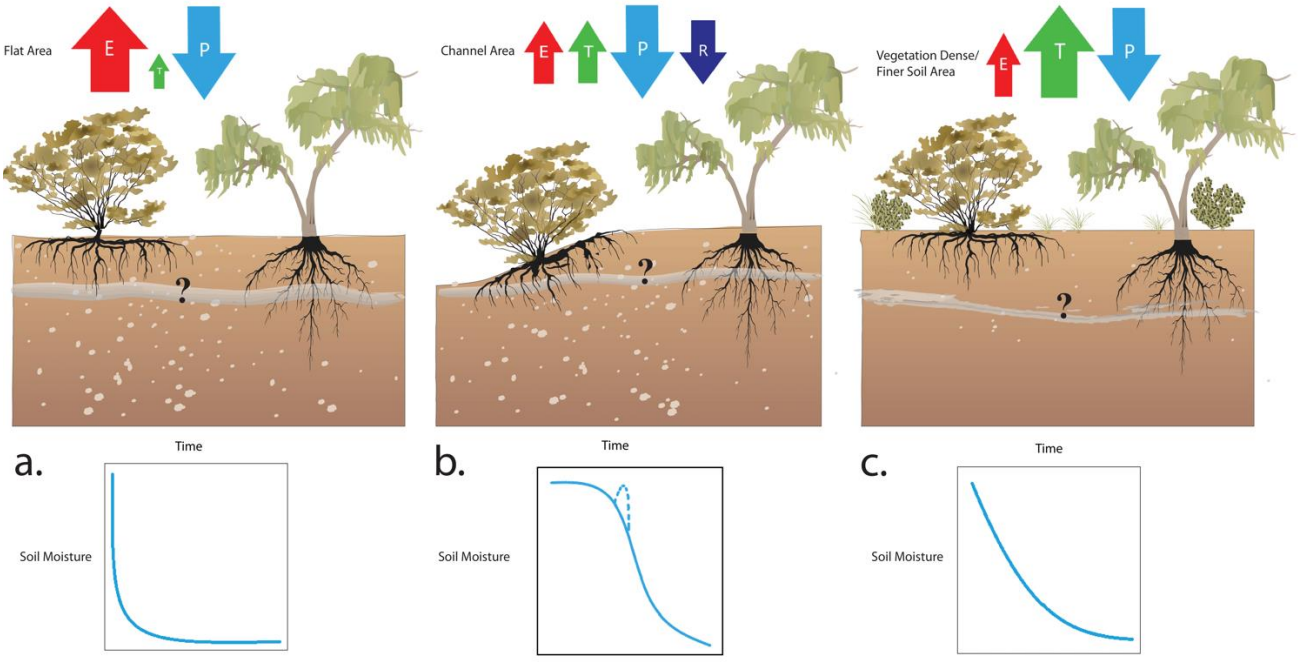

Figure 2: Illustration of hypothetical plant activity and soil moisture residence dynamics within the study sites. The arrows represent water fluxes: E- Evaporation, T-Transpiration. P-Precipitation. R-Runoff. The flat area (FA) is expected to have high evaporation, low transpiration resulting in quickly dissipating soil moisture. The channel area (CA) predictions are similar evaporation and transpiration ratios with slower to dissipate soil moisture with occasional stream flow (dashed line). The two vegetation-dense/finer soil (VD/FS) areas are expected to contain low evaporation and high transpiration ratios and longer soil moisture residence time.

1.3 SOIL TEXTURE INFLUENCE ON WATER SOURCING

Desert ecosystems are known to have high spatial heterogeneity in vegetation composition that is possibly mediated by differences in available moisture in the soil (Duniway et al., 2018). Variability in plant available soil water affects plant community composition (in water scarce environments), productivity, and resilience (Duniway et al., 2018; Osakabe et al., 2014). We examined differences in water uptake from different depths and soil textures for the four desert plant species at the JER. Soil texture can determine how soil moisture is available to plants by affecting infiltration, depth of moisture storage, and moisture residence times (Noy-Meir, 1973; Hamerlynck et al., 2000). For instance, high sand and rock content allow water to percolate deeper into the soil due to its high hydraulic conductivity properties (Duniway et al., 2018) and clay

increases moisture retention and has lower water conductivity (Hamerlynck et al., 2000). Therefore, surficial soil texture can influence soil moisture residence times, potentially extending or shortening the periods of time under which plants can use source water and directly affecting their water sourcing strategies (Figure 2). Our expectations are that soil texture in the shallow profile will affect the type of water sourced by the grasses and shrubs.

1.4 VEGETATION COMPETITION INFLUENCE ON WATER SOURCING

Vegetation competition among plant species occurs when resources are scarce and can lead to limitation in plant growth, survival, and reproduction (Vilà and Sardans, 1999). This competition only occurs if a resource is available in limited quantities, such as water in desert environments. Soil water availability is a major component of the competition between vegetation species and it occurs in the rooting zones of neighboring plant species that share a space (Picon-Cochard, 2001b). Root distribution in the soil profile, root water uptake capacity, and water-use efficiency determines the success of these desert species (Xu and Li., 2006; Grossnickle, 2012). For example, shrubs monopolizes soil moisture and nutrients once established leading to the displacing of other species (Barrow et al., 1996). Dense canopy cover also leads to less evaporation of soil water due to the shade created by vegetation on the soil surface. This shielding from direct sunlight helps maintaining a cooler microclimate relative to that of exposed soils.

Stable water isotopes are commonly used to determine the source of water used by plants constrained by competition (Dawson 1993, Weltzin and McPherson 1997; Picon-Cochard et al., 2001). The water source can be identified by analyzing the isotopes within the xylems of the four vegetation species, considering there is no fractionation during the root water-uptake of plants. In addition, there is a vertical gradient of the soil water istopic signature that occurs during soil moisture replenishment from precipitation and evaporation near the soil surface resulting in an enriched topsoil (Figure 1).

1.5 LANDSCAPE INFLUENCE ON WATER SOURCING

To a large extent, landscape position determines the hydrologic dynamics of a site by favoring or restricting the accumulation and storage of water and the production of runoff as well as the frequency with which that water would flow into and out of an area when available (Duniway et al., 2018). These hydrologic dynamics will in turn determine the soil moisture residence times and therefore the temporal availability of water for vegetation (Duniway et al., 2018). For example, many channel beds of ephemeral arroyos in the piedmonts of Jornada are made of stage V (i.e. highly indurated and impermeable) caliche layers that are thought to aid in the transport of runoff after a precipitation event. I hypothesize that the soils along the banks of those channels exchange moisture with water that is transported from upstream (Figure 2) when a large enough rainfall generates runoff events. Upon initial observation, this site contains greater vegetation cover in comparison to the flatter area, despite their close proximity (100 m). Greater vegetation cover suggests more water availability to support their growth and productivity (Osakabe et al., 2014). Previous studies (Thompson et al., 2020) have demonstrated that the sites within or right next to the channels have a wider range of δ^2H and $\delta^{18}O$ in the soil water compared to soils in higher elevated flat areas. The wider range of isotopic signatures suggests a differing water source infiltrating the soils on the channel banks.

1.6 IMPORTANCE

Plant water uptake is an important element to the global hydrological cycle considering transpiration accounts for >60% of global terrestrial evapotranspiration (Oki and Kanae, 2006). Understanding these key ecohydrological processes of desert plant species can also help us better understand biogeochemical cycling (Schimel et al. 2001), ecosystem productivity (Huenneke et al., 2002), and woody plant encroachment (Grover and Musick, 1990) within the Chihuahuan Desert. In turn, the water uptake patterns of plants that are capable of thriving under extreme arid

conditions can better inform their active role in mediating the hydrological processes at the soil-vegetation-atmosphere continuum for large swaths of lands to improve land management and ecosystem preservation and restoration activities under a changing climate.

1.7 OBJECTIVES

In summary, the objectives of this study were to: (1) determine if the topsoil layer (0-20 cm depth) holds water for plant water use throughout their growing season, or if they switch their water source to deeper water sources, (2) demonstrate if differences in landform in a piedmont affect the source of water available to plants, (3) determine how vegetation competition with finer soil texture and differing canopy cover affect water sourcing of four different desert species, (4) evaluate the degree of isotopic mixing within the 0-10 cm and 10-20 cm soil on a temporal scale. Addressing these study questions will allow us to understand water sourcing strategies and annual patters of water-use for desert species residing in the Northern Chihuahuan Desert.

CHAPTER 2: METHODS

2.1 SITE DESCRIPTION

The study site is located within the United States Department of Agriculture/Agricultural Research Service Jornada Experimental Range (JER) in Southern New Mexico. The Jornada Experimental Range (783 km^2) is located 37 km to the northeast of Las Cruces, NM on the Jornada del Muerto Plain. It sits in between the Rio Grande floodplain (elevation 1,275 m) on the west and the San Andres Mountains (elevation 3,790 m) on the east. The study was conducted on four distinct sites within the southeastern piedmonts of JER (Figure 3). The first site is within a channelized area (32°35'1.68" N, 106°37'58.80" W), the second site is in a higher elevated, flat area (32°34'59.88" N, 106°37'55.20" W), and two others are within large drainage, low-lying areas showing substantially denser vegetation cover and finer soils than the surrounding terrain (1: 32°35'3.29" N, 106°37'57.20" W, and 2: 32°35'7.25" N, 106°37'55.49" W).

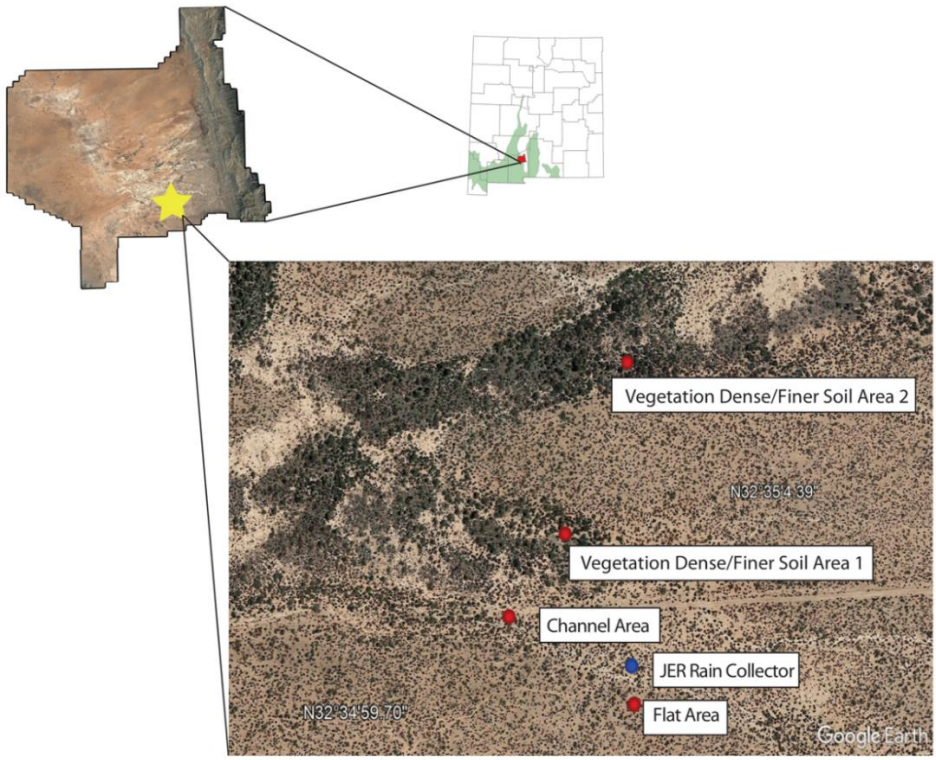

Figure 3: Map of the study area. (a) State of New Mexico (white), Chihuahuan Desert (green), and the Jornada Experimental Range (red). (b) Outline of the Jornada Experimental Range with the study area marked with a yellow star. (c) Satellite view of the three sites.

In the past 100-150 years, a succession of grasslands to woody shrub species have taken place, effectively changing the ecosystem. Vegetation surveys from the 1850s showed there was abundant grass cover and low-density isolated patches of shrub cover in the JER (Drewa and Havstad, 2001; Gibbens et al. 2005). However, there has been a dramatic shift in vegetation species from grass to shrubs. Desert plant species such as mesquite, creosote, and tarbush have colonized the region to become the most abundant plants in the JER (Gibbens et al. 2005). A changing climate, reduced fire frequency, and over grazing have been cited as the main factors for the replacement of grasses and the conversion from grassland to shrubland in JER (Drewa and Havstad, 2001; Gibbens et al. 2005; Caracciolo et al., 2016).

The Jornada Experimental Range experiences frequent sunshine, low relative humidity, large daily temperature ranges, and irregular precipitation both spatially and temporally (Gibbens et al 2005). This region has an average of 245.1 mm/year of precipitation bimodally distributed with the largest amount occurring between July and October during the north American monsoon (Douglas et al., 1993), and with a second peak in November to February (Wainwright, J., 2006). There are some years in which the monsoonal rains begin mid-June. Summer monsoonal precipitation originates in the tropical region of the Pacific, whereas the winter, frontal storms originate on the northern part of the Pacific Ocean (Wainwright, J., 2006). The mean annual temperature is 14.70 °C, with a mean annual minimum temperature of 4.7 °C and a mean annual maximum temperature of 24.7 °C.

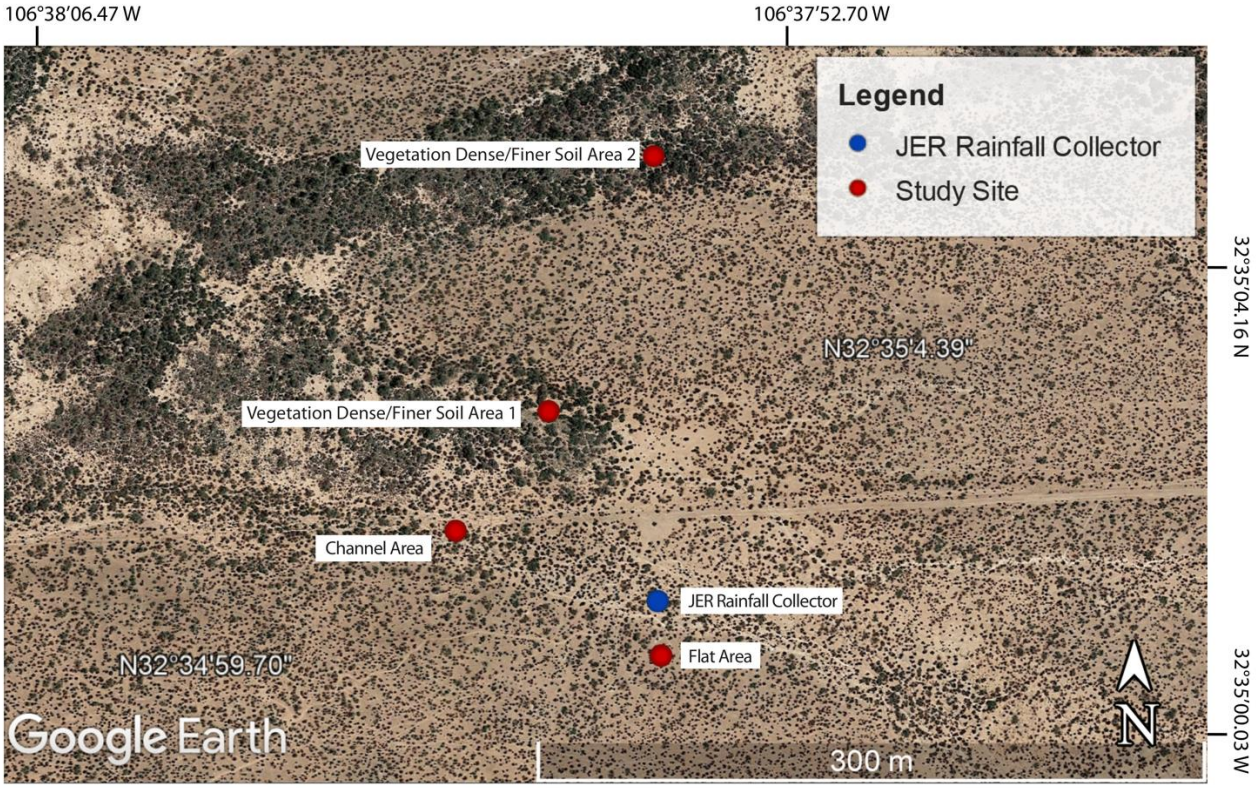

Figure 4: Satellite image of the sampling locations within the JER. The four sites are marked in red and the rain collector is marked in blue. The channel area (CA) is located on a low-lying, ephemeral channel (32°35'1.68" N, 106°37'58.80" W). The flat area (FA) is located on a higher, elevated flat area (32°34'59.88" N, 106°37'55.20" W). The vegetation dense/finer soil area 1 is located within a vegetation dense area with finer soil texture (32°35'3.29" N, 106°37'57.20" W). The vegetation dense/finer soil (VD/FS) area 2 is also located within a vegetation dense area with finer soil texture relative to the channel and flat area (32°35'7.25" N, 106°37'55.49" W).

The JER is located within an intermountain basin with no external drainage with much of the soil originating from fluvial material deposited by the ancestral Rio Grande (Gibbens and Lenz, 2001). Deposition of calcareous dust that is later transported with infiltrating water into the soil profile has promoted the formation of a calcium carbonate horizon ($CaCO_3$) also known as caliche over time (Gibbens and Lenz, 2001). The depth of this caliche reflects the varying average depths of infiltration fronts in the soil and therefore it varies between the study sites, with the caliche horizon in the flat area (FA) being deeper than in the channel area (CA). In the study area, the caliche horizon is frequently exposed in the channels of ephemeral arroyos, forming the channel

beds where runoff is transported. The depth at which the caliche is found in the vegetation dense/finer soil (VD/FS) sites is unknown. The four sites are located on piedmont terrain (Figure 4), at the leading edge of an alluvial fan which sediments originated from Paleozoic limestones (Monger et al., 2006). Soils on the four study sites are considered to be part of the Middle Tank Gravelly category, with a general gravelly sandy loam texture (Monger et al., 2006).

2.2 SAMPLE COLLECTION FOR ISOTOPIC ANALYSIS OF VEGETATION, SOIL AND RAINFALL WATER

Water samples for isotopic analysis were obtained from vegetation stems, soil, and precipitation in the study site at the JER. Precipitation samples were obtained from a rainfall collector buried in the ground collecting water through a funnel that sticks out of the surface and trickles down to a 50 mL centrifuge tube that contains mineral oil to prevent evaporation. When collected, rainfall samples were capped, wrapped in Parafilm and placed in a cooler with ice until transported to the laboratory where they are placed inside a fridge. In this study, two rainfall collectors were used to obtain the local meteoric water line, the JER rainfall collector is located 20-200 meters from the four study sites and a second collector is located at the University of Texas at El Paso (UTEP) outside of the Earth, Environmental and Resource Sciences department (90 km from study site). Sampling of vegetation water was conducted from a total of 17 individual plants: Four from the channel area (two creosote and two mesquite samples), four from the flat area (two creosote and two mesquite sample samples), and eight from the vegetation dense/finer soil area (two creosote, two mesquite, two tarbush, and two grass samples). The procedure to collect the stem samples was to cut a healthy-looking twig with a diameter of 0.2 to 0.5 cm and length of 5-8 cm with gardening shears. The samples are then wrapped in Parafilm and stored in a Ziplock bag, placed in a cooler with ice packs for their transport to the laboratory. This process is repeated for each plant specimen sampled at each study site. Soil samples were collected using a small shovel

to dig a soil pit for different depths. The first sample was taken at 0-10 cm in depth and the second at 10-20 cm, right below the first. Soil samples were placed in crystal containers of 100 g capacity. Each container was filled to the top and its lid sealed with parafilm and placed in cooler for their transport to the laboratory. Precipitation, vegetation, and soil samples were collected bi-weekly when possible and monthly at the least. Due to the proximity of the UTEP rainfall collector, precipitation samples were more frequently collected at that location. All samples were stored in a refrigerated environment in the Ecohydrology Lab at the University of Texas at El Paso until analyzed. A detailed protocol for the collection of samples is provided in Appendix A.

2.3 MICROMETEORLOGICAL DATA

Precipitation, air temperature, and vapor pressure deficit data were obtained from both the Systems Ecology Laboratory's (SEL) and Ecohydrology Lab meteorological instrument network located at the JER. The SEL tower is located at 32°34'55.05 N, 106°38'6.04 W, about 300-500 meters away from the two study sites (Figure 5). The Ecohydrology Lab tower is located at 32°35'0.55 N, 106°37'41.08 W, about 400-450 meters away from the study sites. The data from these two towers were combined for a more complete dataset, due to there being gaps in the timeseries and incorrect values. Air temperature and relative humidity was measured in degrees Celsius (°C) and percent, respectively, using a Vaisala HMP probe HMP45C at the SEL tower and a Vaisala HMP155 at the Ecohydrology Lab's tower. Vapor pressure deficit was obtained from relative humidity and air temperature calculations and was processed with ReddyProc in R. Precipitation data (mm) was obtained using two Texas tipping bucket rain gauges (TE525, Campbell Scientific) at the SEL tower.

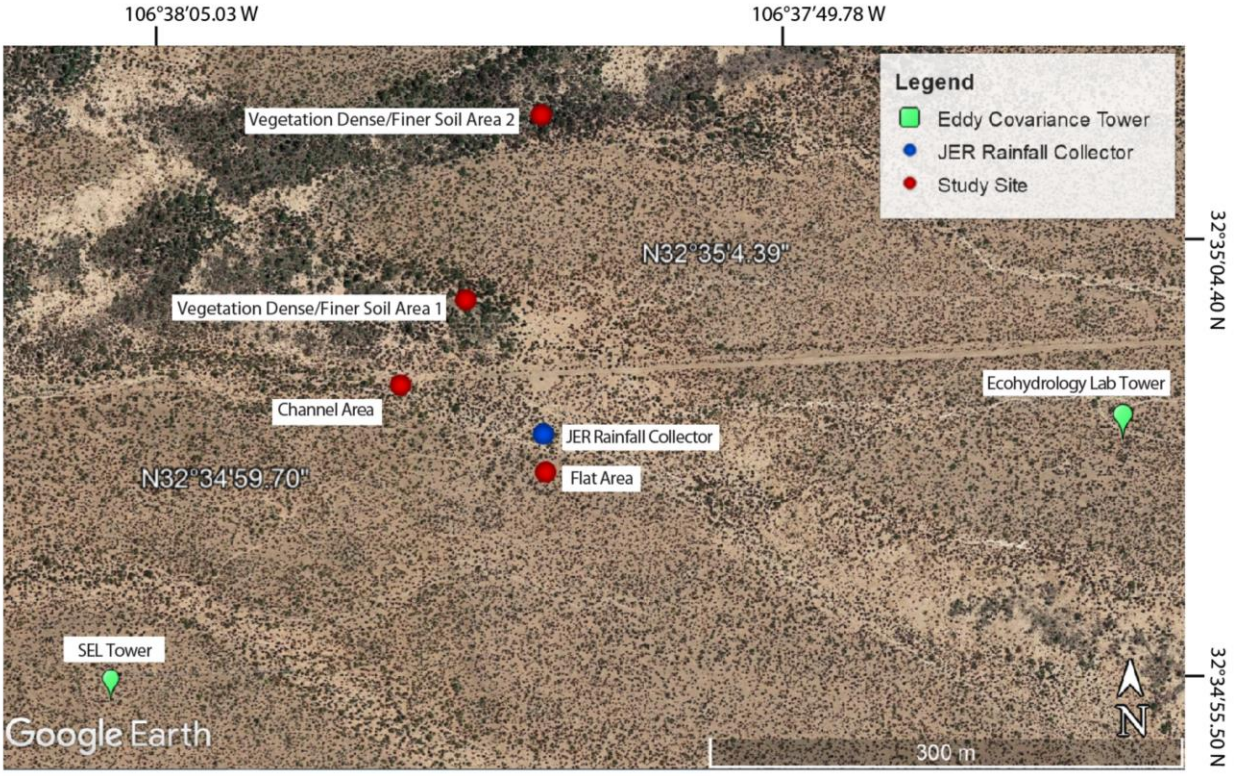

Figure 5: Satellite image of the eddy covariance towers relative to the study sites. The Systems Ecohydrology Laboratory's (SEL) moisture and meteorological instrument network and ecohydrology lab tower (green), study sites (red), and the JER rainfall collector (blue) at the Jornada Experimental Range (JER).

2.4 WATER EXTRACTION FROM VEGETATION AND SOIL SAMPLES

A cryogenic vacuum extraction system was assembled for the purpose of extracting water from plant stems (Figure 6). This system was used to extract water from stems collected from May 16, 2019 through October 2, 2021. This method is capable of extracting water from plants and soil without isotopic fractionation of the water at a transfer rate of ~98% (Araguas-Araguas et al, 1995; West et al, 2006). This set up consists of an Edwards Vacuum Pump, Fisherbrand Isotemp Digital Block Heaters, glass assembly with vacuum valve, stainless steel cold trap, laboraratory jacks, laboratory stand, and PolyScience immersion probe cooler (Figure 6). The cryogenic vacuum distillation method works by fully evaporating the water from the sample by heating it in the sample tube at 100 °C and then trapping the vapor in a collection tube with a temperature of ~-50 °C. The heat is produced through a heating block that is in contact with the sample tube and the

trapping is done by freezing the water vapor in a collection tube submerged in an immersion cooler with isopropyl alcohol at -50 °C. The vegetation samples were prepared by sectioning them into 1 cm long pieces with gardening shears and placing them in a glass assembly with a vacuum valve. A thin piece of glass wool (diameter of the glass vial) is placed on top of the stem sample to to keep stems from floating in the glass assembly. The glass assembly contains a cock valve, glass tube (connecting the sample tube and trapping tube), screw joints, quartz wool, a trapping and a sample tube (See Appendix B for details). This glass assembly is effective in maintaining the vacuum throughout the distillation process. It is critical to conduct a leak test with the vacuum pump prior to proceeding with the distillation to ensure an almost complete vacuum. Once the vacuum is induced within the glass assembly, we place the sample tube in the block heater and the collection tube in the cold bath to distil for two hours at 100 °C. When distillation is completed, the vegetation samples were removed from the instrument to thaw for 10-15 minutes. Then, water samples were sealed and stored in a refrigerated environment until analyzed for hydrogen (δ^2H) and oxygen ($\delta^{18}O$). Vacuum distillation methods are highly effective to avoid condensation of water while exposed to heating (West et al, 2006). See Appendix B for a detailed protocol for conducting cryogenic vacuum extractions and processing of liquid water samples.

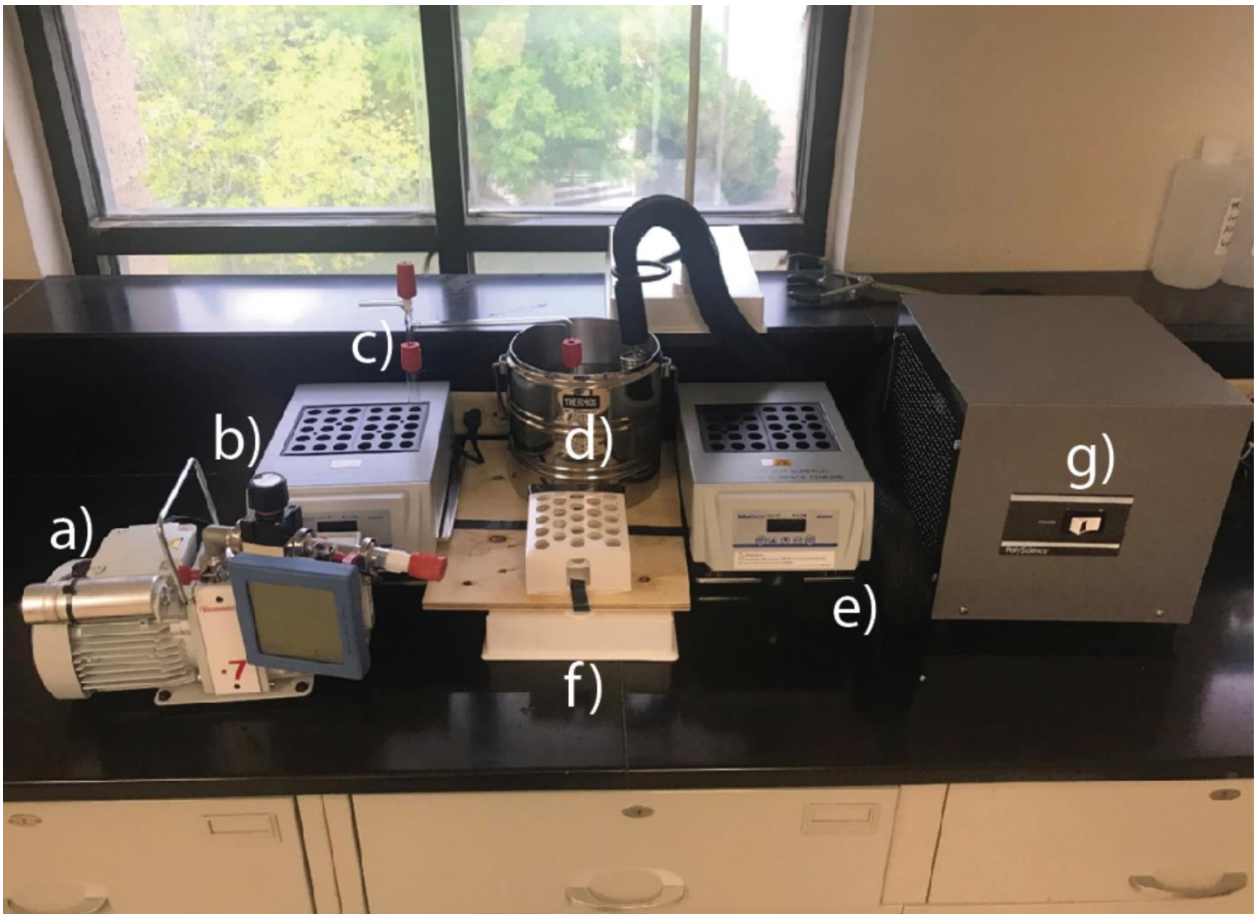

Figure 6: Cryogenic vacuum extraction line for vacuum distillation of plant samples for isotopic analysis. a) Edwards Vacuum Pump, b) Fisherbrand Isotemp Digital Block Heaters, c) Glass assembly with vacuum valve, d) stainless steel cold trap, e) laboraratory jacks, f) laboratory stand, and g) PolyScience immersion probe cooler.

2.5 STABLE WATER ISOTOPE ANALYSIS

All isotopic measurements were made using a wavelength-scanned cavity ring-down spectroscopy analyzer (Picarro L2130-i). The stable isotope composition of water (^{18}O and ^{2}H) is presented as delta (δ) values in units of per mill (‰), where $\delta = ((R_{sample}/R_{standard}) - 1) \times 1000$. Samples and standards are the isotope ratios of $^{2}H/^{1}H$ and $^{18}O/^{16}O$ and used the international standard Vienna Standard Mean Oceanic Water (VSMOW). There were soil, stem and precipitation samples analyzed from October 2018 through October 2021. The analyzer is equipped with two attachments, an induction module and a vaporizer module with an autosampler. Soil samples were analyzed with the Picarro L2130-i paired with the induction module (IM-

CRDS). The induction module is used for isotopic analysis of matrix-bound water and was used to extract the water from the soil. The soil samples are prepared by pouring soil into 3.3 mm (internal diameter) metal sample tubes and filling both ends with quartz wool to secure the soil in place. The sample is placed in a 4 mL glass vial and inserted into the induction module where a metal needle heats the sample to more than 100 °C and the resulting vapor is injected in to the L2130-i. For each soil sample 5 repetitions are carried.

For the vegetation samples, and due to the high volatile organic compounds (VOCs) content of some stems, plant water extraction and processing was performed using a two step process: 1) first a cryogenic vacuum extraction system was installed to obtain liquid stem samples, then 2) the extracted liquid samples were run through the IM-CRDS and fed into the L2130-i. The first step reduces the presence of VOCs in the distilled water extracted water and the second step eliminates any remnants of VOCs in the water samples by passing the sample through a Micro-Combustion Cartridge filtering the VOCs through oxidation (to CO_2) (Johnson et al, 2017). To do this, liquid stem water is placed on glass microfiber filter paper and secured with a metal strip. The metal strip with the sample is placed in a 4 mL glass vial and inserted into the induction module to conduct 6 repetitions.

Water samples from precipitation obtained with the rainfall collectors were analyzed using the Picarro L2130-i with the vaporization module A0211 connected to an autosampler. The samples were analyzed under the 'high precision' setting with 7 sample repetitions. Samples collected from JER and UTEP must have the mineral oil and soil filtered out using a syringe and a 45 µm filter. Once filtered, samples were placed in 2 mL glass vials with a septa cap where the robotic arm of the autosampler would extract the liquid water and inject it in the vaporizer working at 110 °C to be delivered as water vapor into the L2130-i.

2.6 SOIL TEXTURE ANALYSES AT EACH SAMPLING LOCATION

Soil texture analyses for each study site location were performed to verify differences in the shallow soil properties on these sites. Sampling for soil texture analysis was done by obtaining two soil samples from the four study sites at the JER. We utilized a gardening shovel, ziplock bags, and a ruler to obtain at least 100 g of soil at 10 cm and 20 cm from the surface. The soil samples were done 1-3 m away from the vegetation sampled throughout the study. These samples are then taken to the lab for sieving and PARIO analysis. To prepare for analysis, 50 g of the soil samples must have salts flushed out with distilled water (Note: There is no need to flush out organics since the research sites have very low organic content in the soil). When the soil is dry, it is placed in a 1 L bottle with distilled water and Natriumhexametaphosphate ($Na_6O_{18}P_6$) to be placed in a shaker. The sample is then placed in the PARIO (Durner et al., 2017), an instrument that records soil suspension pressure. This instrument is connected to a computer-based automated integral suspension pressure method through the PARIO software. Another 50 g of soil are sieved to obtain coarse percentage data to input into the PARIO user interface to obtain a textural triangle. See Appendix B for a detailed protocol for preparing soil samples for analysis, sieving, and operating the PARIO instrument.

2.7 VEGETATION COVER ANALYSES AT EACH SAMPLING LOCATION

Vegetation cover estimates were obtained for each sampling location to provide quantitative-based evidence of the differences on canopy cover among the sites using the Canfield Line Intercept method (Canfield, 1941). The line intercept method was developed by Canfield in 1941 to estimate vegetation canopy cover and species composition (Canfield, 1941). The method was applied by extending a measuring tape 40 m in length across each of the four study sites (Figure 7). Three parallel transects were conducted for each site (each transect collocated 5 m apart). The objective of this method is to identify plants, or lack thereof, that intercept the

measuring tape and record that distance. Vegetation cover was calculated by adding the intercept distances and calculating the total as a proportion of the measuring tape length. The values were multiplied by 100 to convert the unit into a percentage (%). For the purposes of this project, we took note of bare soil, creosote, honey mesquite, tarbush, and grass. The differing species of the family Poaceae were grouped into one category called ‘grass’.

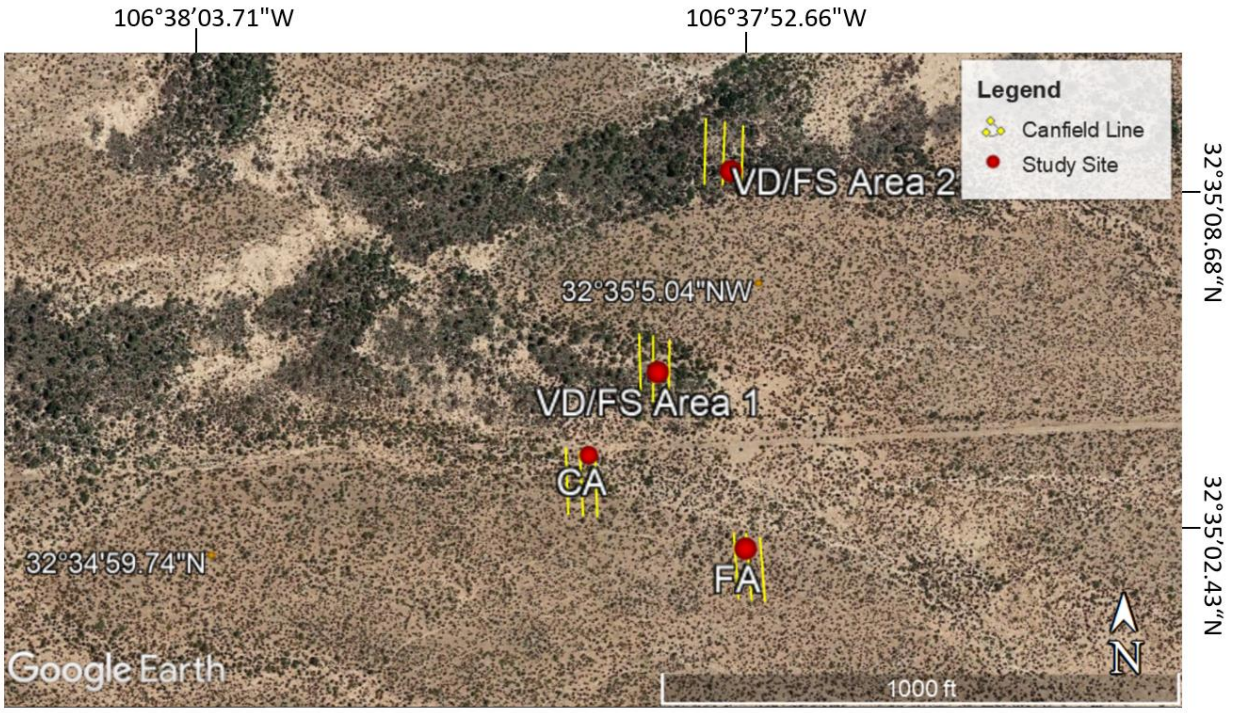

Figure 7: Satellite image of the Canfield line intercept survey done at the four study sites. The red lines represent the study location and the yellow lines indicate where the Canfield line intercept survey was completed.

CHAPTER 3: RESULTS

3.1 HYDROLOGICAL CONDITIONS

3.1.1 Precipitation

Precipitation and air temperature data was obtained from two nearby eddy covariance towers (<100 m) from the study sites from January 2018 through October 2021. Precipitation can occur throughout the year but has a seasonal pattern, similar to air temperature (Figure 8). The monsoon season occurs July through October and coincides with the highest temperatures. There are relatively smaller precipitation events during the fall and winter seasons. The total precipitation during the study period was 726.2 mm from October 2018 through November 2021. The 381.3 mm (52.5 %) of rain occurred during the monsoon season (July-October) and 344.9 mm (47.5 %) occurred during the dry season (November-June). The data gaps in the precipitation and air temperature are due to instrument malfunction.

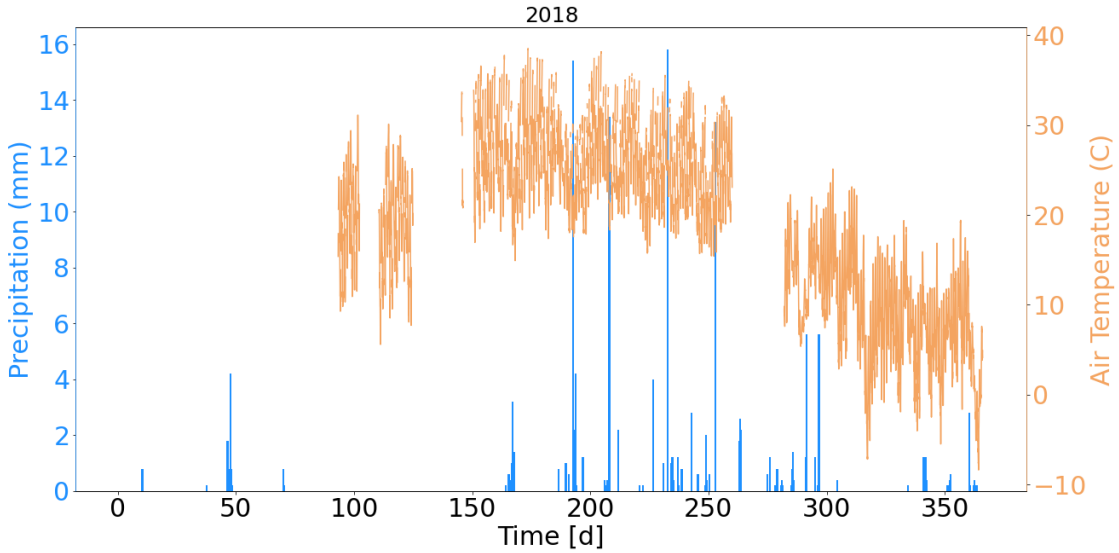

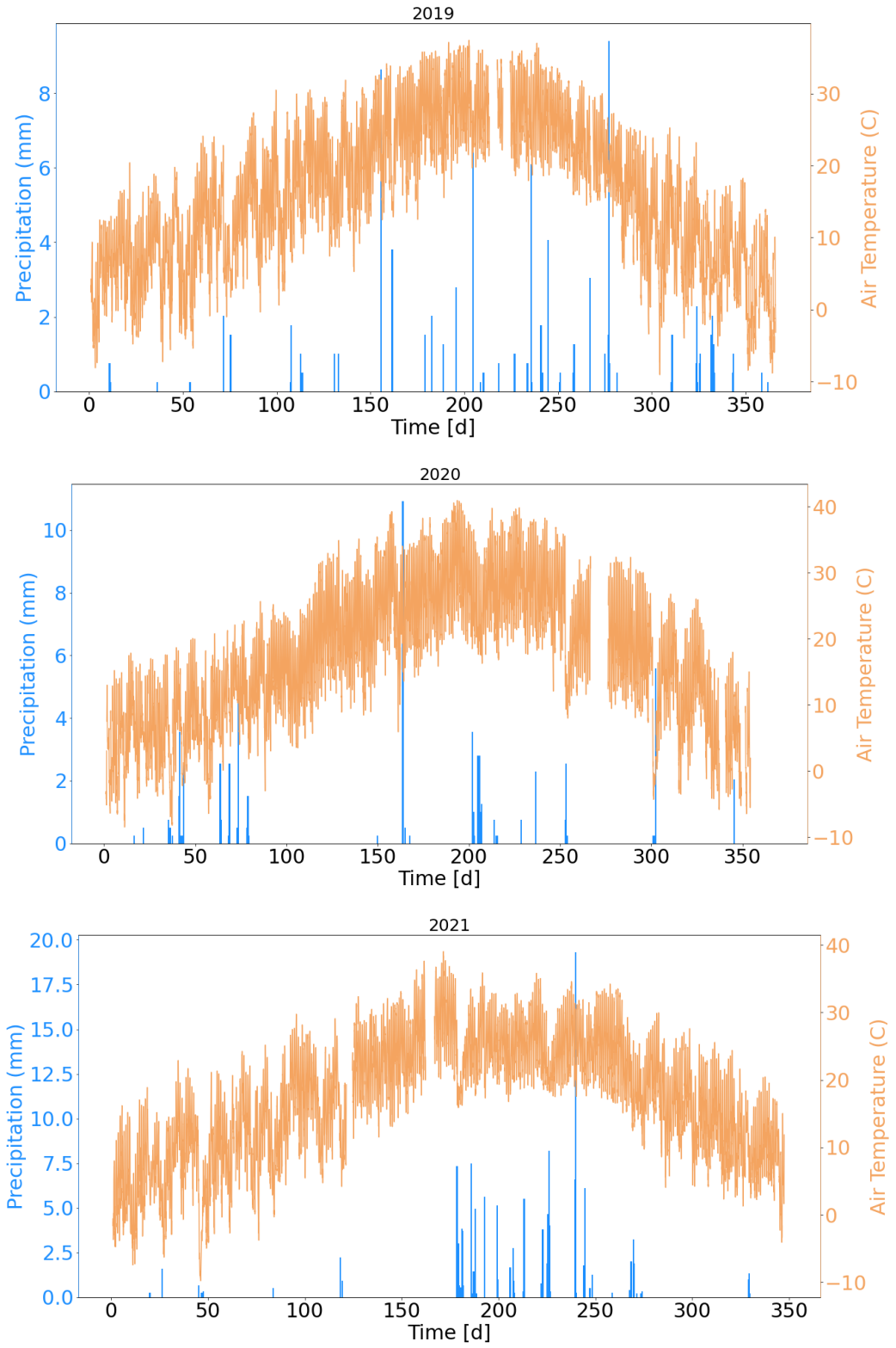

Figure 8: Half hourly precipitation (mm) and air temperature (C) at the Jornada Experimental Range during the study period. Data was obtained from the Systems Ecology Laboratory (SEL) and Ecohydrology Lab weather gauges near the study sites.

3.1.2 Vapor Pressure Deficit

Vapor pressure deficit (VPD) was also obtained from two nearby eddy covariance towers (<100 m) from the study sites from January 2018 through November 2021. VPD was calculated utilizing relative humidity and air temperature data from the meteorological instruments. VPD shows a seasonality with the highest values being during the summer season and lowest values during the winter season (Figure 9). That is due to high moisture content and high temperatures during the summer, whereas, winter has low moisture and low temperature conditions. Warmer temperatures raise the saturation vapor pressure, however, humidity remains low in this region. The highest VPD conditions are reached during the months of July-August throughout the study period (average 19.6 hPA). During the summer period, VPD lowers momentarily after precipitation events and rebounds subsequently. The data gaps in precipitation and air temperature are due to instrument malfunction.

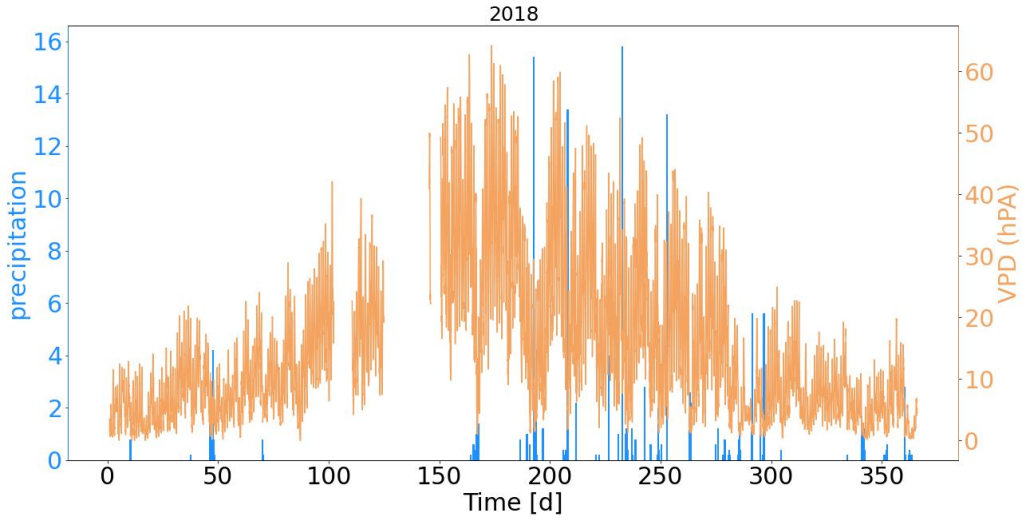

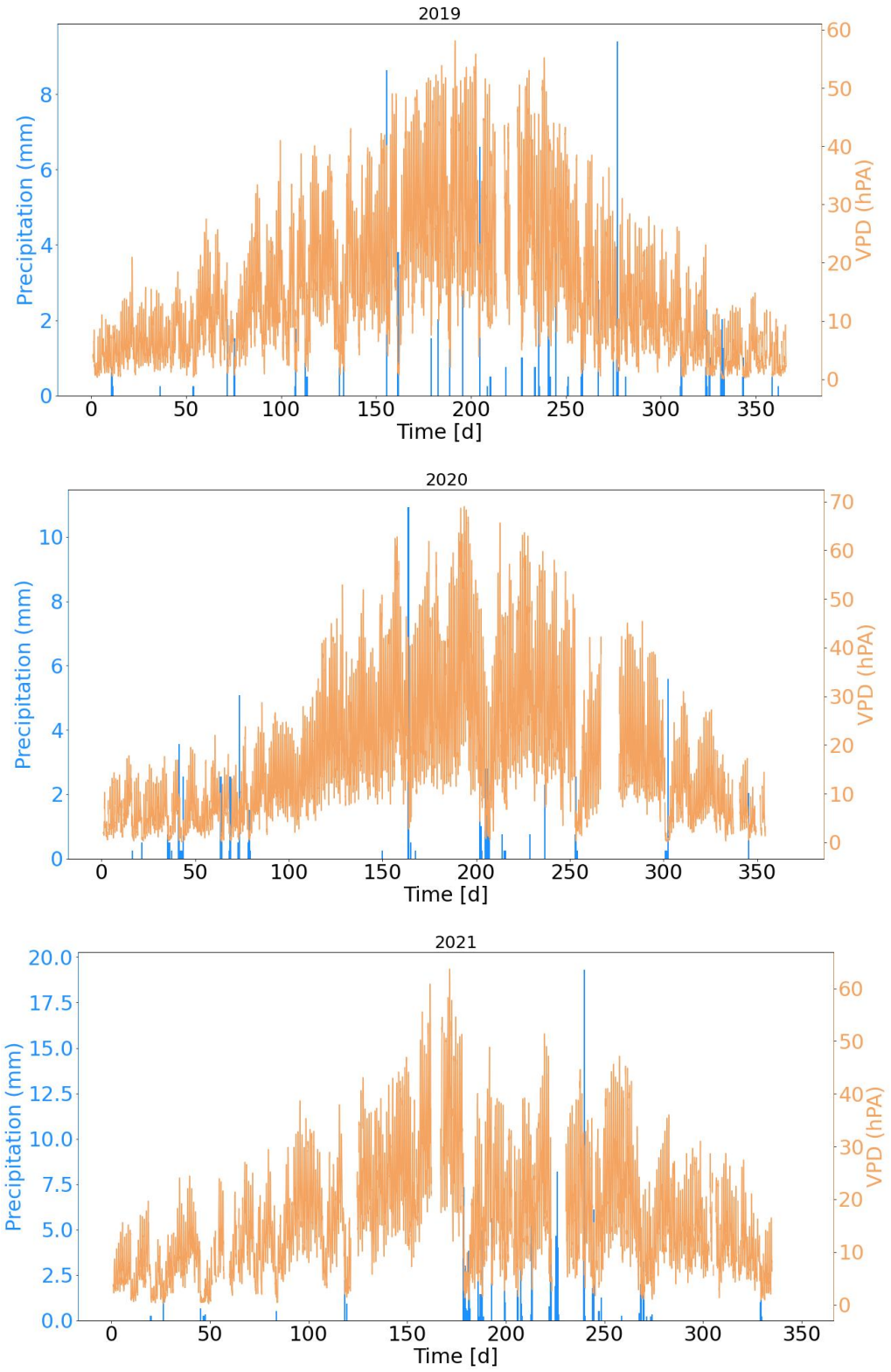

Figure 9: Half-hourly precipitation (mm) and VPD (hPA) at the Jornada Experimental Range during the study period. Data was obtained from the Systems Ecology Laboratory (SEL) and Ecohydrology Lab weather gauges near the study sites.

3.1.3 Cumulative Precipitation

Cumulative precipitation was calculated by summing the precipitation total of a given day with the previous days (Figure 10). This water input is treated as spatially constant throughout the study sites, suggesting that each site received the same quantity. Precipitation was variable throughout the duration of the study. Cumulative precipitation was highest (308.4 mm) in 2018 and lowest in the year 2020 (156.2 mm). The year 2018 was the only year to exceed average precipitation conditions (245.1 mm) in the JER. The year 2020 had the largest increase at the start of the year out of the four years, with ~100 mm of rain during the winter season. The year 2021 had the slowest start for precipitation, with a huge increase occurring during the monsoon season. During the monsoon season, cumulative precipitation increases rapidly and slows down during the dry season. Tipping bucket rain gauge measurements are not precise during intense precipitation events and relatively calm precipitation events.

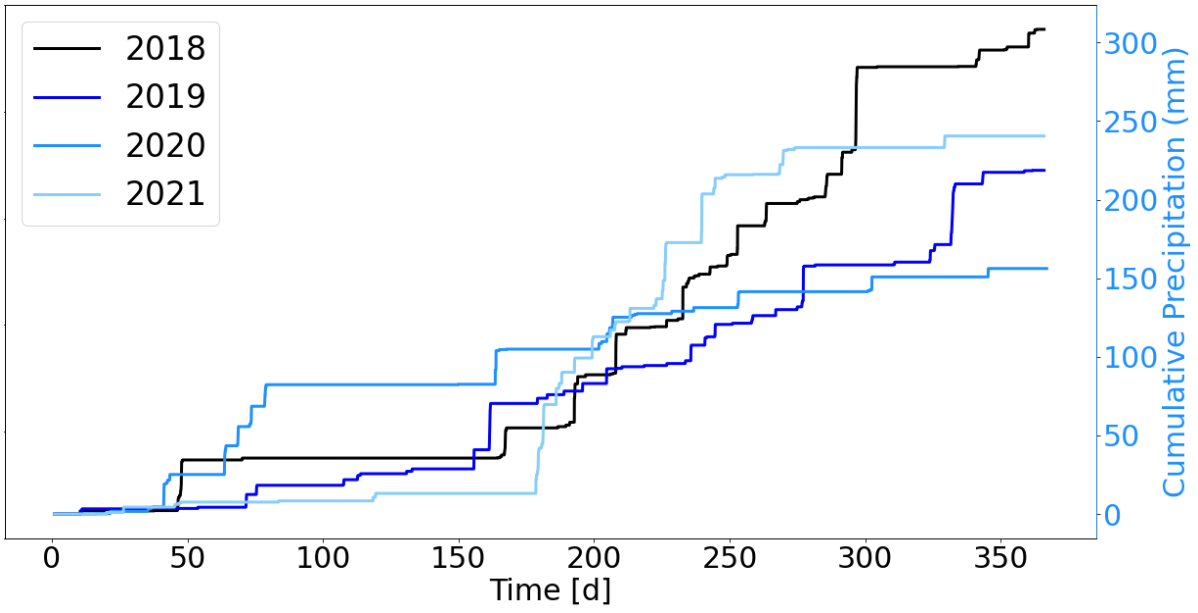

Figure 10: Half hourly precipitation expressed as cumulative precipitation (mm) at the Jornada Experimental Range during the study period. Data was obtained from the Systems Ecology Laboratory (SEL) and Ecohydrology Lab weather gauges near the study sites. Values on the x-axis are expressed in days of the year (365 days for normal years and 366 for leap years) and the y-axis is cumulative precipitation in (mm).

3.2 SOIL TEXTURE ANALYSIS

Soil texture analysis for each site and depth was done using a PARIO instrument. For the analysis, there were two repetitions done for each site and depth. The results for the four study sites were placed on one soil texture triangle (Figure 11). Generally, the soils at all of the study sites proved to be sandy in nature with some variation. Most of the soils at 10 cm at the sites appear to be finer texture than soil at 20 cm from the surface. The soil from the VD/FS Area 2 at 10 cm appears to have the finest soil with the lowest sand content and highest silt content. The soil at the VD/FS area 1 at 10 cm appears to contain the highest sand content out of all the samples and fastest infiltration rate (sandy in texture). Both of the CA and FA soil samples appear to be a sandy loam to sandy clay loam texture.

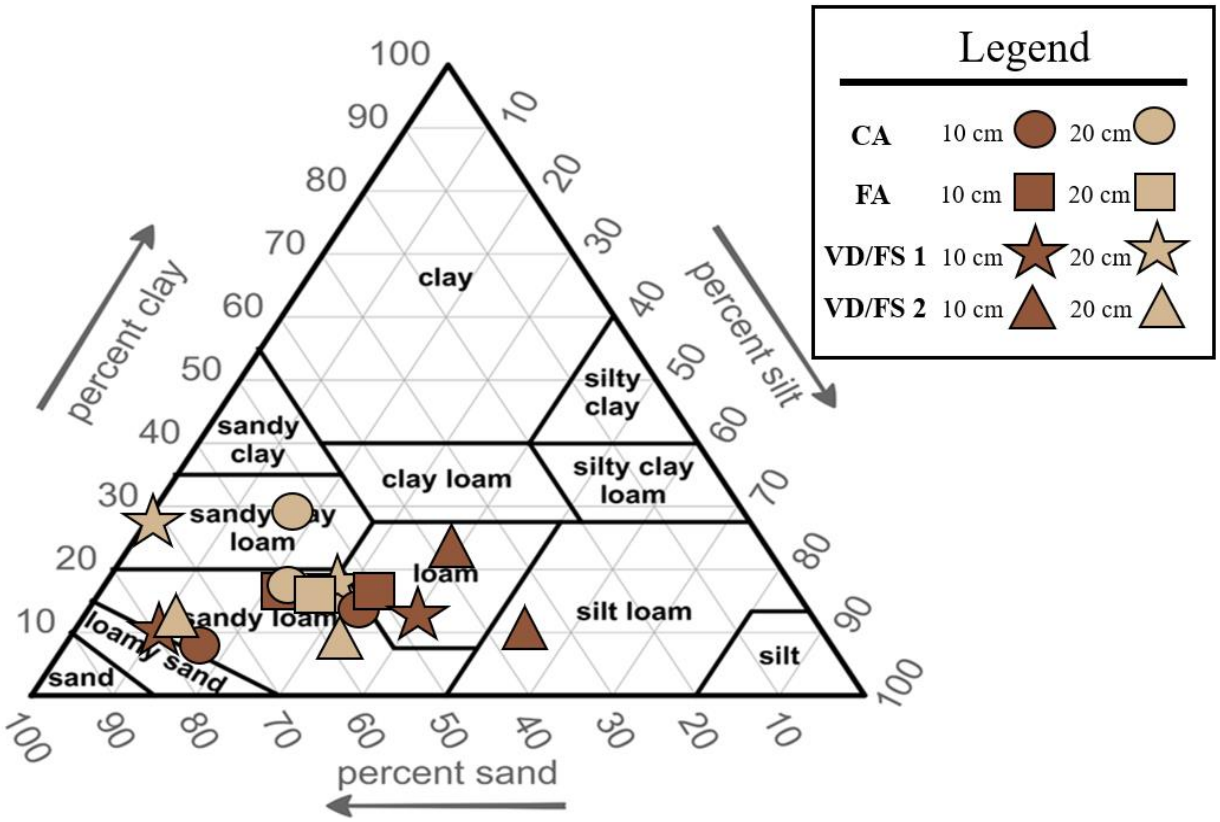

Figure 11: Soil textural triangle containing samples from each site and depth. The shapes represent a different site and the color represent a different depth (10 cm and 20 cm).

3.3 CANFIELD'S LINE INTERCEPT SURVEY

A Canfield line intercept survey was conducted to obtain the density and composition of the vegetation within each site. There were three 40 m long parallel transects conducted at each site. The spacing between the three transects at each respective site was about 5 m in length. The values in the bar graph present the mean of the three canfield surveys within each site (Figure 12). The results reveal the vegetation density or lack of vegetation within the sites. It becomes apparent that the FA has the lowest amount of canopy cover (with a high bare soil area of 63.33%), whereas the VD/FS Area 2 contains the largest amount of canopy cover (with a low bare soil area of 16.33 %). The FA contains the highest amount of creosote (30.83 %), whereas the VD/FS Area 2 contains the lowest quantity (16.33%). The FA is the only area that does not contain tarbush and grass species. The honey mesquite is most abundant in the CA with a canopy cover of 25.83 % and lowest in the VD/FS Area 1 with a cover of 2.91 %.

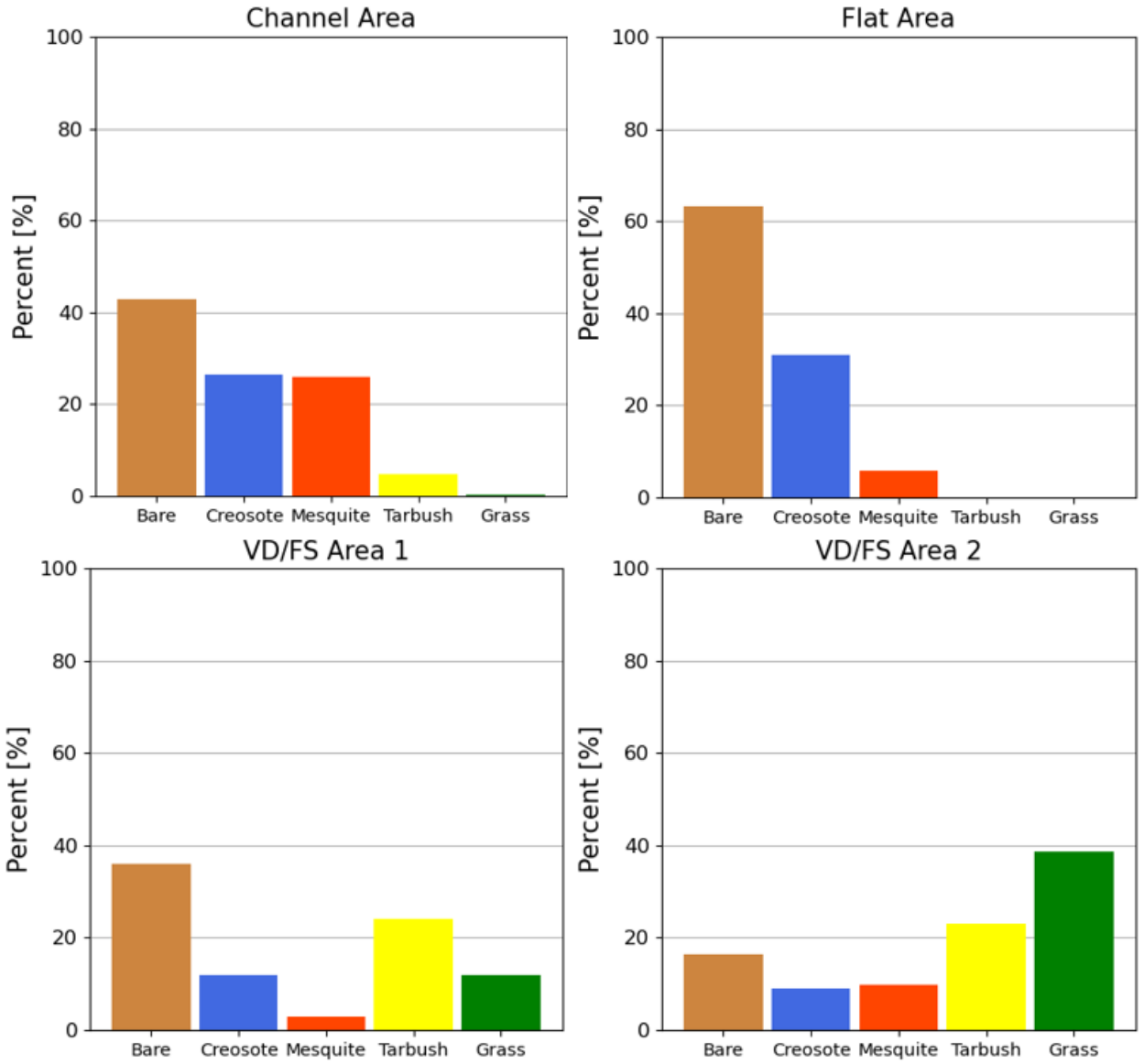

Figure 12: Bar graph containing data from a Canfield's line intercept survey of the vegetation species within the four study sites. The table includes the four sites along with vegetation canopy expressed as a percentage (%).

3.4 STABLE WATER ISOTOPES

3.4.1 Precipitation

There was a total of 57 precipitation samples collected during the study period: 19 precipitation samples collected from a rain collector at JER and 38 collected from UTEP (Figure 13). This contains data for a three year period: the first rain sample was collected in October 2018 and the last in November 2021. There appears to be a seasonal pattern with $\delta^{18}O$ (‰) concentration, with the highest peak during the summer and lowest concentration during winter periods. During the fall and winter periods, $\delta^{18}O$ remains relatively depleted and reaches values as low as -16.88 ‰ in December. Precipitation becomes enriched during the summer period, peaking at 11.00 ‰ in August. The variability in oxygen isotopes (enriched and depleted) throughout the study period is following local precipitation events and the time in which the sample was collected after the event.

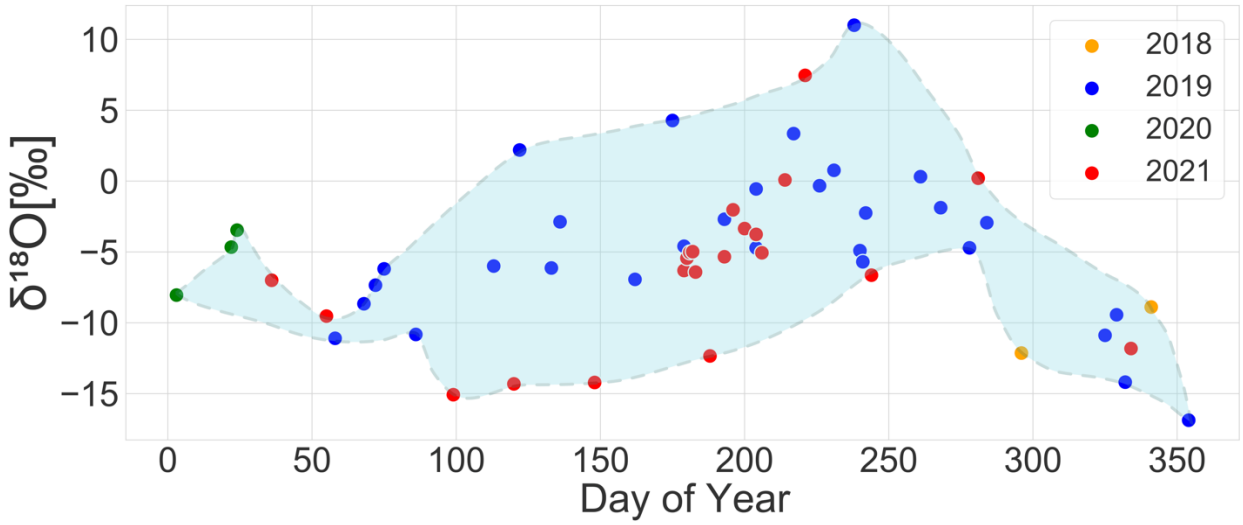

Figure 13: $\delta^{18}O$ (‰) of precipitation samples collected from the years 2018 to 2021. The differing colors represent the year the precipitation was obtained. This data includes samples from both the JER and UTEP rain collectors. Values on the x-axis are expressed in days of the year (365 days for normal years and 366 for leap years) and the y-axis is $\delta^{18}O$ (‰) concentration.

The $\delta^{18}O$ (‰) of rain ranged from -16.88 ‰ to 11.00 ‰ during the study period with an average of $\delta^{18}O$ -5.28 ‰ (TABLE IN APPENDIX C). $\delta^{2}H$ values from rain ranged from -134.17

‰ to 37.36 ‰ with an average of -41.11 ‰ throughout the study. Throughout the monsoon season (July-October), precipitation had an average $\delta^{18}O$ of -2.21 ‰ and -17.55 ‰ of $\delta^{2}H$. Throughout the drier season (November-May), precipitation had an average of -8.05 ‰ for $\delta^{18}O$ and -62.31 ‰ for $\delta^{2}H$. The Global Meteoric Water Line (GMWL) is expressed as a linear regression, which is $\delta^{2}H = 8.0* \delta^{18}O+10$ (Craig, 1961). The Local Meteoric Water Line (LMWL) was determined by local precipitation values, is $\delta^{2}H = 6.4* \delta^{18}O-7.2$ (Figure 14). Climatic and geographic factors result in differences with the LMWL and the GMWL (Craig, 1961).

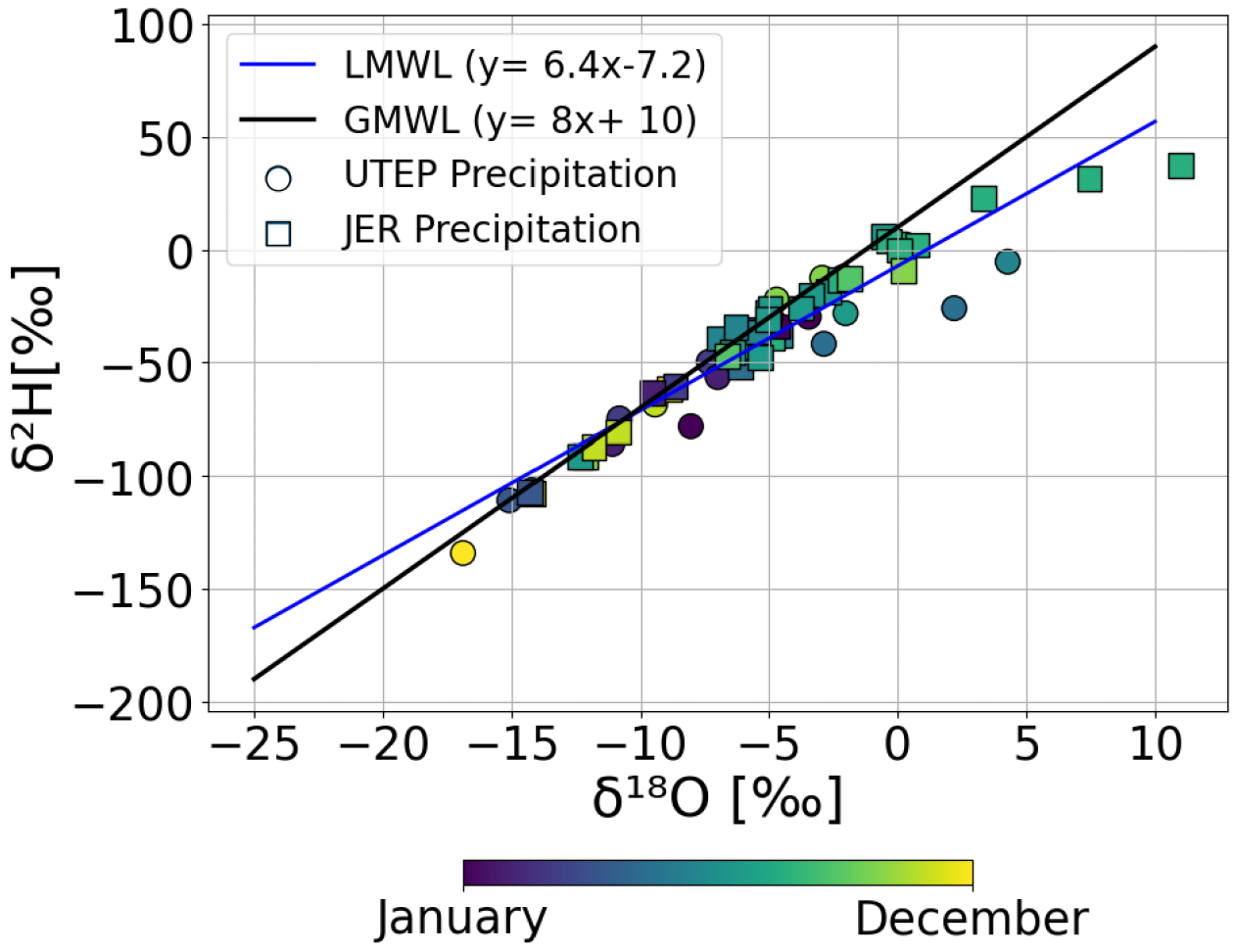

Figure 14: The Global Meteoric Water Line (GMWL) and Local Meteoric Water Line (LMWL). The closed circles represent precipitation collected from the UTEP campus and the open circles were collected from the JER. The colorbar represents the day of the year collected.

3.4.2 Soil Water

There was a total of 207 soil samples collected during the study period: 105 samples from 0-10 cm depth from the surface and 102 samples at 10-20 cm. This contains data for a three year period: the first soil sample was collected in November 2018 and the last in October 2021. The $\delta^{18}O$ (‰) of soil collected at 10 cm ranged from -122.43 ‰ to 4.77 ‰ with an average of -6.34 ‰ and the $\delta^{2}H$ (‰) of soil collected at 10 cm ranged from -115.78 ‰ to -8.70 ‰ with an average of -54.09 ‰. The $\delta^{18}O$ (‰) of soil collected at 20 cm ranged from –16.97 ‰ to 5.28 ‰ with an average of -6.89 ‰ and the $\delta^{2}H$ (‰) of soil collected at 20 cm ranged from -122.43 ‰ to 1.82 ‰ with an average of -55.01 ‰. Soils collected in the CA have an average of $\delta^{18}O$ -6.72 ‰ and $\delta^{2}H$ -55.38 ‰. Soils collected in the FA have an average of $\delta^{18}O$ -5.71 ‰ and $\delta^{2}H$ -53.36 ‰. Soils collected in the VD/FS area 1 have an average of $\delta^{18}O$ -7.17 ‰ and $\delta^{2}H$ -56. 41 ‰ and $\delta^{18}O$ -8.01 ‰ and $\delta^{2}H$ –53.57 ‰ for the VD/FS area 2.

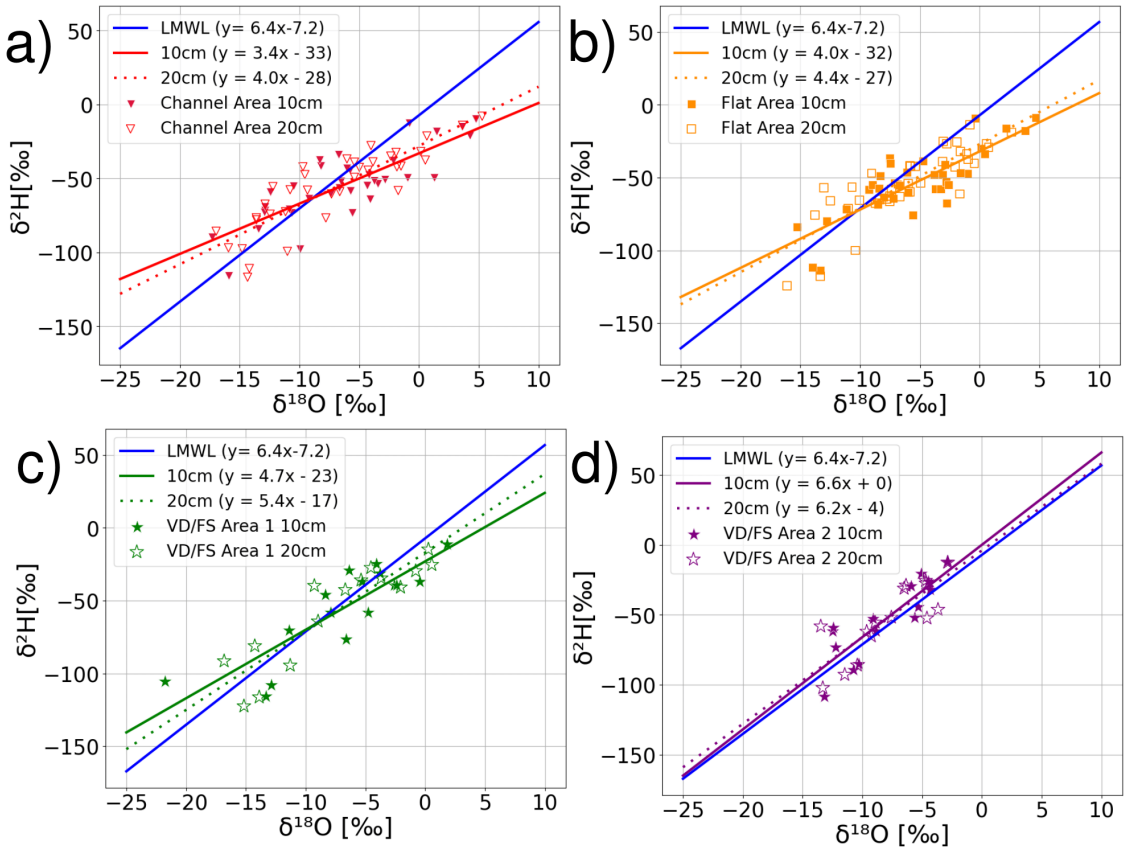

Figure 15: Scatter plots for δ2H and δ18O (‰) for precipitation and soils for the study period. (a) LMWL plotted with CA soil at 10 and 20 cm depth. (b) LMWL plotted with FA soil at 10 and 20 cm depth. (c) LMWL plotted with VD/FS Area 1 soil at 10 and 20 cm depth. (d) LMWL plotted with VD/FS Area 2 soil at 10 and 20 cm depth.

Soils from the four study sites have similar isotope values to each other with most values plotting between -15 ‰ to 0 ‰ $\delta^{18}O$ and -10 ‰ to -100 ‰ $\delta^{2}H$ (Figure 15). For the CA, FA, VD/FS area 1 and 2 some values plot along the LMWL, with most values plotting more enriched in $\delta^{18}O$ and $\delta^{2}H$ than the LMWL. The VD/FS area 1 has the widest range of $\delta^{18}O$ concentrations and the FA has the widest range of $\delta^{2}H$. The linear regressions for each depth (10 cm and 20 cm) collected at the four study sites is included in Figure 15. The linear regression of the 10 cm soil in each site appears to be more enriched in $\delta^{18}O$ and $\delta^{2}H$ than the 20 cm depths. The linear regression for the two depths (10 cm and 20 cm) in the VD/FS area 2 are more similar in slope than the VD/FS area 1 being the most distinct from each other.

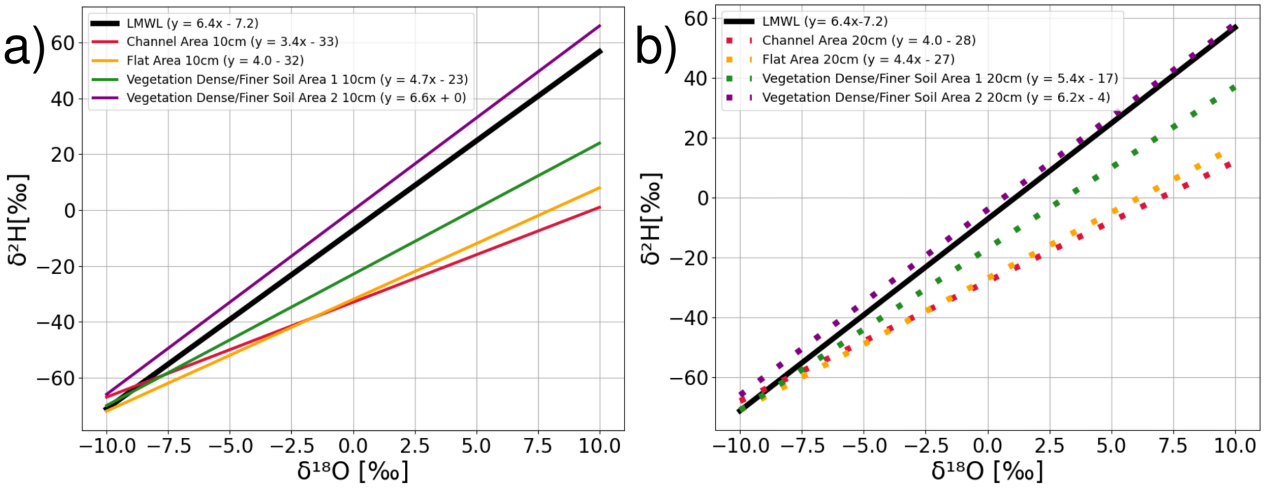

Figure 16: Linear regression plot of $\delta^{18}O$ and $\delta^{2}H$ (‰) within the four study sites' soils with precipitation. (a) LMWL with the soils of the four study sites at 10 cm plotted against $\delta^{18}O$ and $\delta^{2}H$ (‰). (b) LMWL with the soils of the four study sites at 20 cm plotted against $\delta^{2}H$ and $\delta^{18}O$.

To evaluate the differences in soil water isotope behavior (enriched or depleted), soil slopes were plotted together (Figure 16). This includes the $\delta^{2}H$ vs $\delta^{18}O$ (‰) with the four sites at 10 cm

and 20 cm depth with their respective linear regressions. The soils at 10 cm and 20 cm are consistent with each other at both depths. The CA is the most enriched in both depths (y = 3.4*x – 33 at 10 cm, and y = 4.0*x – 28 at 20 cm), and the VD/FS area 2 is the most similar to the LMWL in both depths (y = 6.6*x + 0 at 10 cm, and y = 6.2*x – 4 at 20 cm).

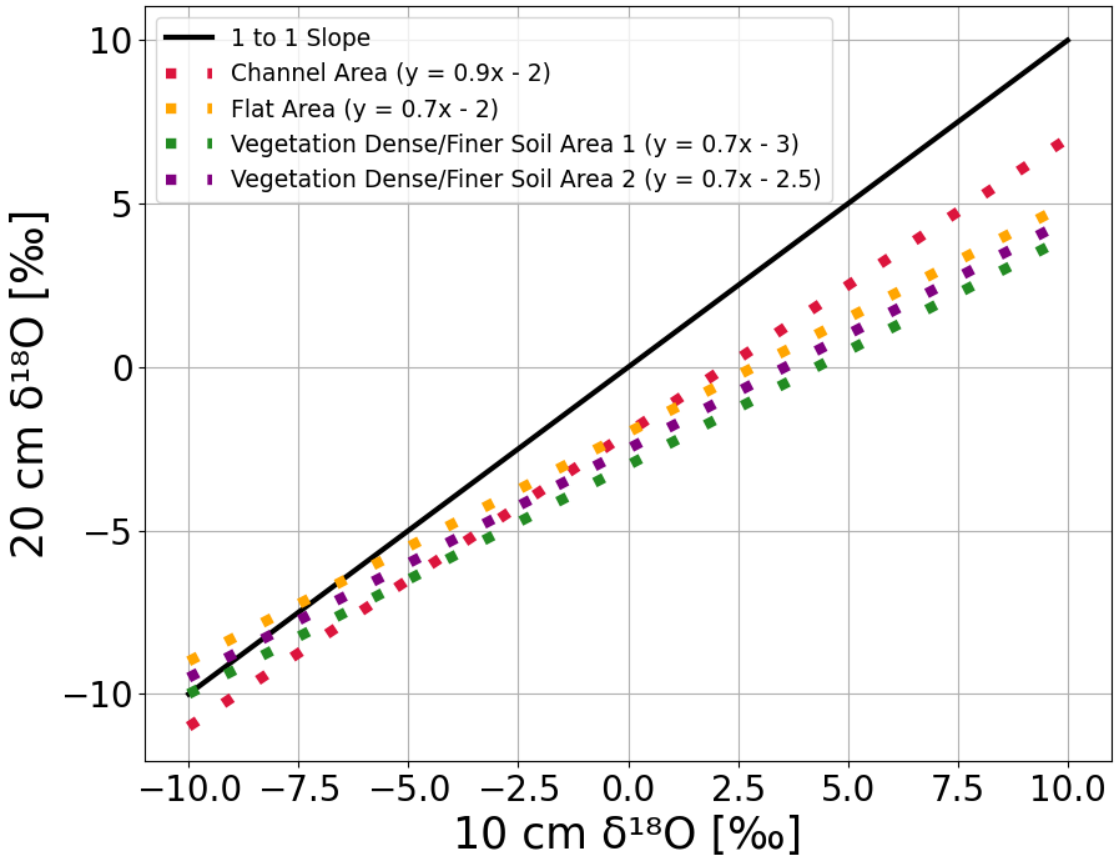

Figure 17: $\delta^{18}O$ and $\delta^{2}H$ (‰) plot of 10 cm vs 20 cm of $\delta^{18}O$ for the soils within the four sites at JER. The differing color represents the line of regression of a distinct site.

To assess the behavior with water dynamics at 10 cm and 20 cm, $\delta^{18}O$ (‰) was plotted against the two depths (Figure 17). These linear regressions describe how well mixed and connected the two depths (10 cm and 20 cm) are isotopically. This mixing variable depends on how different the values are at the two depths for a given sampling date throughout the study period. The two VD/FS sites and FA appear to be the most partitioned out the study sites with slopes of y = 0.7*x – 3 at the site 1, y = 0.7*x – 2.5 at site 2, and y = 0.7*x – 2 for the FA. The CA

appears to be the most isotopically well mixed at 10 cm and 20 cm with a linear regression of y = 0.9*x – 2. The differences in linear regressions suggest differing hydrological dynamics within the sites.

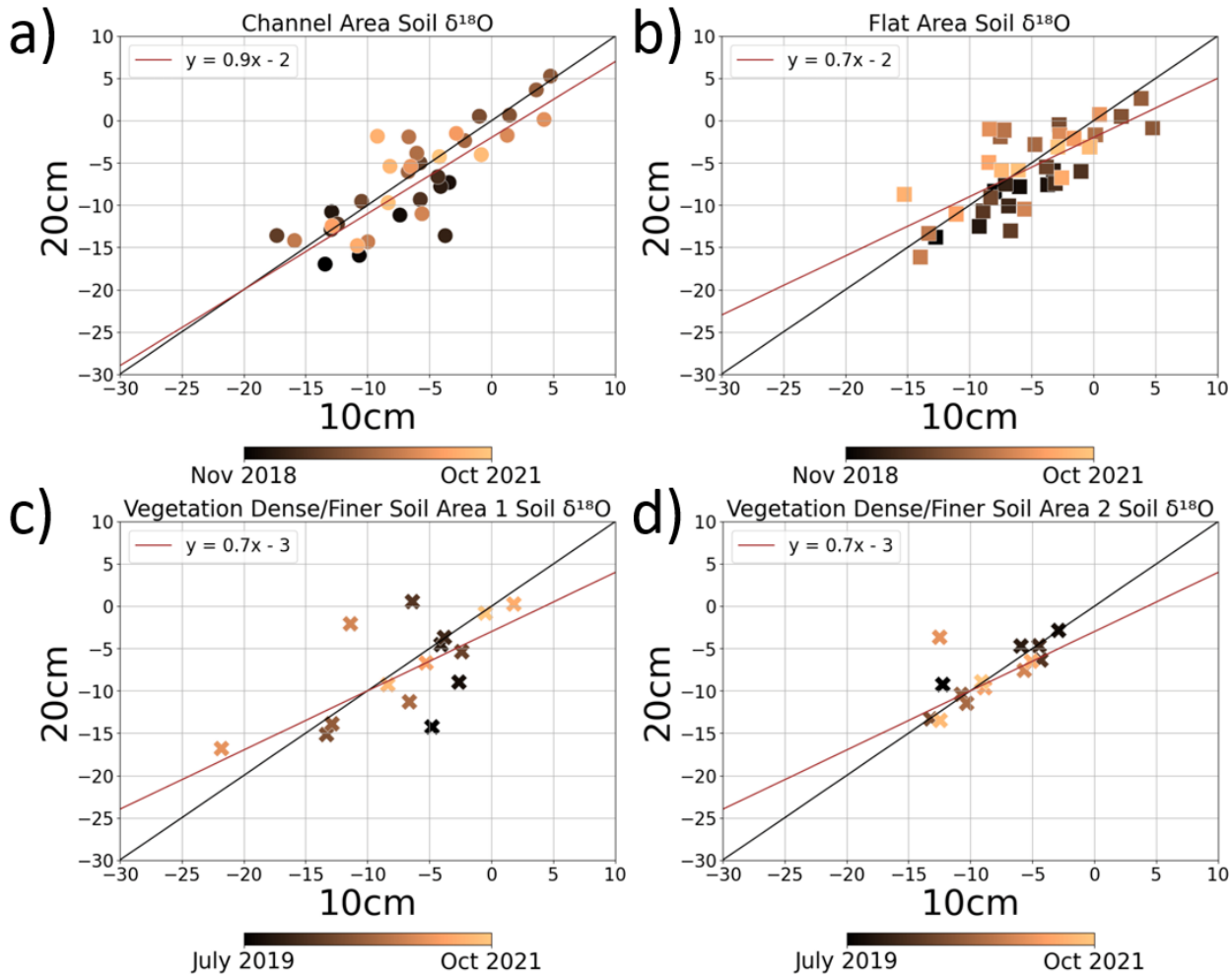

Figure 18: Plots comparing the soil behavior of samples within each of the four study sites at each depth (10 cm vs 20 cm). (a) $\delta^{18}O$ (‰) from soil samples collected in the CA at 10 cm and 20 cm. (b) $\delta^{18}O$ (‰) from soil samples collected in the FA at 10 cm (‰) from soil samples collected in the VD/FS area 2 at 10 cm and 20 cm.

The one to one plots in Figures in 18, 19, and 20 can allow us to make comparisons about their type of water by observing which sites become enriched and depleted in $\delta^{18}O$ at differing rates. To assess the differences in soil water behavior between the four sites at each depth, the

depths of $\delta^{18}O$ (‰) were plotted. It becomes evident that at 10 cm, each site experiences the most change isotopically, it becomes enriched and depleted faster than the depth at 20 cm (Figure 18). The FA, VD/FS area 1 and 2 experience the most change at 10 cm with a slope of y = 0.7 x. The CA has the most similar relationship isotopically at 10 cm and 20 cm. The copper colorbar describes the date of collection, with the dark colored samples being the earliest collected samples.

To evaluate the differences in soil water isotope behavior between the four sites and each depth in the soil, $\delta^{18}O$ (‰) in each site was plotted against those in the other four sites (Figure 19). The results reveal that the sites have similar $\delta^{18}O$ (‰) values to each other. However, when examining their linear regression, some of the sites have a wider range (more enriched or depleted) than the other sites. Such as the VD/FS area 1 vs the CA at 20 cm, have the least similar isotopic relationship, as a result of the VD/FS area 1 having the wider range of $\delta^{18}O$ (‰) isotopes. This trend can be observed throughout the other sites as well. The exception is the VD/FS area 1 vs the CA at 10 cm having a one to one relationship, suggesting they behave similarly. The sites comparing the soil water behavior with VD/FS 2 area show a similar behavior (Figure 20), to those in Figure 19. The VD/FS Area 2 vs the VD/FS Area 1 at 20 cm appears to have the most distinct behavior to each other with a slope of y = 0.5 x – 3. However, the VD/FS area 2 vs flat at 10 cm, the VD/FS area 2 vs CA at 20 cm, and the VD/FS area 2 vs VD/FS area 1 at 10 cm appear to have a one to one relationship, suggesting that they have a similar behavior isotopically to each other. There also appears to have a seasonal pattern with the $\delta^{18}O$ (‰) isotopes appearing lighter during the winter season than those during the summer, monsoonal season.

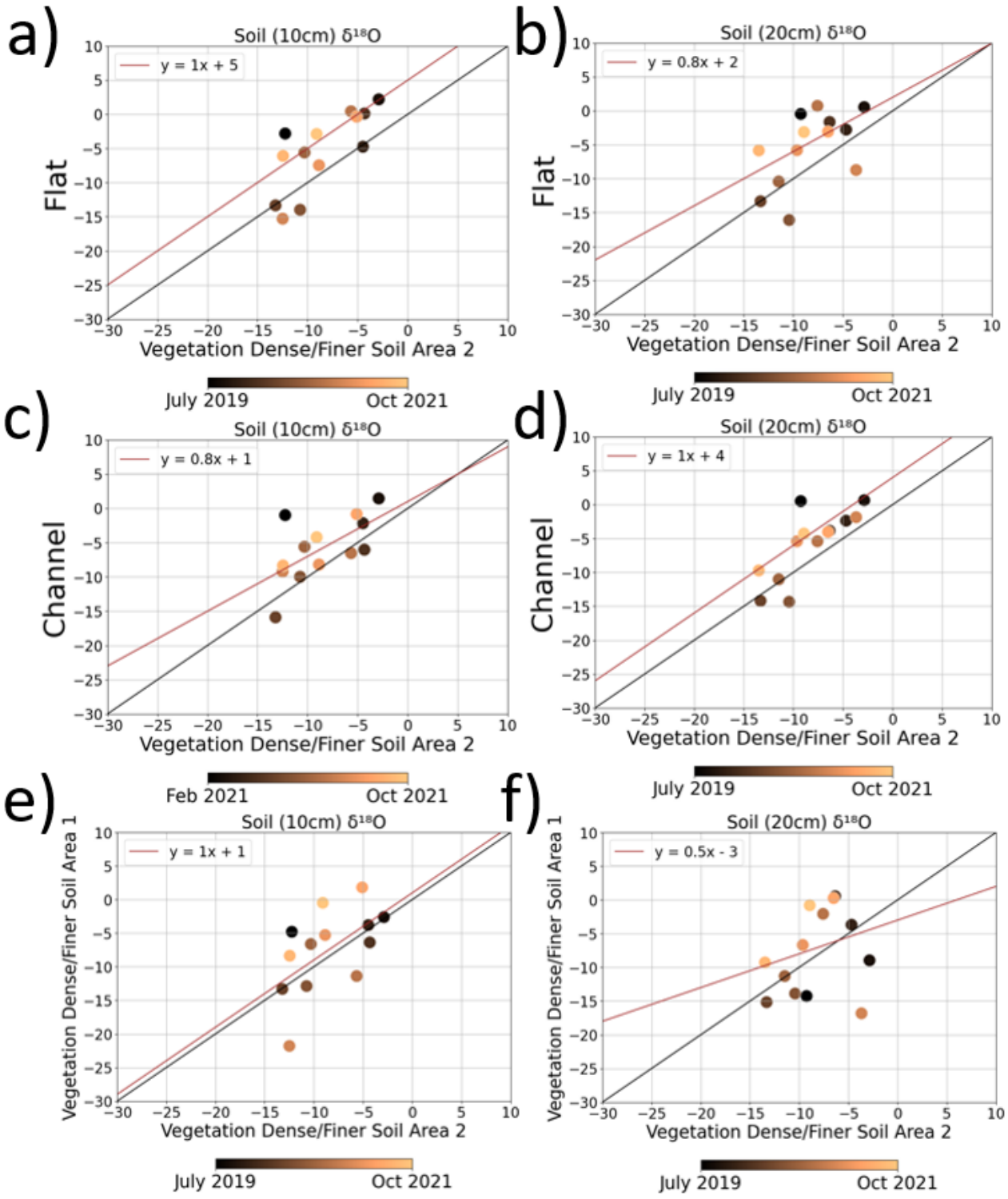

Figure 19: Plots comparing the soil behavior of samples each of the study sites to one another. (a) $\delta^{18}O$ (‰) soil at 10 cm CA vs Flat. (b) $\delta^{18}O$ (‰) soil at 20 cm CA vs Flat. (c) $\delta^{18}O$ (‰) soil at 10 cm VD/FS 1 vs CA. (d) $\delta^{18}O$ (‰) soil at 20 cm VD/FS 1 vs CA. (e) $\delta^{18}O$ (‰) soil at 10 cm VD/FS 2 vs VD/FS 1. (f) $\delta^{18}O$ (‰) soil at 20 cm VD/FS 2 vs VD/FS 1.

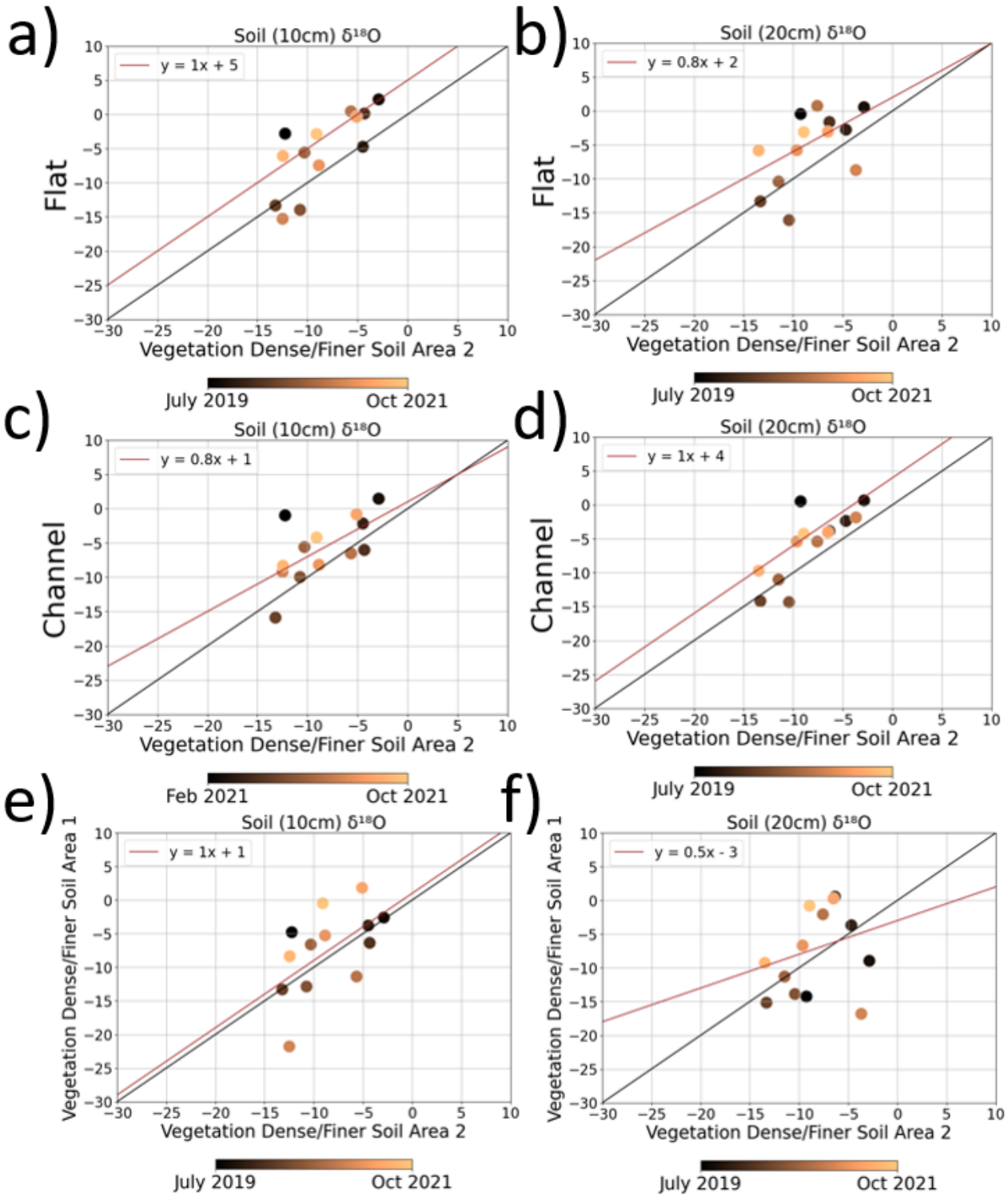

Figure 20: Continuation of plots comparing the soil behavior of samples each of the study sites to one another. (a) $\delta^{18}O$ (‰) soil at 10 cm VD/FS 2 vs Flat. (b) $\delta^{18}O$ (‰) soil at 20 cm VD/FS 2 vs Flat. (c) $\delta^{18}O$ (‰) soil at 10 cm VD/FS 2 vs CA. (d) $\delta^{18}O$ (‰) soil at 20 cm VD/FS 2 vs CA. (e) $\delta^{18}O$ (‰) soil at 10 cm VD/FS 2 vs VD/FS 1. (f) $\delta^{18}O$ (‰) soil at 20 cm VD/FS 2 vs VD/FS 1.

3.4.3 Vegetation Stem Water

There were a total of 201 vegetation samples throughout the study period: 110 of creosote, 64 mesquite, 29 tarbush and 15 grass. This contains data from a two and a half year period: the first sample collected in May 2019 and the last in October 2021. There are some gaps in the data due to not being able to extract the water cryogenically. This was due to vacuum loss during the vacuum distillation process to extract water from the vegetation stems.

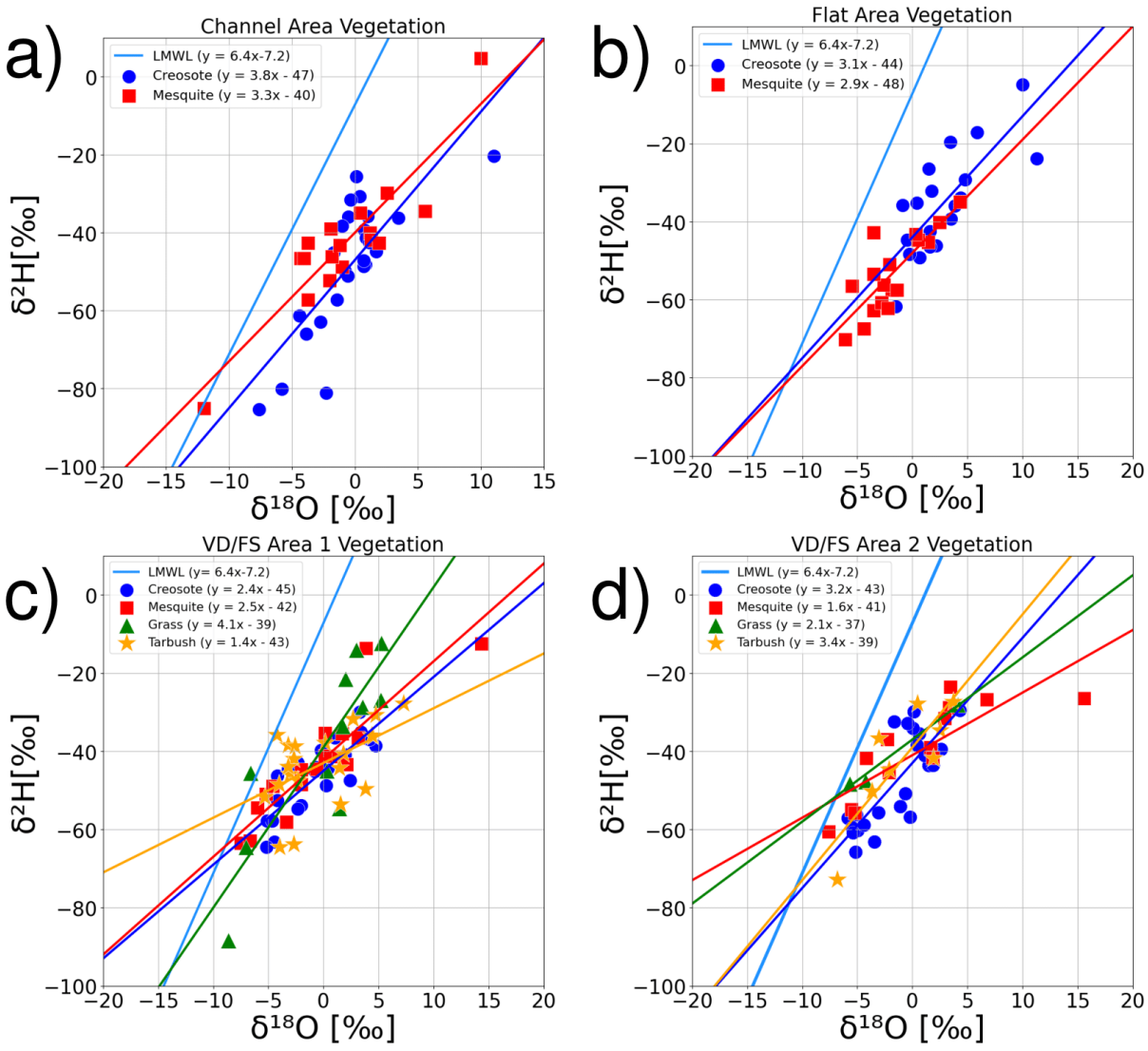

Figure 21: $\delta^{18}O$ and $\delta^{2}H$ (‰) concentration plot of the vegetation within the four sites with the LMWL. a) CA vegetation within the study site with LWML. b) FA vegetation within the study site with LWML. d) VD/FS Area 1 vegetation within the study site with LWML. c) VD/FS Area 1 vegetation within the study site with LWML.

Vegetation samples collected in the four study sites with some differences in their range (Figure 21). Most of the CA samples tend to plot between -5 ‰ to 5 ‰ $\delta^{18}O$ and -30 ‰ to -65 ‰ $\delta^{2}H$ with several outliers. In the FA, the vegetation samples tend to plot between -5 ‰ to 5 ‰ $\delta^{18}O$ and -20 ‰ and -70 ‰ $\delta^{2}H$ with few outliers. The samples in the VD/FS area 1 plot between -7 ‰ to 5 ‰ $\delta^{18}O$ and-30 ‰ to -65 ‰ $\delta^{2}H$. The samples in the VD/FS area 2 plot between -6 ‰ to 5 ‰ $\delta^{18}O$ and -20 ‰ to -70 ‰ $\delta^{2}H$. In the CA, the honey mesquite plots at a wider range of $\delta^{18}O$ and $\delta^{2}H$ than the creosote within the same site. In the FA, the creosote tends to plot more enriched in $\delta^{18}O$ and $\delta^{2}H$ than honey mesquite, which plots lighter than creosote. In the VD/FS area 1, the grass resembles the LMWL with a slope of $y = 4.1*x - 39$ and the tarbush obtaining the most enriched water with a slope of $y = 1.4*x - 43$. In the VD/FS area 2, tarbush resembles the LMWL the most with a slope of $y = 3.4*x - 39$ and the mesquite being the most enriched with a slope of $y = 1.6*x - 41$ at the site.

3.5 RELATIONSHIPS BETWEEN PRECIPITATION, SOIL WATER, AND VEGETATION STEM WATER

The violin plots from Figures 22 and 23, assess the differences in distribution between precipitation, soils, and vegetation species. The ranges of $\delta^{18}O$ of precipitation and soil water overlap (Figure 22), however, precipitation samples tend to be more enriched in $\delta^{18}O$ than the soils. Overall, the soil at 10 cm in the VD/FS 1 are more enriched and depleted in $\delta^{18}O$ than the other sites. In addition, the soil collected at 10 cm for the sites tend to be more enriched than those collected at 20 cm, with the exception of the CA. Looking closer, both of the soil depths at the VD/FS area 2 are less enriched and depleted of $\delta^{18}O$ than the other study sites. Honey mesquite in the VD/FS area 2 is the most enriched and depleted in $\delta^{18}O$, whereas, creosote in the VD/FS area 1 is the least enriched and depleted when examining their ranges in $\delta^{18}O$.

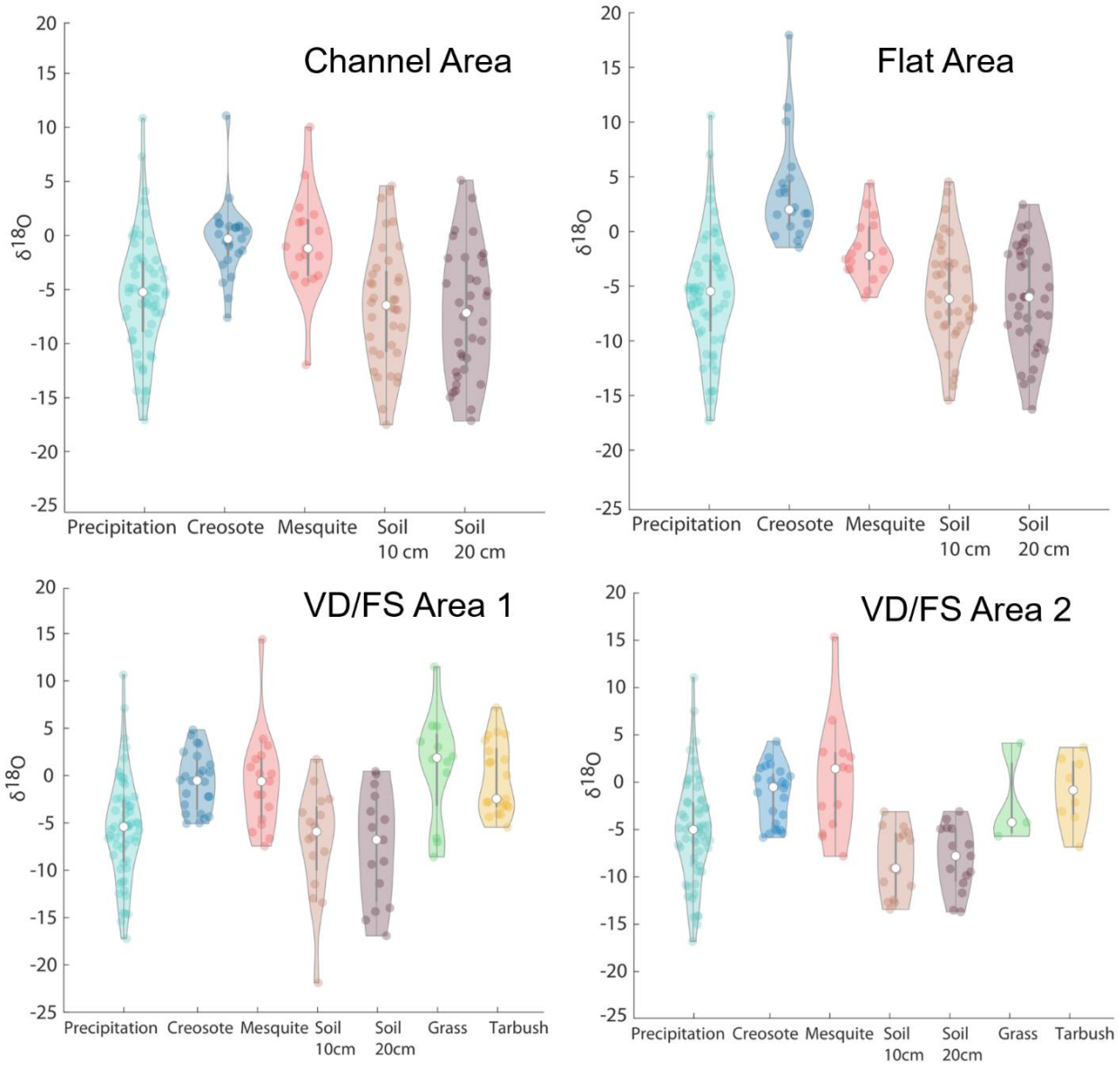

Figure 22: Violin plots for data within each study site in units of $\delta^{18}O$ (‰). Each plot represents one of the four study sites with precipitation, vegetation and two soil depths (10 cm and 20 cm). Each site contains Creosote and Mesquite, whereas VD/FS 1 and 2 areas contain tarbush and grass.

The violin plot from Figure 23, assesses the difference between each vegetation species within each study site. Overall, honey mesquite in the VD/FS 2 site is the most enriched and depleted in $\delta^{18}O$ within each study site, whereas, grass in the VD/FS 2 has the smallest range isotopically. Creosote has the largest range within the FA with a range of 19.4 in $\delta^{18}O$ (‰). In addition, honey mesquite has the largest range within the VD/FS 2. Tarbush and grass are the most

isotopically depleted and enriched within the VD/FS 1 area. Overall, each vegetation species has a differing average and range of $\delta^{18}O$ within each study site.

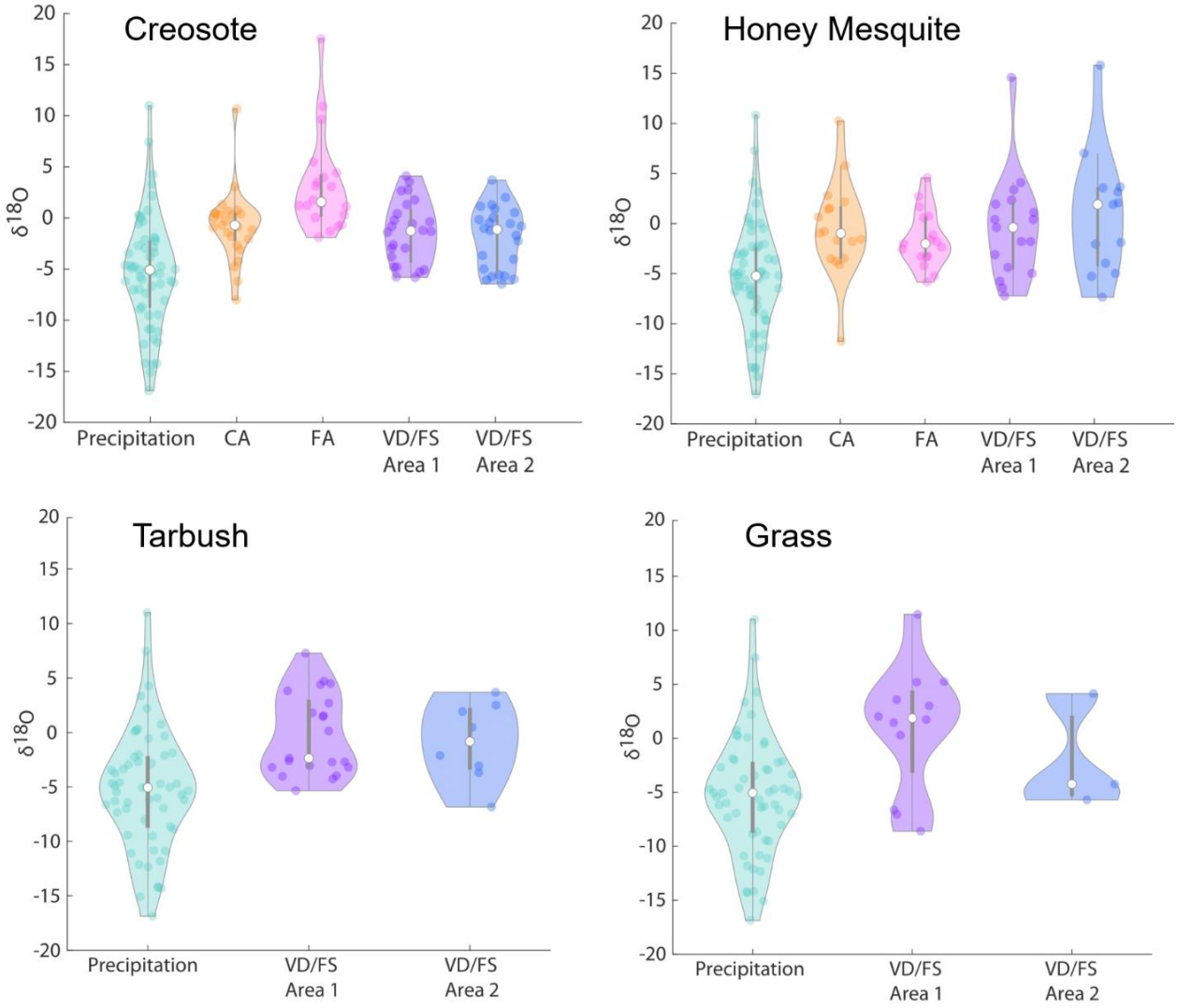

Figure 23: Violin plots for data of vegetation within each study site in units of $\delta^{18}O$ (‰). Each plot represents one of the four vegetation species with precipitation and vegetation samples. Creosote and Mesquite were collected for each of the four study sites, whereas tarbush and grass were only collected within the VD/FS 1 and 2 areas.

For the purposes of this work, we came up with a new concept to plot all of the data. The polar plots in Figures 24, 25, 26, and 27 illustrate the relationship between precipitation, soil water, and vegetation stem water. The radial axes are in the units of $\delta^{18}O$ and is divided into four quadrants to represent the seasons. The 360 degrees in the polar plots were adapted into days with this simple conversion: 1/360 * 365 to obtain days. These polar plots show differences in seasonality and detect changes in isotopic composition with ease. In addition, precipitation is represented as a polygon with points to discern when vegetation and soil deviate from precipitation. The overlap between the samples suggests similarity in isotopic signature and therefore similarity in water sourcing. The vegetation and soil depth are plotted as lines with the points, whereas precipitation is plotted as a polygon with points. However, there are some soil and vegetation samples represented as points due to the lack of continuity with sampling in Spring of 2021. This includes data from the four sites for years 2019 and 2021, being the most complete years in terms of data collection.

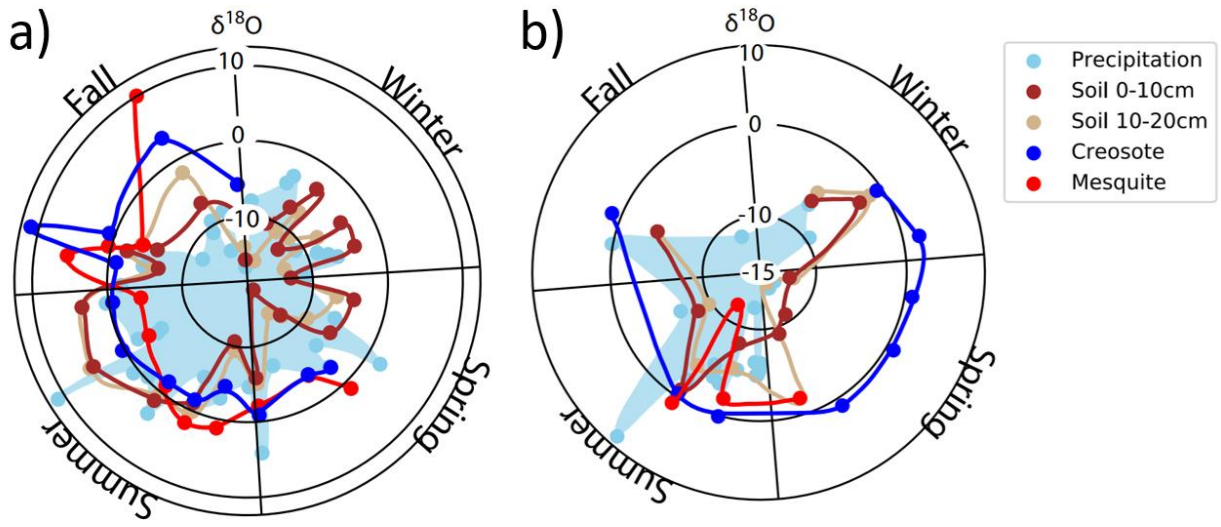

Figure 24: Polar plots of $\delta^{18}O$ (‰) concentration of precipitation, soil water at 10 cm and 20 cm, and vegetation within the CA for the years 2019 and 2021 (left to right). (a) Polar plot of δ18O concentration of rain, soil, and two vegetation species in the CA from 2019. (b) Polar plot of $\delta^{18}O$ concentration of rain, soil, and two vegetation species in the CA from 2021.

Precipitation isotopic signatures for 2019 and 2021 follow a seasonal pattern where isotopes are depleted during the winter season and highly enriched during the summer season (Figure 24, 25, 26, 27). The most enriched precipitation sample is in late August 2021 with 11.00 ‰ $\delta^{18}O$. Both of the CA polar plots from 2019 and 2021, include precipitation, creosote, honey mesquite, soil at 10 cm, and soil at 20 cm (Figure 24). The first collected sample of creosote in May 2019, plots identical to precipitation $\delta^{18}O$, whereas honey mesquite has a more enriched isotopic signature on that collection date. From May through October 2019 in CA, honey mesquite and creosote remained relatively depleted in $\delta^{18}O$ until they both spiked in early October 2019, with $\delta^{18}O$ values of 5.56 ‰ and 11.05 ‰ respectively. During the winter and spring season 2019 in CA, the two soil depths fluctuated from enriched to depleted in $\delta^{18}O$. During the summer season in 2019, soil depths at 10 cm and 20 cm were very well mixed isotopically in $\delta^{18}O$ with an average of 2.22 ‰ at 10 cm and 2.53 ‰ at 20 cm July to September. During most of the summer period in CA, both soil depths remained more isotopically enriched than the vegetation samples, whereas during the other seasons, vegetation tends to plot more enriched (Figure 24).

The creosote from 2021, tends to plot at a small range of -0.56 ‰ to 1.70 ‰ $\delta^{18}O$ with an average of 0.60 ‰ $\delta^{18}O$ (Figure 24). Whereas, honey mesquite in 2021, plots at a larger range of -11.99 ‰ to -1.22 ‰ $\delta^{18}O$ and an average of -4.23 ‰ $\delta^{18}O$. Honey mesquite has a similar signature to precipitation during the early summer season in 2021. The first samples of soil at 10 cm and 20 cm in 2021, plot very similar to that of precipitation. For a majority of the samples at the CA in 2021, soil at 0-10 cm tends to plot very similar to soil at 10-20 cm, with the exception of late spring and early summer. Due to honey mesquite being dormant and losing some samples in the cryogenic vacuum extraction process, there were only four honey mesquite samples from June through September of that year.

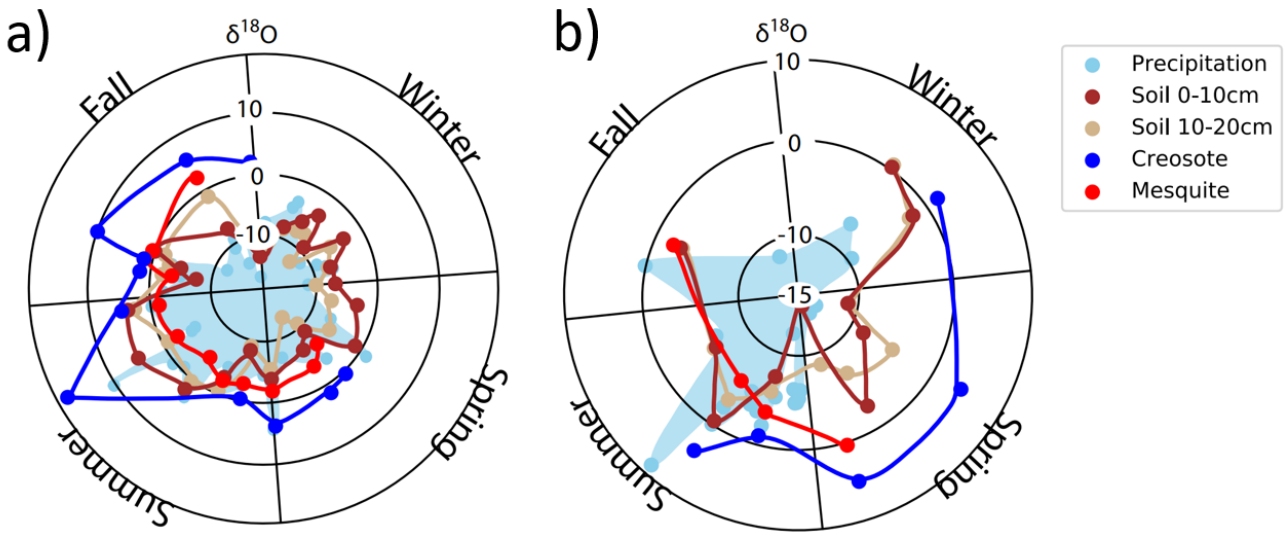

Figure 25: Polar plots of $\delta^{18}O$ concentration of precipitation, soil water at 10 cm and 20 cm, and vegetation within the FA for the years 2019 and 2021 (left to right). (a) Polar plot of $\delta^{18}O$ concentration of rain, soil, and two vegetation species in the FA from 2019. (b) Polar plot of $\delta^{18}O$ concentration of rain, soil, and two vegetation species in the FA from 2021.

Both of the FA polar plots from 2019 and 2021 include precipitation, creosote, honey mesquite, soil at 10 cm, and soil at 20 cm. For the FA in 2019, honey mesquite tends to have a smaller range relative to creosote (Figure 25), with values from -6.09 ‰ to 2.48 ‰ $\delta^{18}O$ and an average of -2.00 ‰ $\delta^{18}O$. Creosote tends to plot at a larger range of -0.28 ‰ to 17.91 ‰ $\delta^{18}O$. Creosote has two spikes in 2019, the largest one in late August and the second in October. Looking closer, creosote remains more enriched in the FA than Mesquite throughout the year of 2019. In addition, creosote has a similar isotopic signature to precipitation in late June 2019. In the FA in 2019, soil at 0-10 cm tends to be more isotopically fractionated than soil at 10-20 cm throughout the majority of the study year.

For the FA in 2021, the creosote tends to plot heavier isotopically relative to honey mesquite, similar to 2019 in the same area (Figure 25). Honey mesquite has a range of -5.5 ‰ and 0.3 ‰ $\delta^{18}O$ with an average -2.7 ‰ $\delta^{18}O$, whereas, creosote has a range of -0.9 ‰ and 4.4 ‰ $\delta^{18}O$ with an average of 2.1 ‰ $\delta^{18}O$ at FA 2021. Both soil depths in the FA in 2021, are isotopically

well mixed throughout most of the winter season, with an average of -0.6 ‰ at both 10 cm and 20 cm $\delta^{18}O$. In the month of June 2021, the soil depth at 10 cm in the FA is isotopically similar to precipitation collected for that date. Due to honey mesquite being dormant and losing some samples in the cryogenic vacuum extraction process, there were only four mesquite samples for June through October that year (Figure 25).

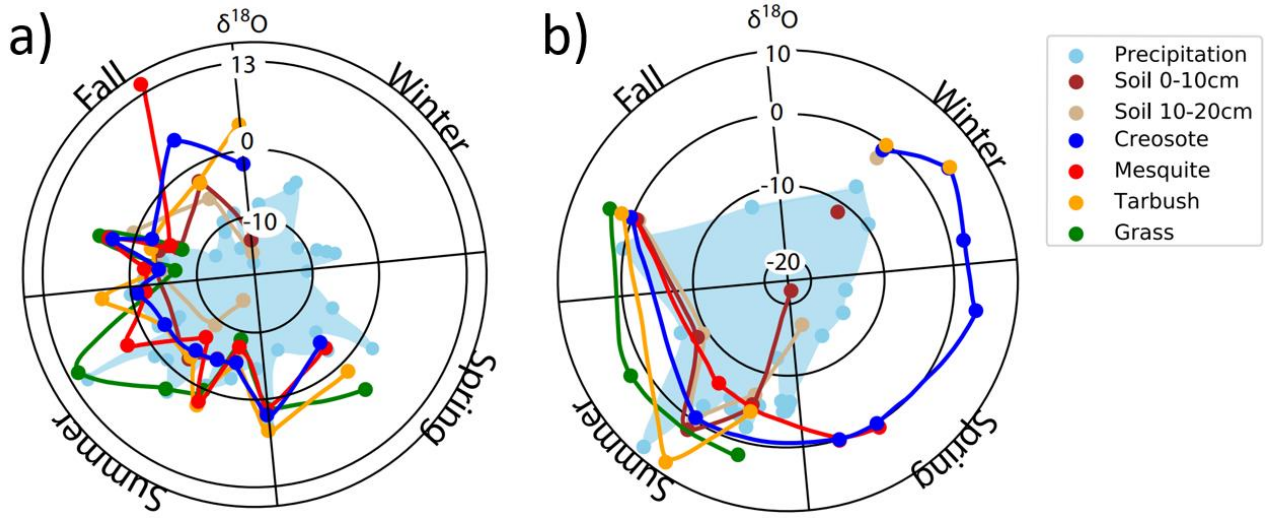

Figure 26: Polar plots of $\delta^{18}O$ concentration of precipitation, soil water at 10 cm and 20 cm, and vegetation within the VD/FS Area 1 for the years 2019 and 2021 (left to right). (a) Polar plot of $\delta^{18}O$ concentration of rain, soil, and two vegetation species in the VD/FS Area 1 from 2019. (b) Polar plot of $\delta^{18}O$ concentration of rain, soil, and two vegetation species in the VD/FS Area 1 from 2021.

Both of the VD/FS area 1 polar plots from 2019 and 2021, include precipitation, creosote, honey mesquite, grass, tarbush, soil at 10 cm, and soil at 20 cm. This area contains two vegetation species that were not collected at the CA and FA area, which are grass and tarbush. In the VD/FS Area 1 site, $\delta^{18}O$ in vegetation tend spike in accordance to each other (Figure 26). This means vegetation species in this site appear to follow the precipitation isotopic signature. In the VD/FS 1 area in 2019, creosote has a range of -5.1 ‰ to 4.7 ‰ $\delta^{18}O$ with an average of -1.7 ‰ $\delta^{18}O$, honey mesquite has a range of -7.5 ‰ to 14.3 ‰ $\delta^{18}O$ and an average of -0.2 ‰ $\delta^{18}O$, tarbush has a range

of -5.4 ‰ to 4.7 ‰ $\delta^{18}O$ and an average of -0.5 ‰ $\delta^{18}O$, and grass has a range of -8.6 ‰ to 11.5 ‰ $\delta^{18}O$ with an average of 0.5 ‰ $\delta^{18}O$.

In the VD/FS Area 1 2021 the first two Tarbush, one soil at 10 cm, and another at 20cm are represented as points due to the lack of continuity with sampling during the spring season (Figure 26). The VD/FS Area 1 in 2021 shows a different scale than the other plots during the year 2021 due to light $\delta^{18}O$ values at the 10 cm. The creosote within the VD/FS 1 area, tends to plot at a range of -0.7 ‰ to 4.2 ‰ $\delta^{18}O$ with an average of 1.1 ‰ $\delta^{18}O$, whereas honey mesquite plots closely to creosote on this site with a range of -6.0 ‰ to 0.9 ‰ $\delta^{18}O$ and an average of -1.9 ‰ $\delta^{18}O$. In February 2021, tarbush plotted similar to creosote suggesting a similar isotopic composition of $\delta^{18}O$ to each other. The first honey mesquite sample collected in 2021 at the VD/FS 1, has a similar isotopic signature to that of creosote on the same date collected. Grass has a range of 1.7 ‰ to 3.6 ‰ $\delta^{18}O$ with an average of 2.4 ‰ $\delta^{18}O$ and tarbush has a range of -4.3 ‰ to 7.3 ‰ $\delta^{18}O$ with an average of 1.0 ‰ $\delta^{18}O$. The soil at both depths in this site tends to be well mixed isotopically with an average of -7.6 ‰ $\delta^{18}O$ for 10 cm and -5.9 ‰ $\delta^{18}O$ for 20 cm.

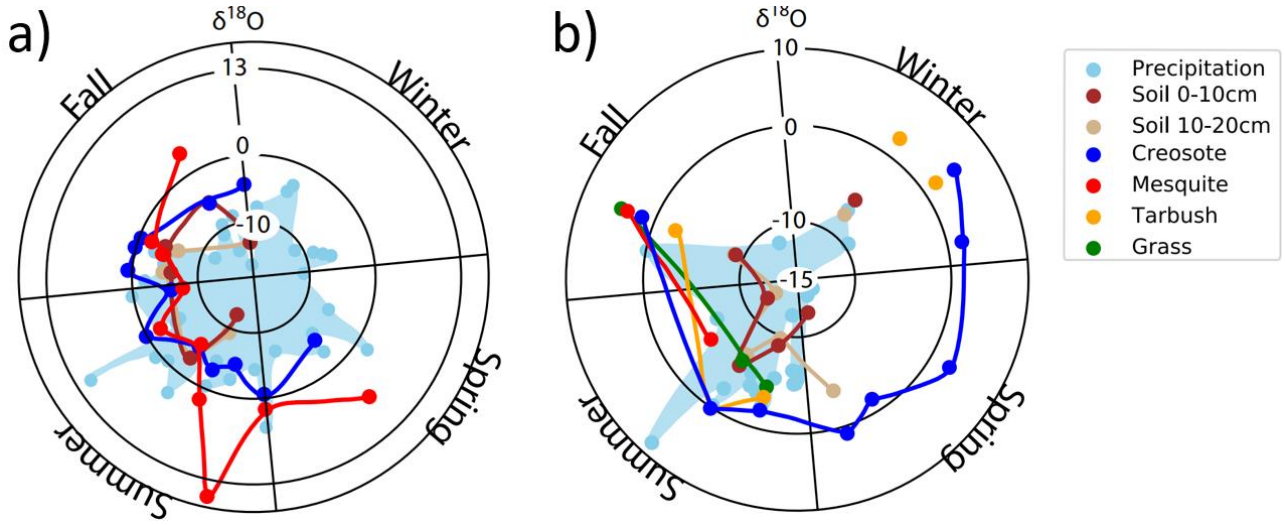

Figure 27: Polar plots of $\delta^{18}O$ concentration of precipitation, soil water at 10 cm and 20 cm, and vegetation within the VD/FS Area 2 for the years 2019 and 2021 (left to right). (a) Polar plot of $\delta^{18}O$ concentration of rain, soil, and two vegetation species in the VD/FS Area 2 from 2019. (b) Polar plot of $\delta^{18}O$ concentration of rain, soil, and two vegetation species in the VD/FS Area 2 from 2021.

The VD/FS Area 2 polar plot from 2021 include precipitation, creosote, honey mesquite, grass, tarbush, soil at 10 cm, and soil at 20 cm. However, the VD/FS Area 2 in 2019 only contains precipitation, honey mesquite, creosote, soil at 10 cm and soil at 20 cm, due to lack of resources to extract sufficient water from stem samples. In the VD/FS area 2 in 2019, honey mesquite peaked at 15.6 ‰ $\delta^{18}O$ July 2019, whereas creosote peaked at 0.6 ‰ $\delta^{18}O$ in September 2019 (Figure 27). Honey mesquite has a range of -7.6 ‰ to 15.6 ‰ $\delta^{18}O$ and an average of 0.7 ‰ $\delta^{18}O$, whereas creosote has a smaller range of -5.8 ‰ to 0.6 ‰ and an average of -2.8 ‰ $\delta^{18}O$. The soils at depths 10 cm and 20 cm remained isotopically well mixed during the summer and early fall with an average of -6.9 ‰ $\delta^{18}O$ at 10 cm and -7.4 ‰ at 20 cm $\delta^{18}O$ during that season.

In the VD/FS 2 area in 2021 the first two tarbush, one soil at 10 cm, and 20 cm are represented as points due to the lack of continuity with sampling during the spring season. Creosote has a range of -1.6 ‰ to 4.3 ‰ $\delta^{18}O$ with an average of 1.2 ‰ $\delta^{18}O$ (Figure 27). Honey mesquite only had 2 samples in this year, with a range of 5.2 ‰ to 3.4 ‰ $\delta^{18}O$ and an average of -0.9 ‰ $\delta^{18}O$. In addition, grass in this site has a range of -5.71 ‰ to 4.1 ‰ $\delta^{18}O$ with an average of -1.9 ‰ $\delta^{18}O$ and tarbush had a range of -3.7 ‰ to 2.5 ‰ $\delta^{18}O$ with an average of -0.7 ‰ $\delta^{18}O$. In mid-June, tarbush resembled precipitation with a signature of -3.1 ‰ $\delta^{18}O$. Both tarbush and creosote in the VD/FS Area 2, resembled that of precipitation in early August with a signature of 0.5 ‰ and 0.4 ‰ $\delta^{18}O$, respectfully (Figure 27).

CHAPTER 4: DISCUSSION

4.1 SOIL TEXTURE INFLUENCE ON VEGETATION WATER SOURCING

We speculated that the corresponding soil within the study sites would have an effect on the isotopic signature of the soil water available to plants because of differing hydrological processes. There were four distinct study sites within the JER that we analyzed the soil texture at 10 cm and 20 cm. Our expectations are that finer soils increase soil water residence times due to small soil pore space, whereas coarser soils contain more soil pore space. Generally, the soils at the four study sites proved to be sandy in nature with some variation (Figure 11). The VD/FS area 2 shows to be site with the finest soil at 10 cm with both samples being a loam and silty loam. One of the soil samples of the VD/FS 1 at 10 cm contains low sand and high silt content as well. This could be due to higher vegetation density and a decrease in erosion as a result. With airborne particles, suspended in the air there is an increase in particle dropping of soil trapped in the canopy of vegetation (Ram, 2014).

We expected both the VD/FS Areas to experience less evaporation due to its finer soil texture leading to higher water residence times (Figure 2). When assessing the soil water isotopic signatures in Figure 15 and Figure 16, it is evident that VD/FS 2 experiences the least amount of evaporation with a slope of $y = 6.6x + 0$ (at 10 cm) and $y = 6.2x – 4$ (at 20 cm) when considering the LMWL in the region is $\delta^2H = 6.4* \delta^{18}O - 7.2$. Our rationale for the results is that the more a line of regression deviates from the LMWL, the more evaporation occurred. These two VD/FS Areas do not deviate far from the LMWL suggesting that they experience relatively low fractionation and therefore low evaporation. The violin plots in Figure 22 show that the VD/FS Area 2 displays the smallest range in $\delta^{18}O$ isotopes, which is an indication that this site experiences the least amount soil water fractionation. This could be another indication that the site is experiencing the least amount of evaporation in the soil. The VD/FS Area 1 also experiences little

evaporation relative to the FA and CA, with a slope of y = 4.7x - 23 (at 10 cm) and y = 5.4x - 17 (at 20 cm). This explanation lines up with field observations, since these two sites support the largest amount of vegetation density and species (Table 2), suggesting greater water content and therefore greater water availability to support vegetation. Another factor contributing to the low evaporation at the VD/FS Areas is their greater vegetation density, especially grass cover. This vegetation cover is likely shielding the soil from the sun's heat, leading to less soil water evaporation. This supports the hypothetical illustration from Figure 2, predicting low evaporation and high transpiration at these two sites. The CA and FA sites appear to be more isotopically enriched in $\delta^{18}O$ and $\delta^{2}H$, with shallower line of regressions (Figure 15 and 16). Soil texture may not be an influence on the soil dynamics on these two sites because they contain similar soil texture, with most in the sandy loam and sandy clay loam category (Figure 11).

During the study period, some of the sites seem to have isotopically mixed soils at the 10 cm and 20 cm depth. This suggests that the soils at 10 cm and 20 cm contain the same type of water. This could occur after a larger precipitation event that infiltrates both depths. The polar plots in figures 24, 25, 26, and 27 shed light shed light on these temporal and spatial soil water dynamics with $\delta^{18}O$. The CA soil is well mixed isotopically during summer 2019 and winter 2021 (Figure 24). Whereas, the VD/FS Area 1 soil is isotopically mixed during the summer 2021 (Figure 26) and for VD/FS Area 2 summer 2019 and 2021 showed a similar pattern (Figure 27). The one to one plots in figures 18, 19, and 20 compare the soil water of each site with depth. This can allow us to make comparisons about their type of water by observing which sites become enriched and depleted in ^{18}O at differing rates. The four sites in figure 18 show that the soil water at 10 cm becomes enriched and depleted in $\delta^{18}O$ more than the depth of 20 cm (Figure 18). The site that appears to be the most isotopically similar at 10 cm and 20 cm is the CA. When comparing the

sites with each other, the VD/FS Area 1 and CA behaves alike at 10 cm, whereas, they are the most distinct at 20 cm (Figure 19). Similarly, the VD/FS Area 2 and FA at 10 cm also become enriched and depleted isotopically at similar ways (Figure 20). The VD/FS Area 2 vs the CA at 20 cm behave similar and so do the VD/FS Area 2 vs the VD/FS 1 at 10 cm.

4.2 VEGETATION SPECIES INFLUENCE ON VEGETATION WATER SOURCING

One of our questions was whether vegetation competition within each site would have an effect on sourcing due to differing rooting depths. There were four study sites and four desert vegetation species within the JER to test this hypothesis. Each site had a unique vegetation composition and density: the CA is predominantly creosote and honey mesquite, FA is mostly creosote, VD/FS Area 1 contains mostly creosote, tarbush, and grass, and VD/FS Area 2 is mostly grass and tarbush with some creosote and honey mesquite (Figure 12). This vegetation composition reveal the differing water uptake patterns due to differing rooting systems. The VD/FS Area 2 has the highest amount of canopy cover with the bare soil percentage being a low 16.33% and the FA has the lowest canopy cover with a bare soil percentage of a high 63.33%.

Similar to soil water samples, vegetation isotopic data may give us some insight into their behavior by interpreting their $\delta^{18}O$ and $\delta^{2}H$ values. Despite the fact that the vegetation samples were overall more enriched in $\delta^{18}O$ and $\delta^{2}H$ in comparison to the soil samples, there are patterns in their isotopic concentrations that may offer some aid in interpretating the values. However, there were some outliers that can be subject to discussion. Honey mesquite at the VD/FS Area 1 in November 2019, displays a high value of 14.4 ‰ $\delta^{18}O$. This sample might be using water from a precipitation event in August 2019 with a $\delta^{18}O$ concentration of 11.00 ‰. Another explanation for the abnormally high value is exposure to organic contamination during the cryogenic extraction process. The creosote from the FA in August 2019 with a value of 17.9 ‰ $\delta^{18}O$ might have also

been exposed to organic contamination during the distillation process. Both of these samples were analyzed an additional time to confirm the values.

In Figure 21 within the CA, creosote and honey mesquite tend to have a wider range in isotopic composition of $\delta^{18}O$ and $\delta^{2}H$ in comparison to the FA, suggesting that the CA vegetation have access to water that the FA does not. In the CA, creosote and mesquite have overlapping values that may suggest a similar water source or an isotopically well mixed soil profile. The FA creosote and honey mesquite tend to have two distinct patterns in the water sourcing: the creosote tends to obtain a soil water source that is more isotopically enriched than the honey mesquite (Figure 21), which may be a source closer to the surface (Figure 1). The honey mesquite in this area tends to have a smaller range that is more isotopically depleted, which may infer a deeper source in the soil profile (Figure 22). The vegetation in the VD/FS Area 1, appear to follow a mutual water source, especially in the year 2019 (Figure 26). Looking closer, it is clear that the plants are increasing and decreasing in conjunction with precipitation. This could be an indication of vegetation taking in the water following precipitation events. This is a viable explanation because honey mesquite, creosote, tarbush, and grass are able to absorb moisture from near the surface due to the location of their rooting systems (Meyer, 1971; Hyder et al., 2002; Schwinning, 2011). The VD/FS Area 2 displays this similar competitive behavior in the year 2021 (Figure 27). In the year 2019, tarbush and grass were not able to be cryogenically extracted due to poor water content, however, the data that we do have, shows that creosote and honey mesquite may be obtaining a similar source (Figure 27).

When assessing just the vegetation species (Figure 23), each has a different behavior in accordance with the site. The honey mesquite in the FA tends to have a preferential source in comparison to the wider isotopic range in the CA. This smaller range suggests a preferential source

because that water contains a more similar isotopic signature. The honey mesquite in both the VD/FS Areas tend to follow a similar behavior, suggesting a similar water source (Figure 26 and 27). The creosote tends to obtain a more enriched source on average in the flat area and a relatively depleted source in the channel (Figure 23). Vegetation such as the tarbush species, have a similar range in $\delta^{18}O$ which suggest they both have the same water source (Figure 23). Grass in in the VD/FS Area 1 tends to have a wider range than the grass in the VD/FS Area 2 (Figure 23), which may be a result of the differing evaporation dynamics affecting the shallow water composition or lack of sufficient data for that site.

4.3 LANDSCAPE INFLUENCE ON VEGETATION WATER SOURCING

Our final question was whether the location landscape would have an effect on the soil water available for plant uptake. There were four study sites within the JER to test the hypothesis of landscape has an effect on vegetation water sourcing due to different hydrological inputs. The four distinct locations within a piedmont included: a low-lying channelized area, a higher elevation flatter area, and two stream discharge sites within a piedmont.

The soil water isotope samples may give some insight into the different hydrological fluxes within each site. There are overlapping values within the four sites but have different ranges in isotopes despite one known input, which is precipitation. This differing range within each site may illuminate what the soil water behavior is. For instance, the CA contains a relatively wide range of isotopes that may infer differing hydrological fluxes. The FA is within close proximity of the CA and contains a similar soil texture, however, they display a differing range of values. This wide range of values in the CA may indicate additional runoff from upstream that is combining with water previously in the soil profile (Figure 22). Since the FA is located slightly higher in elevation compared to the CA, it might not be receiving that additional water that the channel has access to.

That is a viable explanation because in this site there is an arroyo with an exposed caliche horizon that may be draining into the site. This caliche horizon in this area appears to be well-developed, which may have low permeability. Precipitation events that are large enough, are likely transported from uphill on to the site with the aid of this well-developed caliche horizon. That would explain the lighter isotopes coming from higher elevations and lower average temperatures (Poage, 2001), or intense precipitation events (Renée Brooks et al, 2010).

CHAPTER 5: CONCLUSIONS

The results from the 37-month long study in the Jornada Experimental Range show that there are factors that influence the water available for the creosote, honey mesquite, tarbush, and grass throughout their growing season. We established that the soil texture had an influence on the evaporation processes in each site, therefore influencing the water available for vegetation use. After completing a soil texture analysis, it became evident that the VD/FS Area 2 contained the finest soil and the CA and FA contained a sandier texture. When assessing the soil water isotope signatures, it is apparent that VD/FS 2 experiences the least amount of evaporation and the VD/FS 1 also experiences little evaporation. This is evident because these two sites resemble the LMWL the most out of the four study sites. This lines up with field observations because we are assuming that the finer soil texture properties are increasing the water residence time and the high canopy cover in the site is providing sufficient shade that likely prevents further evaporation. The VD/FS Area 1 does not contain as much canopy cover relative to VD/FS Area 2, nonetheless, the slope resembles the LMWL. This suggests that the soil texture might be increasing the water's residence time, without the aid of canopy cover that the VD/FS Area 2 receives. These results support the hypothetical illustration from Figure 2, predicting low evaporation and high transpiration as a result of soil texture. The CA and FA show different water dynamics with their differing isotopic ranges despite their similar soil texture. They appear to be more enriched than the VD/FS Areas, suggesting that the CA and FA experience a higher degree of evaporation. This may be due to their sandier soil texture affecting their water residence time. These findings suggest the sites may contain differing quantities of water for plant uptake.

One of our questions was whether vegetation competition would have an effect on sourcing due to differing rooting depths. Even though the vegetation samples were overall more enriched

in $\delta^{18}O$ and $\delta^{2}H$ in comparison to the soil samples, there are patterns in their isotopic concentrations that may offer support in interpreting the values. In the CA, creosote and honey mesquite have a similar range in values, which may suggest a similar water source or an isotopically well mixed soil profile (Figure 21). The FA creosote and honey mesquite tend to have two distinct patterns in the water sourcing: the creosote tends to obtain a soil water source that is more enriched than the honey mesquite (Figure 21), which may be a source closer to the surface. The honey mesquite in the FA tends to have a smaller range that is more isotopically depleted, which may infer a deeper source in the soil profile (Figure 22). The vegetation in the VD/FS Areas, appear to follow a mutual water source in the soil profile because their isotopic values increase and decrease in conjunction with those of precipitation. This could be an indication of vegetation taking in water following precipitation events or caliche might be affecting water infiltration, which leaves vegetation with only a surficial water source.

Our final question was whether the location of the landscape would have an effect on the soil water available for vegetation. There are overlapping values within the four sites but have different ranges in isotopes despite one known input, which is precipitation. The FA is within close proximity to the CA and is composed of similar soil texture, however, they display isotopic different values. For instance, the CA contains a relatively wide range of isotopes that may suggest different hydrological fluxes. The wide range of values in the CA may indicate additional runoff from upstream that is combining with water previously in the soil profile. This runoff may be transported with the aid of exposed caliche in the arroyo that leads into the CA. The VD/FS Areas may not be as influenced by the landscape as the CA, even though they are considered as a stream discharge sites. The VD/FS Area 2 contain a very small range of values that might suggest that runoff may not be an additional input of water for the site.

5.1 FUTURE WORK

Future work should investigate other possible sources of water such as water retained at the caliche in the soil profile or moisture deeper than at 20 cm. This project could also benefit from understanding the plant root systems and how they are influenced by caliche acting as a barrier. It would also be important to consider additional water sources such as runoff in the in the channel area by taking samples from upstream. This would help to understand isotopic mixing that influences water composition at the site.

REFERENCES

Araguás-Araguás, L., Rozanski, K., Gonfiantini, R., & Louvat, D. (1995). Isotope effects accompanying vacuum extraction of soil water for stable isotope analyses. Journal of Hydrology, 168(1–4), 159–171. https://doi.org/10.1016/0022-1694(94)02636-p

Barrow, Jerry R., E. Durant McArthur, Ronald E. Sosebee, and Robin J. Tausch. "Proceedings: Shrubland Ecosystem Dynamics in a Changing Environment." Ogden, UT: U.S. Department of Agriculture, Forest Service, Intermountain Research Station, 1996. https://doi.org/10.2737/INT-GTR-338.

Brunel, J.-P., Walker, G. R., & Kennett-Smith, A. K. (1995). Field validation of isotopic procedures for determining sources of water used by plants in a semi-arid environment. *Journal of Hydrology*, *167*(1–4), 351–368. https://doi.org/10.1016/0022-1694(94)02575-v

Canfield, R. H. (1941). Application of the line interception method in sampling range vegetation. Journal of Forestry, 39(4), 388–394. https://doi.org/10.1093/jof/39.4.388

Caracciolo, D., Istanbulluoglu, E., Noto, L. V., & Collins, S. L. (2016). Mechanisms of shrub encroachment into Northern Chihuahuan Desert grasslands and impacts of climate change investigated using a cellular automata model. Advances in Water Resources, 91, 46–62. https://doi.org/10.1016/j.advwatres.2016.03.002

Craig, H. (1961). Isotopic variations in meteoric waters. Science (New York, N.Y.), 133(3465), 1702–1703. https://doi.org/10.1126/science.133.3465.1702

Dawson, T. E. (1993). Water sources of plants as determined from xylem-water isotopic composition: Perspectives on plant competition, distribution, and water relations. In J. R. Ehleringer, A. E. Hall, & G. D. Farquhar (Eds.), Stable Isotopes and Plant Carbon-water Relations (pp. 465–496). Elsevier

Dawson, T. E., Mambelli, S., Plamboeck, A. H., Templer, P. H., & Tu, K. P. (2002). Stable isotopes in plant ecology. *Annual Review of Ecology and Systematics*, *33*(1), 507–559. https://doi.org/10.1146/annurev.ecolsys.33.020602.095451

Drewa, P. B., & Havstad, K. M. (2001). Effects of fire, grazing, and the presence of shrubs on Chihuahuan desert grasslands. Journal of Arid Environments, 48(4), 429–443. https://doi.org/10.1006/jare.2000.0769

Douglas, M.W., Maddox, R.A., Howard, K., Reyes, S., AUG 1993. The Mexican monsoon. J. Clim. 6 (8), 1665e1677. http://dx.doi.org/10.1175/1520-0442(1993)006.

Dubbert, M., Caldeira, M. C., Dubbert, D., & Werner, C. (2019). A pool-weighted perspective on the two-water-worlds hypothesis. *The New Phytologist*, *222*(3), 1271–1283. https://doi.org/10.1111/nph.15670

Duniway, M. C., Petrie, M. D., Peters, D. P. C., Anderson, J. P., Crossland, K., & Herrick, J. E. (2018). Soil water dynamics at 15 locations distributed across a desert landscape: insights from a 27-yr dataset. Ecosphere (Washington, D.C), 9(7), e02335. https://doi.org/10.1002/ecs2.2335

Durner, W., Iden, S. C., & von Unold, G. (2017). The integral suspension pressure method (ISP)

for precise particle-size analysis by gravitational sedimentation: ISP METHOD FOR PARTICLE-SIZE ANALYSIS. Water Resources Research, 53(1), 33–48. https://doi.org/10.1002/2016wr019830

Ehleringer, J.R., Dawson, T.E., 1992. Water uptake by plants: perspectives from stable isotope composition. Plant Cell and Environment 15, 1073–1082.

Fargione, J., & Tilman, D. (2005). Niche differences in phenology and rooting depth promote coexistence with a dominant C4 bunchgrass. Oecologia, 143(4), 598–606. https://doi.org/10.1007/s00442-005-0010-y

Gibbens, R. P., & Lenz, J. M. (2001). Root systems of some Chihuahuan Desert plants. Journal of Arid Environments, 49(2), 221–263. https://doi.org/10.1006/jare.2000.0784

Gibbens, R. P., McNeely, R. P., Havstad, K. M., Beck, R. F., & Nolen, B. (2005). Vegetation changes in the Jornada basin from 1858 to 1998. Journal of Arid Environments, 61(4), 651–668. https://doi.org/10.1016/j.jaridenv.2004.10.001

Grieu, P., Lucero, D. W., Ardiani, R., & Ehleringer, J. R. (2001). The mean depth of soil water uptake by two temperate grassland species over time subjected to mild soil water deficit and competitive association. Plant and Soil, 230(2), 197–209. http://www.jstor.org/stable/42951139

Grossnickle, S. C. (2012). Why seedlings survive: influence of plant attributes. New Forests, 43(5–6), 711–738. https://doi.org/10.1007/s11056-012-9336-6

Grover, H.D., Musick, H.B., 1990. Shrubland encroachment in southern New Mexico, USA.: an analysis of desertification processes in the American Southwest. Climatic Change 17, 305–330.

Hamerlynck, E. P., Mcauliffe, J. R., & Smith, S. D. (2000). Effects of surface and sub-surface soil horizons on the seasonal performance of Larrea tridentata (creosotebush): Larrea tridentata and desert soils. Functional Ecology, 14(5), 596–606. https://doi.org/10.1046/j.1365-2435.2000.t01-1-00469.x

Henrickson J, Johnston MC (2007) A flora of the Chihuahuan Desert region. Published by J Henrickson, Los Angeles, CA, USA

Hennessy, J. T., Gibbens, R. P., Tromble, J. M., & Cardenas, M. (1983). Water properties of caliche. Journal of Range Management, 36(6), 723. https://doi.org/10.2307/3898195

Huenneke, L. F., Clason, D., & Muldavin, E. (2001). Spatial heterogeneity in Chihuahuan Desert vegetation: implications for sampling methods in semi-arid ecosystems. Journal of Arid Environments, 47(3), 257–270. https://doi.org/10.1006/jare.2000.0678

Huenneke, L. F., Anderson, J. P., Remmenga, M., & Schlesinger, W. H. (2002). Desertification alters patterns of aboveground net primary production in Chihuahuan ecosystems: DESERTIFICATION ALTERS CHIHUAHUAN NPP PATTERNS. Global Change Biology, 8(3), 247–264. https://doi.org/10.1046/j.1365-2486.2002.00473.x

Hyder, P. W., Fredrickson, E. L., Estell, R. E., & Lucero, M. E. (2002). Transport of phenolic compounds from leaf surface of creosotebush and tarbush to soil surface by precipitation. Journal of Chemical Ecology, 28(12), 2475–2482. https://doi.org/10.1023/a:1021432018512

Johnson, J. E., Hamann, L., Dettman, D. L., Kim-Hak, D., Leavitt, S. W., Monson, R. K., & Papuga, S. A. (2017b). Performance of induction module cavity ring-down spectroscopy (IM-CRDS) for measuring δ18 O and δ2 H values of soil, stem, and leaf waters: Performance of induction module cavity ring-down spectroscopy. Rapid Communications in Mass Spectrometry: RCM, 31(6), 547–560. https://doi.org/10.1002/rcm.7813

Jorquera, M. A., Shaharoona, B., Nadeem, S. M., de la Luz Mora, M., & Crowley, D. E. (2012). Plant growth-promoting rhizobacteria associated with ancient clones of creosote bush (Larrea tridentata). Microbial Ecology, 64(4), 1008–1017. https://doi.org/10.1007/s00248-012-0071-5

Kemp, P. R. (1983). Phenological patterns of chihuahuan desert plants in relation to the timing of water availability. The Journal of Ecology, 71(2), 427. https://doi.org/10.2307/2259725

Li, J., Okin, G. S., Alvarez, L., & Epstein, H. (2007). Quantitative effects of vegetation cover on wind erosion and soil nutrient loss in a desert grassland of southern New Mexico, USA. Biogeochemistry, 85(3), 317–332. https://doi.org/10.1007/s10533-007-9142-y

MacMahon JA (1979) North American deserts: their floral and faunal components. In: Goodall DW, Perry RA (eds) Arid-Land Ecosystems: Structure, Functioning and Management, IBP 16, vol 1. Cambridge University Press, Cambridge, UK, pp 21–82

McCole, A. A., & Stern, L. A. (2007). Seasonal water use patterns of Juniperus ashei on the Edwards Plateau, Texas, based on stable isotopes in water. Journal of Hydrology, 342(3–4), 238–248. https://doi.org/10.1016/j.jhydrol.2007.05.024

McDonnell, J. J. (2014). The two water worlds hypothesis: ecohydrological separation of water between streams and trees?: The two water worlds hypothesis. *WIREs. Water*, *1*(4), 323-329. https://doi.org/10.1002/wat2.1027

Meyer, R. E. (1971). *Morphology and anatomy of honey mesquite*. U.S. Department of Agriculture.

Monger, H. C., Mack, G. H., Nolen, B. A., & Gile, L. H. Regional Setting of the Jornada Basin.

Noy-Meir, I. (1973). Desert ecosystems: Environment and producers. *Annual Review of Ecology and Systematics*, *4*(1), 25–51. https://doi.org/10.1146/annurev.es.04.110173.000325

Oki, T., & Kanae, S. (2006). Global hydrological cycles and world water resources. Science (New York, N.Y.), 313(5790), 1068–1072. https://doi.org/10.1126/science.1128845

Osakabe, Y., Osakabe, K., Shinozaki, K., & Tran, L.-S. P. (2014). Response of plants to water stress. Frontiers in Plant Science, 5, 86. https://doi.org/10.3389/fpls.2014.00086

Picon-Cochard, C., Nsourou-Obame, A., Collet, C., Guehl, J. M., & Ferhi, A. (2001b). Competition for water between walnut seedlings (Juglans regia) and rye grass (Lolium perenne) assessed by carbon isotope discrimination and delta18O enrichment. Tree Physiology, 21(2–3), 183–191. https://doi.org/10.1093/treephys/21.2-3.183

Poage, M. A. (2001). Empirical relationships between elevation and the stable isotope composition of precipitation and surface waters: considerations for studies of paleoelevation change. American Journal of Science, 301(1), 1–15. https://doi.org/10.2475/ajs.301.1.1

Qian, J., Zheng, H., Wang, P., Liao, X., Wang, C., Hou, J., Ao, Y., Shen, M., Liu, J., & Li, K. (2017). Assessing the ecohydrological separation hypothesis and seasonal variations in water use by Ginkgo biloba L. in a subtropical riparian area. Journal of Hydrology, 553, 486–500. https://doi.org/10.1016/j.jhydrol.2017.08.021

Ram, S. S., Majumder, S., Chaudhuri, P., Chanda, S., Santra, S. C., Maiti, P. K., Sudarshan, M., & Chakraborty, A. (2014). Plant canopies: bio-monitor and trap for re-suspended dust particulates contaminated with heavy metals. Mitigation and Adaptation Strategies for Global Change, 19(5), 499–508. https://doi.org/10.1007/s11027-012-9445-8

Renée Brooks, J., Barnard, H. R., Coulombe, R., & McDonnell, J. J. (2010). Ecohydrologic separation of water between trees and streams in a Mediterranean climate. Nature Geoscience, 3(2), 100–104. https://doi.org/10.1038/ngeo722

Schlesinger, W. H., Marion, G. M., & Fonteyn, P. J. (1989). Stable isotope ratios and the dynamics of caliche in desert soils. In *Stable Isotopes in Ecological Research* (pp. 309–317). Springer New York.

Schimel, D. S., House, J. I., Hibbard, K. A., Bousquet, P., Ciais, P., Peylin, P., Braswell, B. H., Apps, M. J., Baker, D., Bondeau, A., Canadell, J., Churkina, G., Cramer, W., Denning, A. S., Field, C. B., Friedlingstein, P., Goodale, C., Heimann, M., Houghton, R. A., … Wirth, C. (2001). Recent patterns and mechanisms of carbon exchange by terrestrial ecosystems. Nature, 414(6860), 169–172. https://doi.org/10.1038/35102500

Schwinning, S., Sandquist, D. R., Miller, D. M., Bedford, D. R., Phillips, S. L., & Belnap, J. (2011). The influence of stream channels on distributions of Larrea tridentata and Ambrosia dumosa in the Mojave Desert, CA, USA: patterns, mechanisms and effects of stream redistribution. Ecohydrology: Ecosystems, Land and Water Process Interactions, Ecohydrogeomorphology, 4(1), 12–25. https://doi.org/10.1002/eco.116

Sohel, M. S. I., Grau, A. V., McDonnell, J. J., & Herbohn, J. (2021). Tropical forest water source patterns revealed by stable isotopes: A preliminary analysis of 46 neighboring species. Forest Ecology and Management, 494(119355), 119355. https://doi.org/10.1016/j.foreco.2021.119355

Szutu, D. J., & Papuga, S. A. (2019). Year-round transpiration dynamics linked with deep soil moisture in a warm desert shrubland. Water Resources Research, 55(7), 5679–5695. https://doi.org/10.1029/2018wr023990

T.E. Dawson, S. Mambelli, A.H. Plamboeck, P.H. Templer, K.P. Tu Stable isotopes in plant

ecology Annu. Rev. Ecol. Syst., 33 (2002), pp. 507-559, 10.1146/annurev.ecolsys.33.020602.095451

Thompson, H. E, Ramirez, O., Dagda-Torres, A., Gutiérrez-Jurado, H.A (2020). Water sourcing strategies of highly resilient vegetation in desert soils: stable isotope analysis of a northern chihuahuan desert ecosystem. The University of Texas at El Paso, El Paso, TX.

Van Auken, O. W. (2009). Causes and consequences of woody plant encroachment into western North American grasslands. Journal of Environmental Management, 90(10), 2931–2942. https://doi.org/10.1016/j.jenvman.2009.04.023

Vilà, M., & Sardans, J. (1999). Plant competition in mediterranean-type vegetation. Journal of Vegetation Science: Official Organ of the International Association for Vegetation Science, 10(2), 281–294. https://doi.org/10.2307/3237150

Wainwright, J., 2006, Climate and Climatological Variations in the Jornada Basin, in Havstad, K.M., Huenneke, L.F., and Schlesinger, W.H., eds., Structure and Function of a Chihuahuan Desert Ecosystem: The Jornada Basin Long-Term Ecological Research Site: New York, NY, Oxford University Press, p. 44-80.

Walker, C. D., & Richardson, S. B. (1991). The use of stable isotopes of water in characterising the source of water in vegetation. Chemical Geology, 94(2), 145–158. https://doi.org/10.1016/0168-9622(91)90007-j

Weltzin, J. F., & McPherson, G. R. (1997). Spatial and temporal soil moisture resource partitioning by trees and grasses in a temperate savanna, Arizona, USA. Oecologia, 112(2), 156–164. https://doi.org/10.1007/s004420050295

West, A. G., Patrickson, S. J., and Ehleringer, J. R.: Water extraction times for plant and soil materials used in stable isotope analysis, Rapid Commun. Mass Sp., 20, 1317–1321, doi:10.1002/rcm.2456, 2006.

Wu, H., Zhao, G., Li, X.-Y., Wang, Y., He, B., Jiang, Z., Zhang, S., & Sun, W. (2019). Identifying water sources used by alpine riparian plants in a restoration zone on the Qinghai-Tibet Plateau: Evidence from stable isotopes. The Science of the Total Environment, 697(134092), 134092. https://doi.org/10.1016/j.scitotenv.2019.134092

Xu, H., & Li, Y. (2006). Water-use strategy of three central Asian desert shrubs and their responses to rain pulse events. Plant and Soil, 285(1–2), 5–17. https://doi.org/10.1007/s11104-005-5108-9

APPENDIX A: PROTOCOL FOR COLLECTING SAMPLES FOR ISOTOPIC ANALYSIS WITH THE PICARRO L2130-I ANALYZER

Martha E. Gardea[1]

[1]Department of Earth, Environmental and Resource Sciences, University of Texas at El Paso, TX 79968, USA

1. SUMMARY

The purpose of this appendix is to describe the sample collection protocol for precipitation, vegetation, and soil samples in the study area. This consists of four study location within a piedmont slope at the Jornada Experimental Range in the Northern Chihuahuan Desert. The samples were collected at a bi-weekly to monthly interval. There were four sites within the piedmont in which we collected from: a channelized area, a flat area, and two vegetation dense/finer soil areas. Precipitation samples were collected using a rainfall collector with a few mL of mineral oil to prevent evaporation. There were four vegetation samples collected from the channel area (two creosote and two mesquite samples), four from the flat area (two creosote and two mesquite sample samples), and eight from the two vegetation dense/finer soil areas (two creosote, two mesquite, two tarbush, and two grass samples). These samples were wrapped in Parafilm, placed in a ziplock bag, and stored in a cooler. Soil samples were collected at 0-10 cm from the surface, and another 10-20 cm below the first. The soil sample containers were also wrapped in Parafilm and placed in a cooler during transportation until placed in a refrigerator in the Ecohydrology Lab at the University of Texas at El Paso.

2. SITE DESCRIPTION

The study sites are located 30 km northeast of Las Cruces, New Mexico, within a piedmont slope at the Jornada Experimental Range (JER) of the Northern Chihuahuan Desert. The Jornada Basin Long-Term Ecological Research (LTER) site is surrounded by the Rio Grande Valley towards the west and the San Andres Mountains to the east. The study areas are located in the vicinity of the Systems Ecology Laboratory (SEL) and the Ecohydrology Laboratory eddy covariance towers from the University of Texas at El Paso. Each site within the piedmont has differing vegetation community composition, landscape, and soil texture.

3. SAMPLE COLLECTION

Samples were collected biweekly to monthly at the four sites at the Jornada Experimental Range. There were soil samples at two depths, precipitation, and four desert vegetation species to be collected. Honey mesquite, grass, and tarbush are dormant during a portion of the year and cannot be collected.

3.1 Precipitation sample collection

3.1.1 Approach both rainfall collectors at JER: 32°35'0"N, 106°37'55"W and UTEP: 31°46'12"N, 106°30'21"W.

3.1.2 Collecting a precipitation sample:

3.1.2.1 Move rocks supporting the base of the rainfall collector

3.1.2.2 Remove the lid of the plastic jar holding the 50mL centrifuge tube in place

3.1.2.3 Remove the lid of the 50mL centrifuge tube

3.1.2.4 Twist on new centrifuge tube with ~5mL of mineral oil

3.1.2.5 Place the lid of the new 50mL centrifuge tube on to the tube with the rain water

3.1.2.6 Wrap sample tube with Parafilm

3.1.2.6 Label the tube with date, time, location (ex. 6/11/2022, JER or UTEP, 10:43 am)

3.1.2.7 Store temporarily in cooler with ice packs

3.1.3 Repeat for each collection

3.1.4 Storing precipitation samples in laboratory

3.1.4.1 Upon arrival to the laboratory, place sample in lab refrigerator immediately

3.2 Vegetation Stem Sample Collection

3.2.1 Approach one of the study sites (Flat Area 1 and 2, Channel Area 1 and 2, Vegetation Dense/Finer Soil Area 1 and 2)

3.2.2 Identify vegetation (Creosote, Honey Mesquite, Tarbush, or Grass)

3.2.3 Collecting a stem sample:

3.2.3.1 Locate a healthy twig with a diameter of 0.2 to 0.5 cm

3.2.3.2 Cut the stem that is 5 to 8 cm in length with gardening shears

3.2.3.3 Wrap stem firmly in Parafilm and place in a zip-lock bag

3.2.3.4 Label zip-lock bag with location, plant species, and collection date

3.2.3.5 Store temporarily in cooler with ice packs

3.2.4 Repeat to collect 2 stems from each plant (except grass). For grass, collect a bundle that is 3-4 cm in thickness.

3.2.5 After approaching each study site, there will be a total of six mesquite, six creosote, two tarbush, and two grass samples.

3.5.6 Storing vegetation samples in the laboratory:

3.5.6.1 Upon arrival to the laboratory, place sample in lab refrigerator immediately

3.3 Soil Samples

3.3.1 Approach open soil between the vegetation from the study sites (Flat Area, Channel Area, and Vegetation Dense/Finer Soil Area 1 and 2)

3.3.2 Collecting a soil sample:

3.3.2.1 Use a small shovel to dig a soil pit 10cm deep

3.3.2.2 Fill a container with 100g+ of the soil

3.3.2.3 Parafilm the container

3.3.2.4 Label the container with date, location and depth (ex. 6/11/2022, JER or UTEP, 10:43 am)

3.3.2.5 Place container in a cooler with icepacks

3.3.3 Repeat the procedure for 20cm in depth below the 10cm

3.3.4 Complete this process for all sites

3.3.5 Storing vegetation samples in the laboratory:

3.3.5.1 Upon arrival to the laboratory, place sample in lab refrigerator immediately

APPENDIX B: PROTOCOL FOR SAMPLE ANALYSIS ON THE PICARRO L2130-I ANALYZER, CRYOGENIC VACUUM EXTRACTION AND SOIL TEXTURE ANALYSIS

Martha E. Gardea[1]

[1]Department of Earth, Environmental and Resource Sciences, University of Texas at El Paso, TX 79968, USA

1. SUMMARY

The purpose of this appendix is to present the general protocol that was used to process soil, vegetation, and precipitation samples on the Picarro L2130-I Isotope and Gas Concentration Analyzer (Autosampler and Induction Module), PARIO Plus, and Cryogenic Vacuum Extractor. It demonstrates the general procedure for running samples for isotopic analysis, water extraction from vegetation stems and soil texture analysis. Prior to analysis, samples are stored in a refrigerator in the Ecohydrology Lab at the University of Texas at El Paso.

2. PICARRO ANALYSIS EQUIPMENT AND MATERIALS

2.1 Equipment:

2.1.1 L2130-I Isotope and Gas Concentration Analyzer

2.1.2 External Vacuum Pump

2.1.3 Induction Module (IM)

2.1.4 Omega Engineering Inc. FMA5400A/5500A Series Mass Flow Controller

2.1.5 Dry Air

2.2 Materials:

2.2.1 Water stable isotope standards (Zero, Mid and Depleted)

2.2.2 Syringes (10 μL)

2.2.3 Glass vials (4 mL with septa cap)

2.2.4 Glass microfiber filter paper

2.2.5 Quartz wool

2.2.6 Tri-fold metal strips sample holders

2.2.7 Metal tube sample holders (3.3 mm internal diameter)

2.2.8 Hole punch

2.2.9 Disposable gloves

2.2.10 Syringe filter (0.45 μm)

3. SET UP FOR RUNNING BLANKS AND SAMPLES ON THE PICARRO

3.1 Assemble the analyzer and vacuum pump with the L2130-I Installation User's Manual.

3.2 Remove samples from refrigerator and allow to reach room temperature to avoid condensation when opened.

3.3 Press power switch on the external vacuum pump. Turn on the analyzer using the power switch on the back of the instrument. The analyzer will run on ambient air until it switches from pressure (torr) to water concentration (ppm) on the Graphical User Interface.

3.4 To install the Induction Module (IM):

3.4.1 Connect the IM to the Omega Engineering Inc. FMA5400A/5500A Series mass flow controller.

3.4.2 Then, connect the mass flow controller to the IM and tighten with a wrench. Insert the other opening into the Picarro analyzer.

3.4.3 Open the zero-air gas line to 2.5-4.0 psi and the mass flow controller will be running at 154-156 SCCM, alternating slightly.

3.4.4 Press power switch of the IM and wait until its green light stops flashing.

3.5 Launch the ‘Coordinator Launcher’ on the Picarro desktop. On the ‘Picarro Coordinator Launcher’ window, select ‘IM CRDS’. A window called ‘CRDS Coordinator’ will appear.

3.6 To run blanks:

3.6.1 Run the Coordinator Launcher on the desktop and select IM CRDS.

3.6.2 On the recipe selection, select ‘Calibration- Lower Temperature.’

3.6.3 On data type, select ‘Blank.’

3.6.4 Begin purging by pressing ‘OK’.

3.6.5 Press ‘OK’ after preparing an empty 4 mL vial with a septa on the cap.

3.6.6 Insert the 4 mL vial by turning the lever to the right and pushing the vial into the IM and press ‘OK’.

3.6.7 Once prompted by the CRDS Coordinator, eject the vial by turning the lever further to the right. This process takes 5 minutes per blank sample.

3.6.8 Repeat this process until the maximum H_2O (ppm) concentration is below 250 ppm to run liquid and soils samples safely.

4. HOW TO RUN STANDARDS AND LIQUID SAMPLES

4.1 Verify that the steps above have been completed before proceeding with the standards and liquid samples.

4.2 Preparation of materials needed to run standards and liquid samples:

4.2.1 Vials with septa caps are needed to place sample inside for analysis. The septa in the vial needs to have the glossy side facing out.

4.2.2 Glass microfiber filter paper needs to be cut into smaller and more manageable pieces, a hole punch can be used to get small round pieces.

4.2.3 Tri-fold Metal Envelope Sample Holders are necessary to hold the microfiber filter paper. Separate a strip from the pack of metal envelopes and place a hole punched glass microfiber filter paper inside the clip, with the small opening facing up. Fold the two flaps on the envelope to secure the filter paper in place. Fold one end of the envelope to 90° so it can lay horizontally in the 4 mL vial.

4.3 On the recipe selection, select ‘Calibration- Lower Temperature.’

4.4 On data type, select ‘Sample.’

4.5 On the following window, press ‘OK’ to begin purging.

4.6 While purging, prepare the liquid sample (standard or water sample):

4.6.1 With a 10 μL syringe, obtain 2 μL of water from a standard or liquid water sample. **Note:** With precipitation samples containing mineral oil, the plunger of a syringe must be pulled back to partially fill with air. Then, the needle needs to be submerged to reach the water at the bottom. Inject the air into the water to remove mineral oil from the syringe. Take 2 μL of sample.

4.6.2 Pump the water sample into the tri-fold metal envelope that was prepared on step 4.2.3.

4.6.3 With laboratory gloves or a tweezer, place the metal envelope in the 4 mL vial (with the bent end at the bottom of the vial) and close the lid. **Note:** Do not touch the metal envelope, the moisture from finger tips will contaminate the isotopic signature.

4.7 Once instructed by the CRDS Coordinator, place the vial into the IM as instructed on step 3.6.5.

4.8 Once prompted by the CRDS Coordinator, eject the vial by turning the lever further to the right. This process takes 5 minutes per sample.

4.9 The zero and mid standards were ran prior to the liquid samples. The depleted sample was ran after the liquid samples. 6 repetitions each.

4.10 How to run samples in the autosampler:

4.10.1 Assemble the vaporizer and vacuum pump with the Picarro Autosampler User's Manual. **Note:** This method was only done with precipitation samples. Stems with organic contamination were processed in the IM for accurate readings.

4.10.2 Place a loaded sample tray into the tray holder with 2 mL vial containers. **Note:** Fill with a minimum of 200 μL to minimize isotopic fractionation due to vapor equilibrium).

4.10.3 Verify syringe was installed appropriately. See User's Manual for detailed instructions.

4.10.4 Fill Wash 1 with DI water.

4.10.5 Place septa into vaporizer injector port. **Note:** septa should be replaced every 200-300 repetitions.

4.10.6 Double click the Coordinator Launcher icon in the Picarro desktop. Select 'High Precision' in the drop down menu. Minimize this window.

4.10.7 Select the Autosampler Control icon in the desktop window. The Autosampler User Interface window will appear.

4.10.8 On Job Queue, for every 20 samples (7 repetitions for each) we ran a set of standards (Zero, Mid, and Depleted 5 repetitions each). The method used for this experiment was ‘Picarro Rinse’. Under ‘tray’ all of them will be ‘1’. Checkmark the jobs to be ran. Select ‘Run’. **Note:** Some samples were needed to be filtered to remove soil particles.

4.10.9 While the Autosampler is running, the Autosampler UI window will be disabled.

4.10.10 Once the autosampler has completed the job, remove the vials from the sample tray. Parafilm the lids and store in a refrigerated environment.

4.10.11 Select ‘End’ on the Autosampler UI. Reduce the Vaporizer temperature to match the ambient room temperature before turning off.

5. HOW TO RUN SOIL SAMPLES

5.1 Verify that the steps in section 3. have been completed before proceeding with the soil samples.

5.2 Materials needed to run soil samples:

5.2.1 Vials with septa caps are needed to place sample inside for analysis. The septa in the vial needs to have the glossy side facing out.

5.2.2 Metal tube sample holders need to be prepared by rolling quartz wool into a small ball that fits at the end of the tube (to prevent soil from spilling out).

5.3 On the recipe selection, select ‘Clay Loam.’ Note: This recipe is appropriate for the soil texture of the study site. Other recipes are more fitting for different soil textures.

5.4 On data type, select ‘Sample.’

5.5 On the following pop-up window, press ‘OK’ to begin purging.

5.6 Preparing soil for analysis:

5.6.1 Using a laboratory spatula, scoop soil into the metal tube until it is nearly filled with soil. Take another quartz wool ball to stuff the other end of the tube.

5.6.2 Place metal tube in 4 mL vial with septa and inject into the IM.

5.6.3 Each sample takes 12 minutes to complete. Repeat 5 times for each soil sample.

6. CRYOGENIC VACUUM EXTRACTION EQUIPMENT MATERIALS

6.1 Equipment:

6.1.1 Polyscience P40N7A101B IP-35 Immersion Probe Cooler

6.1.2 Edwards E2M0.7 Vacuum Pump

6.1.3 2 Fisherbrand Isotemp Digital Dry Baths/Block Heaters

6.1.4 Thermos Stainless Steel Nitrogen Cold Trap (???)

6.1.5 Laboratory Heating and Drying Oven

6.2 Materials:

6.2.1 Chemglass Life Sciences glass assembly with vacuum valve (custom glass welding to connect the sample tube and a trapping tube)

6.2.2 3 mL plastic syringe

6.2.3 Duran Wheaton Kimble 16 x 100 disposable culture tubes with GL18 thread screw caps

6.2.4 99% Isopropyl Alcohol

6.2.5 Parafilm

6.2.6 2 Laboratory Jacks 8in x 8in

6.2.7 Fisherbrand 2 mL screw thread autosampler vials

6.2.8 Quartz wool

7. PROCEDURE TO BEGING EXTRACTING WATER FROM STEMS

7.1 Set up the equipment and materials:

7.1.1 Mount both block heaters on each laboratory jack and connect to appropriate power supply. Adjust the jack height as needed.

7.1.2 Thermos Stainless Steel Nitrogen Cold Trap is placed in between the mounted block heaters.

7.1.3 Laboratory stand is placed behind the stainless steel nitrogen cold trap to support the immersion cooler's probe.

7.1.4 To assemble the Edwards E2M0.7 Vacuum Pump follow the Edwards instruction manual.

7.1.5 Place the immersion probe cooler next to the equipment assembly (with enough space between the assembly.

7.1.6 Pour the 99% isopropyl alcohol in stainless steel nitrogen cold trap until ~60% filled (enough to have the vegetation stem in the vial completely submerged).

7.2 Remove vegetation samples from refrigerator and allow to reach room temperature to avoid condensation when opened.

7.3 Begin by submerging the immersion cooler probe in the cold trap and clamping it on to the laboratory stand to keep it in place. Press the power switch to begin cooling.

7.4 Turn on block heaters power switch near the power cord. Set the temperature to 100 °C:

7.4.1 Confirm 'Heat indicator' light is on or blinking.

7.4.2 Press the 'set/cal' button.

7.4.3 Press the up, down and shift buttons until desired temperature is reached.

7.4.4 Press the 'set/cal' button again.

7.4.5 Choose 99:59 for continuous heating.

7.4.6 Wait 5 seconds and the instrument will begin heating.

7.5 Placing vegetation samples in glass assembly:

7.5.1 Set aside 20 disposable culture tubes with screw caps to begin filling with stems.

7.5.2 Unwrap vegetation sample that was stored in Parafilm and cut up into small, 1 cm long pieces. Label each tube with appropriate sample ID.

7.5.3 Place a thin piece of quartz wool (diameter of tube) above the vegetation sample.

7.5.4 Assemble the screw cap by referring to the instructions within the packaging.

7.5.5 Screw sample vial below the cock valve and the trapping tube on the other end of the glass assembly.

7.6 Repeat procedure for 10 more sample vials.

8. HOW TO EXCTRACT WATER FOR SAMPLE ANALYSIS

8.1 Submerge the sample vials in the isopropyl alcohol until stems are partially frozen (~10 minutes).

8.2 How to operate the Edwards E2M0.7 Vacuum Pump:

8.2.1 Plug the vacuum to the appropriate power source.

8.2.2 Remove one sample from the isopropyl alcohol bath.

8.2.3 Make sure cock valve on the glass assembly is closed and the isolation valve is open.

8.2.4 Connect the glass assembly with the vacuum and make sure the screw is tight.

8.2.5 Open the cock valve and close the isolation valve. Make sure the pressure reads 2 mbar or less for at least 15 seconds.

8.2.6 When a vacuum is achieved successfully, remove the glass assembly and place the sample tube in the block heater and the collection tube in the alcohol bath.

8.3 Repeat for the desired outcome of samples. Unplug the vacuum pump when finished.

8.4 Wait two hours for distillation to be completed before removing glass assembly from the instrument.

8.5 Remove glass assemblies from the alcohol bath and place upright to allow the frozen water to thaw and collect at the bottom of the tube.

8.6 Once water is liquid, remove collection tube from assembly and extract the water using a 3 mL syringe. Place in a 2 mL vial and refrigerate.

8.7 Repeat for every sample in alcohol bath.

8.8 After the desired amount of samples are completed, turn off the immersion cooler with the power switch. Remove immersion cooler probe from alcohol bath to dry. Cover the Thermos container filled with alcohol to prevent evaporation. Turn off both block heaters by pressing ‘start/stop’ and then pressing the power switch on the back.

9. SOIL TEXTURE ANALYSIS EQUIPMENT AND MATERIALS

9.1 Equipment:

9.1.1 1 PARIO sensor and 2 PAIRO flasks

9.1.2 Computer (to launch PARIO Control software)

9.1.3 Four Soil Sieves (2 mm, 0.50 mm, 0.25 mm, 0.053 mm)

9.1.4 Laboratory Hot Plate with Magnetic Stirrer

9.1.5 HANNA Instruments Portable Water Conductivity and Soil Activity Meter

9.1.6 Branson 2510 Ultrasonic Cleaner

9.1.7 Scientific Industries SI-1100 Roto-Shake Genie Rocker

9.2 Materials:

9.2.1 Ashless filter paper grade No. 40

9.2.2 16 oz funnels

9.2.3 Weighing boats

9.2.4 Deionized water

9.2.5 1,000 mL beaker

9.2.6 50 g/L $Na_6O_{18}P_6$

10. PROCEDURE TO PREPARE FOR SOIL TEXTURE ANALYSIS

10.1 Verify that sample is at least 100 g of soil and contains less than 1.5 % organic content.

10.2 Procedure for salt removal:

10.2.1 With a 2mm sieve, filter out 50g of soil with any particles larger than 2mm.

10.2.2 Place weighing boat on scale and tare weight.

10.2.3 Weigh the 50 g of <2 mm sample into weighing boat and record the weight. Record sample ID, date and time. Label weighing boat.

10.2.4 Fold filter paper into a cone shape and place in funnel. Pour weighted soil into the filtered funnel. Repeat for each sample.

10.2.5 Place a beaker below the funnel to catch discharge. Pour deionized water into the funnel until filled to the brim.

10.3 Procedure to measure specific conductivity measurements:

10.3.1 Turn on the water conductivity meter with the on/off button. **Note:** To calibrate instrument, refer to the Instruction Manual.

10.3.2 Submerge the probe into the discharged water (at least 5 cm). Pour more deionized water into the soil until it reads less than 0.4 mS/cm.

10.3.4 Dispose of the discharged water into the sink. Allow samples to air dry in the funnel for at least 24 hours. If it is still wet, allow more time to air dry before proceeding.

10.3.5 Once dry, weigh out another boat and record weight. Label the boat as described in 10.2.3.

10.3.6 Scrape off the dry salt-leached sample from the filter paper and place it on weighing boat. Record the weight. **Note:** Verify that as much soil as possible was transferred from the filter paper to the associated boat.

10.3.7 Carefully transfer soil into a 1 L bottle. Add 250 mL of DI water and 100 mL of $Na_6O_{18}P_6$. **Note:** To make dispersion solution fill up a 1,000 mL beaker with DI water, add 50 g of $Na_6O_{18}P_6$, and place on stir plate with stir tab for 24 hours to dissolve $Na_6O_{18}P_6$.

10.3.8 Place prepared mixture on shaker for at least 8 hours.

10.4 Preparing for sieving:

10.4.1 Place four new weighing boats on a scale and record the boat weights. Label according to the four sieves (2 mm, 0.50 mm, 0.25 mm, 0.053 mm).

10.4.2 Place a weighing boat on the scale and tare. Pour approximately 50 g of soil sample into one of the boats and record the weight.

10.4.3 Oven dry the soil sample for 24 hours at 65 °C. Then remove the sample from the oven and record the dry weight.

10.4.5 Pour sample into a 200 mL beaker with 100 g of water. Place the beaker in an ultrasonic cleaner for 10 minutes.

10.5 Sieving procedure:

10.5.1 Rinse sieves with water to remove any debris. Then, stack in order of increasing to decreasing mesh size (top to bottom).

10.5.2 Once the ultrasonic cleaner is finished, stir the soil slurry for about 30 seconds.

10.5.3 Pour the soil slurry into the top sieve. **Note:** Verify that all of the soil is removed from the beaker. If there are soil particles left in the beaker, rinse with deionized water and pour into sieve. Repeat if necessary.

10.5.4 Use deionized water to help the soil transfer through each sieve. Continue until the water is flowing clear to the next sieve.

10.5.5 Scrape as much sample as possible from the sieve and pour into assigned boat from step 10.4.1.

10.5.6 Repeat for all four sieves.

10.6 Oven dry the four boats for 24 hours at 65 °C.

10.7 Remove from oven and record dry weight of each.

10.8 PARIO Plus Mode:

10.8.1 Pour suspended soil sample into Pario Plus sedimentation cylinder. **Note:** Make sure to rinse the soil container with DI water until most of the soil grains are poured into the sedimentation cylinder.

10.8.2 Once the soil container is properly rinsed, fill the sedimentation cylinder with DI water until it reaches the white ‘max fill’ line.

10.8.3 Connect PARIO usb port to laptop and the PARIO LED light should flash 3 times.

10.8.4 Open ‘Pario Control’ software and LED light will flash another 3 times.

10.8.5 Click ‘New Measurement’ on Pario Control interface. On the right-hand corner, insert sample label under ‘Sample Name’ under the Sample Data tab. Under PARIO Mode, select ‘PARIO plus’. On the Suspension Data tab under ‘Mass of Particles’, insert dry mass that was weighted in step 10.3.6. For ‘Mass of Dispersant’ insert 5 g. Homogenization Method is ‘overhead shaking’.

10.8.6 Select the ‘Start’ button and begin overhead shaking for 60 seconds as directed by the PARIO interface. Once the timer ends, remove the PARIO from the DI water and tilt at 45 degree angle and quickly submerge in the sedimentation cylinder. **Note:** Hold on to the rubber stopper when overhead shaking or sample will leak.

10.8.7 Wait for 2.5 hours for the analysis to reach completion.

10.8.8 Weigh a boat and take note of weight. Open the valve to remove the effluent and let it drip into a boat, wait 100 seconds. Place boat containing sample into the oven for 24 hours at 50 C. Once dry, record the dry effluent weight from boat.

10.8.9 To extract the analysis file from the PARIO control program, enter dry weight of sample after salt removal, the mass of the dispersant under ‘suspension data’ (5 g), the percent sand (after sieving), and effluent dry weight. Then export the file.

10.8.9 Disconnect the PARIO from the laptop and rinse it out with DI water. Place PARIO back in cylinder with DI water (to remain at room temperature). Rinse out the PARIO Plus sedimentation cylinder with DI water.

10.8.10 Repeat for every soil sample.

APPENDIX C: DESCRIPTIVE STATISTICS OF ALL DATA

Martha E. Gardea[1]

[1]Department of Earth, Environmental and Resource Sciences, University of Texas at El Paso, TX 79968, USA

Table 1: Descriptive statistics (min, max, average) in $\delta^{18}O$ (‰) and $\delta^{2}H$ (‰) of precipitation, soil, and vegetation samples.

Sample Name	$\delta^{18}O$			$\delta^{2}H$		
	Minimum	Maximum	Mean	Minimum	Maximum	Mean
Precipitation	-16.88 ‰	11.00 ‰	-5.28 ‰	-134.17 ‰	37.36 ‰	-41.11 ‰
All Mesquite	-11.99 ‰	15.56 ‰	-0.73 ‰	-84.98 ‰	4.69 ‰	-45.03 ‰
CA Mesquite	-11.99 ‰	10 ‰	-0.76 ‰	-84.98 ‰	4.69 ‰	-42.74 ‰
FA Mesquite	-6.09 ‰	4.33 ‰	-1.79 ‰	-70.19 ‰	-34.93 ‰	-53.32 ‰
VD/CR 1 Mesquite	-7.48 ‰	14.36 ‰	-0.69 ‰	-63.52 ‰	-12.5 ‰	-43.29 ‰
VD/CR 2 Mesquite	-7.60 ‰	15.56 ‰	0.65 ‰	-60.60 ‰	-23.48 ‰	-39.47 ‰
All Creosote	-7.62 ‰	17.91 ‰	0.12 ‰	-85.36 ‰	13.50‰	-44.29 ‰
CA Creosote	-7.62 ‰	11.05 ‰	-0.42 ‰	-85.36 ‰	-20.39 ‰	-48.25 ‰
FA Creosote	-1.52 ‰	17.91 ‰	3.58 ‰	-61.65 ‰	13.50 ‰	-32.94 ‰
VD/CR 1 Creosote	-5.19 ‰	4.72 ‰	-0.77‰	-64.45 ‰	-29.91 ‰	-46.41 ‰
VD/CR 2 Creosote	-5.84 ‰	4.32 ‰	-1.33 ‰	-65.83 ‰	-29.57 ‰	-47.50 ‰
All Tarbush	-6.84 ‰	7.28 ‰	-0.43 ‰	-72.75 ‰	-27.41 ‰	-42.90 ‰
VD/CR 1 Tarbush	-5.36 ‰	7.28 ‰	-0.25 ‰	-64.48 ‰	-27.78 ‰	-43.25 ‰
VD/CR 2 Tarbush	-6.84 ‰	3.69 ‰	-0.89 ‰	-72.75 ‰	-27.41 ‰	-41.98 ‰
All Grass	-8.61 ‰	11.47 ‰	0.39 ‰	-88.36 ‰	12.39 ‰	-36.44 ‰
VD/CR 1 Grass	-8.61 ‰	11.47 ‰	0.97 ‰	-88.36 ‰	12.39 ‰	-35.21 ‰
VD/CR 2 Grass	-5.71 ‰	4.13 ‰	-1.94 ‰	-48.28 ‰	-28.11 ‰	-41.36 ‰
All Soil 10 cm	-21.79 ‰	4.77 ‰	-6.34 ‰	-115.78 ‰	-8.70 ‰	-54.09 ‰
CA Soil 10 cm	-17.32 ‰	4.77 ‰	-6.30 ‰	-115.78‰	-9.87 ‰	-54.31 ‰
FA Soil 10 cm	-15.28 ‰	4.73 ‰	-5.40 ‰	-113.82 ‰	-8.70 ‰	-53.36 ‰
VD/CR 1 Soil 10 cm	-21.79 ‰	1.82‰	-6.89 ‰	-115.62 ‰	-11.43 ‰	-55.48 ‰
VD/CR 2 Soil 10 cm	-13.20 ‰	-2.88 ‰	-8.20 ‰	-108.36 ‰	-12.16 ‰	-53.92 ‰
All Soil 20 cm	-116.74 ‰	2.65 ‰	-24.12 ‰	-124.37 ‰	4.73 ‰	-36.86 ‰
CA Soil 20 cm	-16.97 ‰	5.28 ‰	-7.14 ‰	-116.74 ‰	-7.90 ‰	-56.45 ‰
FA Soil 20 cm	-16.10 ‰	2.65 ‰	-6.02 ‰	-124.37 ‰	-13.81 ‰	-53.37 ‰
VD/CR 1 Soil 20 cm	-16.82 ‰	0.55 ‰	-7.47 ‰	-122.43 ‰	-14.78 ‰	-57.39 ‰
VD/CR 2 Soil 20 cm	-13.48 ‰	-2.86 ‰	-7.83 ‰	-102.28 ‰	-12.58 ‰	-53.22 ‰
All CA Soil	-17.32 ‰	5.28 ‰	-6.72 ‰	-116.74 ‰	-7.90 ‰	-55.38 ‰
All FA Soil	-16.10 ‰	4.73 ‰	-5.71 ‰	-124.37 ‰	-8.70 ‰	-53.36 ‰
All VD/CR 1 Soil	-21.79 ‰	1.82 ‰	-7.17 ‰	-122.43 ‰	-11.43 ‰	-56.41 ‰
All VD/CR 2 Soil	-13.48 ‰	-2.86 ‰	-8.01 ‰	-108.36 ‰	-12.16 ‰	-53.57 ‰

VITA

Martha Elizabeth Gardea was born in Ciudad Juárez, Chihuahua to Beatriz Gomez and Gustavo Gardea. They grew up in Clovis, New Mexico and graduated from Clovis High School in May 2015. That same year Martha entered Clovis Community College and after a year enrolled in Eastern New Mexico University. Martha majored in Environmental Science and participated in undergraduate research with Dr. Jim Constantopoulos. Martha used X-ray Fluorescence and UV-VIS Spectroscopy to conduct their undergraduate thesis in trace metal distribution within Bonito Lake, New Mexico. Martha received their Bachelor of Science in Environmental Science, with a minor in Geology, in May 2020. The following year, Martha was admitted into the Department of Earth, Environmental, and Resource Sciences at the University of Texas at El Paso, where they pursued their Master of Science degree. During those years, Martha worked as a Research Assistant for the Ecohydrology Laboratory and as a Teaching Assistant the majority of the time. In the Spring of 2022, Martha was awarded Outstanding Graduate Student in Environmental Science by the Department of Geological Sciences at the University of Texas at El Paso. Martha received their Master of Science in Environmental Science May 2022.

Contact Information: megardea4@gmail.com

This thesis was typed by Martha Elizabeth Gardea